NASA TECHNICAL NOTE

NASA TN D-7103

MIXING-HEIGHT MEASUREMENT BY LIDAR, PARTICLE COUNTER, AND RAWINSONDE IN THE WILLAMETTE VALLEY, OREGON

by M. Patrick McCormick, S. Harvey Melfi, Lars E. Olsson, Wesley L. Tuft, William P. Elliott, and Richard Egami

Langley Research Center
Hampton, Va. 23365

NATIONAL AERONAUTICS AND SPACE ADMINISTRATION • WASHINGTON, D. C. • DECEMBER 1972

1. Report No.	2. Government Accession No.	3. Recipient's Catalog No.
NASA TN D-7103		

4. Title and Subtitle	5. Report Date
MIXING-HEIGHT MEASUREMENT BY LIDAR, PARTICLE COUNTER, AND RAWINSONDE IN THE WILLAMETTE VALLEY, OREGON	December 1972
	6. Performing Organization Code
7. Author(s)	8. Performing Organization Report No.
M. Patrick McCormick, S. Harvey Melfi, Lars E. Olsson, Wesley L. Tuft, William P. Elliott, and Richard Egami	L-8279
	10. Work Unit No.
9. Performing Organization Name and Address	502-23-56-04
NASA Langley Research Center Hampton, Va. 23365	11. Contract or Grant No.
	13. Type of Report and Period Covered
12. Sponsoring Agency Name and Address	Technical Note
National Aeronautics and Space Administration Washington, D.C. 20546	14. Sponsoring Agency Code

15. Supplementary Notes

Lars E. Olsson, Wesley L. Tuft from Department of Atmospheric Sciences, Oregon State University, and William P. Elliott, Richard Egami from Department of Oceanography, Oregon State University

16. Abstract

This paper shows the feasibility of using laser radar (lidar) to measure the spatial distribution of aerosols and water vapor in the earth's mixing or boundary layer. From these data the important parameter of actual mixing height was determined, that is, the maximum height to which particulate pollutants actually mix. Data are shown for simultaneous lidar, rawinsonde, and aircraft-mounted condensation nuclei counter and temperature measurements. The synoptic meteorology is also presented. The Willamette Valley, Oregon, was chosen for the measurements because of its unique combination of meteorology, terrain, and pollutant source, along with an ongoing Oregon State University study of the natural ventilation of this valley.

17. Key Words (Suggested by Author(s))	18. Distribution Statement
Laser radar Mixing height Meteorology Atmospheric science	Unclassified – Unlimited

19. Security Classif. (of this report)	20. Security Classif. (of this page)	21. No. of Pages	22. Price*
Unclassified	Unclassified	78	$3.00

*For sale by the National Technical Information Service, Springfield, Virginia 22151

MIXING-HEIGHT MEASUREMENT BY LIDAR, PARTICLE COUNTER, AND RAWINSONDE IN THE WILLAMETTE VALLEY, OREGON

By M. Patrick McCormick, S. Harvey Melfi, Lars E. Olsson,[1]
Wesley L. Tuft,[1] William P. Elliott,[2] and Richard Egami[2]
Langley Research Center

SUMMARY

This paper shows the feasibility of using laser radar (lidar) to measure the spatial distribution of aerosols and water vapor in the earth's mixing or boundary layer. From these data the important parameter of actual mixing height was determined, that is, the maximum height to which particulate pollutants actually mix. Data are shown for simultaneous lidar, rawinsonde, and aircraft-mounted condensation nuclei counter and temperature measurements. The synoptic meteorology is also presented. The Willamette Valley, Oregon, was chosen for the measurements because of its unique combination of meteorology, terrain, and pollutant source, along with an ongoing Oregon State University study of the natural ventilation of this valley.

INTRODUCTION

The objective of this paper is to show the feasibility of using laser radar (lidar) to measure atmospheric parameters important to the study of air pollution. Laser-radar measurements can yield the spatial distribution of aerosols (particles in air suspension) and water vapor in the earth's mixing or boundary layer. From these data the important parameter of actual mixing height can be determined, that is, the maximum height to which particulate pollutants actually mix. Presently, mixing height is determined from twice-daily rawinsonde temperature and wind profiles or aircraft visual observation. These techniques do not necessarily yield the actual mixing height, represent only point measurements in time and space, and are not remote. Laser radar offers the ability to measure the mixing height remotely, instantaneously, and in two dimensions and should provide a very valuable tool for the air-pollution meteorologist.

The data presented in this paper represent the results of a study of the mixing of pollutants in the Willamette Valley, Oregon. This study was conducted jointly by the NASA Langley Research Center and Oregon State University. A map and cross section of the

---

[1] Department of Atmospheric Sciences, Oregon State University.

[2] Department of Oceanography, Oregon State University.

valley are shown in figure 1. Air stagnation over the valley results from a combination of terrain and various meteorological factors including the mixing height. The geographical area has one of the highest meteorological air-pollution potentials in the United States. (See ref. 1.) The region is enclosed by mountains to the east and west and by hills to the north and south. Furthermore, the natural ventilation of the valley region is often restricted by a stable layer of air aloft, which typically defines the actual mixing height. When the stable layer is based below the top of the mountains, air flow into or out of the valley region is greatly restricted. (See refs. 2, 3, and 4.) The effect of this meteorology is evidenced when agricultural field burnings, shown in figure 2, are permitted. The combustion products rise to the top of the mixing layer and laterally diffuse. In a very short time these burnings can greatly reduce the visibility within the mixing layer. (See fig. 3.) This combination of meteorology, terrain, and pollutant source, along with an ongoing Oregon State University (OSU) study of the natural ventilation of this valley, prompted NASA participation.

The joint NASA-OSU experiment compares meteorological data (rawinsonde, pilot balloon, aircraft-mounted temperature and condensation nuclei measurements) taken by Oregon State University and the National Weather Service with laser-radar data taken by NASA. This study represents part (approximately 2 weeks) of a long-term investigation of the natural ventilation of the Columbia-Willamette Valleys being undertaken by the Department of Atmospheric Sciences, Oregon State University.

The authors wish to express their gratitude for the cooperation and support of personnel from the State Department of Environmental Quality in Oregon, the Columbia-Willamette Air Pollution Authority, the Mid-Willamette Valley Air Pollution Authority, the Lane Regional Air Pollution Authority, and the National Weather Service.

SYMBOLS

A	area of the receiver, meters^2
c	speed of light, meters per second
E	laser output energy per pulse, joules
f	backscattering function, meter^{-1}-steradian^{-1}
N	molecular number density, molecules per centimeter^3
q	transmissivity of a model aerosol and molecular atmosphere

$q_s(\lambda,\Delta z)$ transmissivity from scattering volume to laser radar

$q_t(\lambda,\Delta z)$ transmissivity from laser radar to scattering volume

R photomultiplier load resistor, ohms

r range, kilometers

S spectral sensitivity of photomultiplier, amperes per watt

T system optical efficiency

V voltage of photomultiplier, volts

z distance between scatterer and detector, meters

γ system constant

λ wavelength of incident or scattered light, meters

σ_r Raman cross section, meters^2 per steradian

Subscripts:

A aerosol

M molecular

r Raman

OBSERVATIONAL METHODS AND DATA REDUCTION

Vertical profiles of temperature, water vapor, winds aloft (speed and direction), and aerosol concentrations were taken at various times with instrumented aircraft, rawinsondes, pilot balloons, and laser radar. The aircraft used was a Piper Comanche instrumented by personnel from Oregon State University with a temperature probe and condensation (Aitken) nuclei counter. The condensation nuclei counter measures aerosols in the size range greater than 0.001 μm. The aircraft probed the atmosphere over the vicinity of the ground-based laser radar, which was located approximately 600 meters

from the Salem airport. At the airport members of the Salem National Weather Service Station provided rawinsonde vertical profiles of temperature, water-vapor concentration, wind speed and direction, and ground visibility. Pilot balloons, which are small theodolite-tracked balloons providing wind speed and direction, were launched and tracked by OSU personnel.

Two ground-based laser-radar (lidar) systems were used in this investigation. One system measured water-vapor mixing ratio and lidar scattering ratio in the zenith direction only. These quantities are discussed in the following section. The other system measured lidar scattering ratio and was capable of scanning in elevation and azimuth. The zenith system consists of a ruby laser with frequency doubler and a Newtonian telescope-collector. The scanning system consists of a ruby laser and a searchlight-mirror receiver. Photographs of the laser radars are shown in figures 4, 5, and 6. Laser radar represents the optical analog of the familiar microwave radar; a pulse of light approximately 6 meters in length is emitted into the atmosphere and interacts with the molecules and aerosols, scattering light in all directions. A portion of this light is backscattered, collected by a telescope, and recorded as voltage as a function of time (or range). The amplitude of this voltage yields information concerning the scatterers.

A detailed description of all the measurement systems used in this investigation is given in appendix A.

DATA PRESENTATION

Data were taken in Salem, Oregon, from August 26 to September 3, 1970, and separated into 18 periods. The periods are divided into two distinct time intervals: The first consists of data collected during periods 1 to 9 from 2215 P.d.t. (Pacific daylight time) August 26 to 2251 P.d.t. August 28, 1970. (All times in this paper are given in Pacific daylight time.) The second time interval, divided into periods 10 to 18, consists of data collected from 1030 August 31 to 0415 September 3, 1970. The various observations during these time periods are summarized in table 1. The times shown for rawinsonde and winds-aloft data correspond to balloon launch. The times shown for laser-radar and aircraft data correspond to times during which data were taken.

The large-scale weather conditions are of interest as they affect local weather conditions in Salem. These synoptic conditions are discussed for each of the two time intervals in appendix B. The discussions are based on surface weather charts and 850-, 700-, and 500-millibar pressure-height contour maps supplied by the National Weather Service and on surface observations taken at the Salem airport.

A detailed analysis of all the data is given in appendix C. Only a representative portion is discussed in detail in the text. The main topic of discussion is the measure-

ment of actual mixing height determined by lidar data compared with actual mixing height determined by significant vertical variations of temperature, winds aloft, water vapor, and condensation nuclei concentrations.

In the discussion for each period, the following terminology and definitions are used: A temperature inversion refers to an increase in temperature with height and implies very limited vertical mixing. Isothermal refers to constant temperature with height and implies limited mixing. Nearly isothermal refers to a decrease in temperature of zero to 2^{o} C-km^{-1} and also implies limited mixing. An average lapse rate refers to a decrease in temperature of 2^{o} to 7^{o} C-km^{-1} and implies moderate mixing. A nearly-dry-adiabatic lapse rate refers to a decrease in temperature of 7^{o} to 10^{o} C-km^{-1} and implies good mixing. A dry-adiabatic lapse rate refers to a decrease in temperature of 10^{o} C-km^{-1} and also implies good mixing. A superadiabatic lapse rate refers to a decrease in temperature greater than 10^{o} C-km^{-1} and implies intensive mixing. Wind shear refers to a rapid change in wind speed and/or direction with height. A negative vertical gradient refers to a decrease in values with height, and a positive gradient refers to an increase in values with height.

In the graphical presentation and in the discussion, times are given in Pacific daylight time, temperatures are given in degrees Celsius, mixing ratios are given as grams of water vapor per kilogram of dry air, and heights are given in meters referenced to sea level. Winds aloft for the graphical presentation are plotted by using the following symbols and classification:

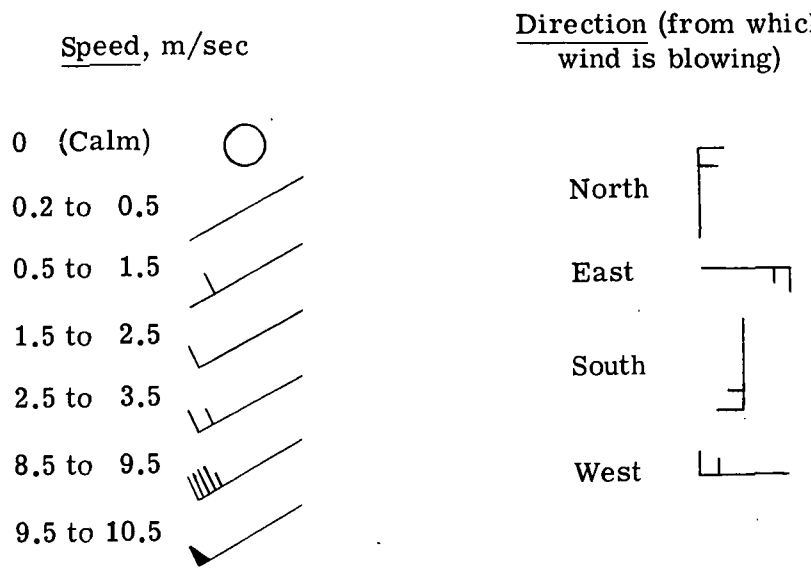

The laser-radar data are presented in three forms: lidar scattering ratio, isopleths of the lidar scattering ratio, and water-vapor mixing ratio. In order to explain these quantities, the general lidar equation must be presented.

After crossover of the laser pulse and receiver field of view, which occurs shortly after laser emission (approximately 100 meters range), the voltage $V(\lambda,z)$ at the oscilloscope for a laser-rader system is given by

$$V(\lambda,z) = \frac{\gamma(\lambda)\, E(\lambda)\, q_t(\lambda,\Delta z)\, q_s(\lambda',\Delta z)\, f(\lambda,z)}{z^2} \tag{1}$$

with

$$\gamma(\lambda) = \frac{cA}{2}\, T(\lambda)\, S(\lambda) R$$

where $f(\lambda,z)$ is the backscattering function at wavelength λ and altitude z, $q_t(\lambda,\Delta z)$ and $q_s(\lambda',\Delta z)$ are the transmissivities from the laser radar to the scattering volume and from the scattering volume to the laser radar, respectively. The symbol λ' refers to a wavelength other than λ, R is the photomultiplier load resistor, $T(\lambda)$ is the system optical efficiency, $S(\lambda)$ is the spectral sensitivity of the photomultiplier, A is the area of the receiver, c is the speed of light, and $E(\lambda)$ is the laser output energy per pulse.

For elastic scattering, that is, the incident and return wavelengths are identical and there is no absorption, this equation reduces to

$$V(\lambda,z) = \frac{\gamma(\lambda)\, E(\lambda)\, q^2(\lambda,\Delta z)\, f(\lambda,z)}{z^2} \tag{2}$$

where $f(\lambda,z) = f_M(\lambda,z) + f_A(\lambda,z)$. The subscripts M and A refer to molecular and aerosol, respectively. The Raman scattered return, which is shifted in wavelength from the laser output, would not include aerosol scattering; thus the voltage at the oscilloscope is given as

$$V(\lambda',z) = \frac{\gamma(\lambda')\, E(\lambda)\, q_t(\lambda,\Delta z)\, q_s(\lambda',\Delta z)\, f_r(\lambda',z)}{z^2} \tag{3}$$

if $f_r(\lambda',z)$ is the Raman scattering function at λ'. The scattering function in the molecular (Rayleigh) and Raman cases is simply the product of the cross section for backscattering and the molecular number density as a function of altitude. In order to calculate the aerosol scattering function, however, assumptions about the aerosol must be made. Usually the particles are assumed to be spherical with a constant size distribution and index of refraction as a function of altitude.

The oscillogram of the voltage-time profile and the output energy are analyzed by a film reader producing a computer card for each data point. Computer processing of these cards yields plots of V/E and z^2V/E as a function of z for each oscillogram, and therefore, for each laser firing. Besides the raw data points, interpolated points corresponding to every 50 or 100 meters in altitude are included. Each profile is then

compared with the oscillogram as a check on the film reading accuracy. The profiles produced in this manner encompass increments of about 1000 meters altitude, depending upon the signal change as a function of altitude. A total composite profile is constructed by computer averaging all 50- or 100-meter altitude points from a given set of oscillograms. The average z^2V/E is computer plotted as a function of z.

For elastic scattering, these values of z^2V/E are divided by values of q^2f_M, where f_M is the scattering function for a model molecular atmosphere and q^2 is the transmissivity of a model aerosol and molecular atmosphere. This model is developed in reference 5. Equation (2) then becomes

$$\frac{z^2V}{q^2f_ME} = \gamma\left(1 + \frac{f_A}{f_M}\right) \tag{4}$$

which is proportional to an aerosol-scattering ratio. In this paper the lidar system is calibrated by normalizing the ratio to 1 in a definite molecular scattering region above the top of the mixing layer. All other data are referenced to this firing. Isopleths of this ratio are constructed by plotting lidar scattering ratio as a function of altitude and time of day or range. Monotonic increases or decreases are assumed between data points.

For Raman scattering, the ratio of water-vapor return to nitrogen return is computer calculated and plotted. This ratio, to a good approximation, is proportional to water-vapor mixing ratio. From equation (3) this becomes

$$\frac{V\left(\lambda_{H_2O},z\right)}{V\left(\lambda_{N_2},z\right)} = \frac{\gamma\left(\lambda_{H_2O}\right) q_s\left(\lambda_{H_2O},\Delta z\right) f_r\left(\lambda_{H_2O},z\right)}{\gamma\left(\lambda_{N_2}\right) q_s\left(\lambda_{N_2},\Delta z\right) f_r\left(\lambda_{N_2},z\right)}$$

and if $q_{N_2} \approx q_{H_2O}$ and $\gamma\left(\lambda_{H_2O}\right) \approx \gamma\left(\lambda_{N_2}\right)$,

$$\frac{V\left(\lambda_{H_2O},z\right)}{V\left(\lambda_{N_2},z\right)} = \frac{\sigma_r\left(\lambda_{H_2O}\right)N_{H_2O}(z)}{\sigma_r\left(\lambda_{N_2}\right)N_{N_2}(z)} = \text{Constant}\,\frac{N_{H_2O}(z)}{N_{N_2}(z)} \tag{5}$$

where σ_r is the Raman cross section and N is the molecular number density of the particular molecular species.

The horizontal bars presented with the laser-radar data represent the one-sigma fluctuation of the data. This shows the amount of fluctuation of the aforementioned ratios during the time the data were taken.

In discussing the data, the actual mixing height measured with the lidar is defined to be the average altitude during which a strong reduction in scattering ratio or aerosol

concentration is observed. This strong reduction normally terminated in scattering-ratio values near 1, corresponding to molecular scattering. For the aircraft-mounted condensation nuclei counter, the mixing height is arbitrarily defined as the altitude at which the concentration becomes less than 500 cm^{-3} (particles per cubic centimeter). It should be noted that the laser radar is most sensitive to aerosols greater than 0.1 μm and the condensation nuclei counter, as previously mentioned, is sensitive to particles greater than 0.001 μm. Therefore, comparing these two techniques of measuring mixing height could yield different results, depending on atmospheric particle size distribution and mixing.

A typical example of the data taken during the experiment is shown in figure 7. Plotted as a function of altitude are the lidar scattering ratio, condensation nuclei count (listed as particle count), and temperature. Also shown are altitude profiles of wind velocity and water-vapor mixing ratio obtained from rawinsondes. These data are from period 4 which includes, as shown in table 1, 1517 to 1800 August 27, 1970. The horizontal bars on the lidar data show the one-sigma fluctuation of the data taken between 1624 and 1710. The winds-aloft data are from rawinsondes launched at 1600 and 1800. The aircraft particle count and temperature data were taken from 1517 to 1537.

The temperature data show a nearly-dry-adiabatic lapse rate below approximately 930 meters and a strong temperature inversion above this altitude. Thus, the vertical mixing should be inhibited by this inversion and therefore the aerosols should be "capped" near this altitude. The condensation nuclei counts remained relatively constant to 1020 meters and, as expected, decreased rapidly near the inversion. The actual mixing height determined by the particle counter was 1100 meters, that is, by the definition used herein, the altitude at which the count became less than 500 cm^{-3}. The lidar system shows a rapid decrease of scattering from 850 to 1250 meters, where the scattering becomes nearly molecular. The actual mixing height as determined by lidar, therefore, is 1050 meters. Also the rawinsonde water-vapor mixing-ratio profile shows a significant decrease in this region. It should be pointed out that both lidar and particle counter determined the mixing height to extend into the temperature inversions.

An isopleth of lidar scattering ratio as a function of altitude and time of day for periods 6 to 9 is shown in figure 8. The numbers indicate the intensity of the scattering; for example, a number 5 corresponds to scattering 5 times as intense as that from a purely molecular atmosphere at that altitude. This type of presentation shows the changes in the atmospheric mixing of aerosols as a function of time of day and altitude. As can be seen in the figure, the air over Salem was relatively clean during the day with very few aerosols in the mixing layer. About 1700 the advection of smoke starts to become evident. A smoke layer begins to form that was fairly stable in space and time and took approximately 4 hours to move over the field of view. These data were taken with the

lidar looking at the zenith only. In order to investigate the spatial cross section of this layer, the scanning lidar made a series of elevation angle measurements pointing to the west of the field site. The results are shown in figure 9, where the isopleth of lidar scattering ratio is plotted as a function of altitude and range. The limiting elevation angle was about 45^{o}, as seen in the figure. The scan data show the layer to be centered, not overhead, but approximately 1400 meters to the west.

Shown in figure 10 is an altitude profile of water-vapor mixing ratio obtained from lidar compared with water-vapor mixing ratio obtained from rawinsonde. The lidar data were related to the rawinsonde data by using a weighted least-squares fit, with the inverse variance as the weighting factor. The horizontal bars indicate one-sigma fluctuation of the data. In general, these data agree very well.

All the data from periods 1 to 18 are presented and discussed in appendix C. A summary of these data is shown in figures 11 and 12. The top of the mixing layer determined by lidar and condensation nuclei counter, the altitude region of temperature inversion, and the region of decreasing water vapor are shown when available for each of the 18 periods. The lidar data show the altitude region of significant decrease in scattering ratio and the average altitude value, which, by the definition used herein, indicates the top of the mixing layer. The condensation nuclei data show the altitude region of significant decrease in count and the altitude at which the particle count is 500 cm^{-3}, which, by the definition used herein, indicates the top of the mixing layer.

Figure 11 indicates that of the nine periods, six had concurrent lidar and particle data and of these six periods, five show the top of the mixing layer as determined by the nuclei counter to lie within the band of decreasing lidar scattering ratio. For the other case (period 2), it lies within 100 meters of the lidar data. It should be pointed out that for period 2 the lidar did not show a well-defined mixing top and all data showed large variations. Furthermore, the top of the mixing layer as determined by these two methods in the five cases are within 50 meters of each other, with an average difference of 22 meters. The other case shows a difference of 170 meters. In all eight periods where there are lidar and temperature data, the lidar decrease lies within a temperature inversion, but for two periods the altitude spread of the nuclei data decrease does not correspond to a temperature inversion. Also, in only two of the nine periods did the water-vapor decrease not include the top of the mixing layer as determined by the lidar and nuclei counter.

In summary, during the first time interval of nine periods there was very good agreement between the lidar and particle-counter techniques for measuring the actual mixing height. Furthermore, the actual mixing height was, in general, found to be associated with a stable layer aloft although not uniquely with the base of this layer, as is normally assumed. The ground visibility measured at the Salem airport decreased with

decreasing mixing height and increased with increasing mixing height. This phenomenon indicates that the mixing height is forming a boundary for the mixing volume. There also appears to be correlation between layers with water-vapor decreases and the actual mixing height but again with no clear boundary relationship.

A summary of periods 10 to 18 is shown in figure 12. Of the six periods with concurrent lidar and particle-counter data, only one (period 15) shows excellent agreement. Also, period 12 indicates that the particle mixing height is within 20 meters of the top of the decrease in lidar scattering ratio. The lidar mixing height lies within stable layers aloft except in period 16, where there was a very shallow inversion. In period 16 the lidar mixing height was found to be slightly below the inversion. In most periods, the lidar mixing height lies within the water-vapor decrease.

The second time interval, in general, does not indicate the marked agreement between the methods as does the first. However, a closer examination of the data for each period of the second time interval shows that most of these data were taken during periods of good mixing with poorly defined lidar mixing heights and that there were also large temporal fluctuations in the lidar data. Also, there was considerably more variability in the synoptic weather conditions during this time interval. Therefore, the second time interval may not be indicative of the comparability of the many methods to sense the actual mixing height.

CONCLUSIONS

As part of a study of the natural ventilation of the Columbia-Willamette Valleys in western Oregon, laser-radar measurements of the aerosol and water-vapor distributions within the mixing layer were coordinated with special aircraft and balloon measurements over Salem, Oregon. Vertical profiles of aerosol concentrations, temperatures, water vapor, and winds were analyzed for 18 periods of special interest. The main emphasis in these analyses was placed on the determination of the actual mixing height by laser-radar scattering data and more conventional techniques. The feasibility of using laser-radar techniques in measurements of the temporal and spatial variations of this actual mixing height was investigated. Comparisons between temperature profiles measured by means of aircraft and rawinsondes were also made.

On the basis of the resulting analysis, the following conclusions were made:

1. There was general agreement between the interpretation of profiles of aerosol concentration measured with an airborne particle counter and with laser radar. The laser-radar profile was, however, assumed to be more reliable, as it was based on a time average of several probings, whereas the profiles measured from an aircraft were based on instantaneous measurement at any given level during a flight. In addition, it must be

stressed that these two aerosol measurements are sensitive to different aerosol sizes. The laser radar is most sensitive to particle sizes >0.1 μm, whereas the particle counter is sensitive to particles >0.001 μm.

2. The top of the aerosol layer, the actual mixing height, in general, was located within a stable layer aloft. This conclusion is in general agreement with findings based on earlier investigations.

3. The shapes of the water-vapor profiles measured with rawinsonde and laser radar were well correlated.

On the basis of the findings presented in this report, laser radar should provide a valuable tool for measurements of temporal and spatial variations of the actual mixing height. Furthermore, the technique lends itself to detailed studies of the distribution of aerosols within the mixing layer.

Langley Research Center,
National Aeronautics and Space Administration,
Hampton, Va., November 9, 1972.

APPENDIX A

MEASUREMENT SYSTEMS

Rawinsonde Observations

Rawinsonde observations were taken daily at 0415 and 1615 at the Salem airport. Seven special observations were taken upon request at approximately 1015 and 2215 on August 27, 28, 31, and September 2. All observations were made under procedures specified in the Federal Meteorological Handbook No. 3 – Radiosonde Observations (ref. 6) and in Circular O, Winds-Aloft Observations (ref. 7). Under these procedures, winds aloft are computed manually using a 2-minute average of both wind speed and direction.

Pilot-Balloon Observations

Pilot-balloon observations were taken every 2 hours on the even-numbered daylight hours of August 27, 28, and September 1 and 2. Single-theodolite tracking of 10- and 30-gram balloons was employed; the azimuth and elevation angles were read every 30 seconds. Winds aloft were calculated by use of a computer at Oregon State University. The wind speed and direction were averaged each minute of the balloon ascent. (See ref. 2.)

As part of the overall investigation, pilot-balloon observations were taken at the same times at various locations within the Columbia-Willamette Valleys and compared. Comparison of winds above 2000 meters indicated that the winds were approximately the same above that altitude over the entire region. Below 2000 meters wind velocities varied at different sites because of the influence of the topography and local meteorology. Also, Salem pilot-balloon observations and rawinsonde winds-aloft observations taken within half an hour of each other were found to compare closely.

When both pilot balloon and rawinsonde winds aloft were available, only pilot-balloon observations are included in the figures. If no pilot-balloon observations were taken or if the observations were incomplete, rawinsonde winds aloft are used.

Aircraft Particle Detector and Temperature Sensor

A small-particle, or condensation nuclei, detector was used for measurements of particle concentration. This robust instrument is portable and well suited for field experiments.

The procedure in using this instrument is very simple. An air sample is drawn by a hand vacuum pump into a chamber, which is lined with a saturated blotting paper for moisture supply. A second chamber is evacuated by the same hand vacuum pump to a desired vacuum pressure. A light source at the top of the sample tube transmits a

collimated light beam through the chamber to a cadmium-selenium photocell located at the base. To make a measurement, a valve connecting the two chambers is quickly opened causing adiabatic expansion and cooling. The supersaturation caused by the expansion activates a fog, the density of which is measured by the extinction of the light reaching the photocell. A galvanometer is calibrated to read particle concentration. The concentration measurement range for this instrument is from 2×10^2 to 1×10^7 cm^{-3}.

The partial-vacuum pressure in the expansion chamber for the measurements was 660 mm Hg or full-vacuum expansions at higher altitudes. The supersaturation for these expansions is of the order of 200 to 300 percent. This supersaturation permits particles as small as 0.001 μm radius to be counted.

Temperature measurements were made with a portable temperature sensor. The unit is self-contained with rechargeable batteries and is very suitable for aircraft experiments. A precision bead thermistor mounted in a radiation shield was the sensing element. Temperature was recorded on an inkless pressure-sensitive paper with six 12° C ranges between -30° and $+32^{\circ}$ C. Date, time, position, and altitude are annotated on the chart.

The accuracy of the temperature varies with aircraft speed because of aerodynamic heating of the sensing element. A comparison of the aircraft profiles with the rawinsonde profiles measured at approximately the same time over Salem showed that the profiles had the same shape, with the aircraft profiles shifted to a higher temperature because of this heating.

Laser-Radar System

Two laser-radar systems were used in this investigation. One system measured in the zenith direction only and was housed in the environmentally controlled mobile van shown in figure 4. This laser-radar system, shown in the closeup photograph in figure 5, consists of a ruby laser with frequency doubler and a Newtonian telescope-collector. The laser and telescope are alined parallel and pointed at the zenith through a hatch in the van roof. Raman and multiple-wavelength scattering experiments were conducted with this system.

The second laser-radar system used is shown in figure 6. It is capable of scanning in elevation and azimuth but cannot operate during daylight hours. It was used for aerosol measurements at $\lambda = 0.6943$ μm only. The basic experimental arrangement for the zenith laser radar is shown in figure 13 and is similar to the scanning system. For both systems a ruby laser is Q-switched with a Pockels cell and thereby produces a 1- to 2-joule, horizontally polarized pulse of approximately 20-nsec duration at 0.6943 μm in a beam width of 5 mrad. The temperature of the ruby rod is controlled to maintain consistent operation of the laser and prevent detuning of the output frequency into water-vapor

absorption lines at 0.69427 and 0.69438 μm. These lines correspond to changing the temperature of the ruby rod 20° C. (See ref. 5.) In the zenith system a temperature-controlled ADP crystal is used to generate the second-harmonic frequency, 0.3472 μm, with an efficiency of about 4 percent. Temperature control of the ADP crystal to within $\pm 1^{\circ}$ F is necessary to maintain peak conversion efficiency. The angle between the laser output axis and the crystal optical axis is approximately 50°, and the alinement is facilitated with a micrometer-adjusted crystal mount. The blue output at 0.3472 μm has an elliptical beam width of about 1 by 5 mrad.

The transmitter output energy for the zenith system contains plane-polarized, 0.6943- and 0.3472-μm radiation propagating effectively as a single beam. This radiation is monitored by a set of parallel beam splitters, directing a small portion of the beam to two vacuum photodiodes. The beam splitters are arranged in such a manner that a minimum amount of the second harmonic is lost to the output radiation. The spectral response of the 0.3472-μm diode is limited by a low-pass color filter, and that of the 0.6943-μm photodiode is limited by a high-pass color filter. To evaluate the rejection capabilities of this monitor, all color and neutral density filters were checked on a spectrophotometer and the laser was pulsed with and without the frequency-doubler crystal placed in front of the laser. Furthermore, with the doubler in place, a cell filled with a copper sulfate solution opaque to 0.6943-μm radiation was used to check if any 0.3472-μm radiation was being seen by the 0.6943-μm photodiode. The output signal of each photodiode is slightly integrated and displayed on one channel of a dual-beam, dual-trace oscilloscope and represents a relative energy measurement for each wavelength at consecutive laser pulsings. The entire transmitter was mounted on a rigid platform, which is micrometer adjustable in two degrees of freedom to permit alinement with the receiver. As the fundamental laser pulse and second harmonic propagate through the atmosphere, a small portion is backscattered and collected by the f/3, 0.41-meter-diameter primary mirror. This radiation is directed onto the secondary mirror, which is mounted at 45° to the primary-mirror axis. The secondary is a front-surface-coated flat mirror cut elliptically for minimum obscuration. The collected radiation is then focused in the plane of an adjustable stop which limits the field of view of the telescope. For the aerosol and multiple-wavelength measurements, a movable mirror deflects the light for collimation by a lens. The collimated light is color separated very efficiently by a dichroic beam splitter set at 45° to the beam axis. The reflectivity of the dichroic beam splitter at 0.3472 μm is about 95 percent, and transmissivity at 0.6943 μm is about 95 percent. The separated red and blue radiation passes through narrow-band interference filters before detection by 14-stage photomultipliers with S-20 photocathode response. The interference filter, centered at 0.6943 μm, has a bandwidth of 6 Å and a peak transmissivity of 62 percent, whereas the filter centered at 0.3472 μm has a bandwidth of 20 Å and a peak transmissivity of 12 percent. The dichroic-beam-splitter—interference-filter combina-

tion was investigated for crosstalk by operating the laser with and without the frequency doubler and by filtering the laser fundamental with a cell containing a copper sulfate solution. Both tests verified the spectral integrity of the photomultiplier input signals.

A third photomultiplier positioned behind the movable mirror, shown in figure 13 is used for the Raman scattering experiment. As in the previous mode of operation, the collected light is collimated and passed through a narrow-band interference filter. The maximum transmission of the filter corresponds to Raman shifted wavelengths. The interference filters used for Raman scatter detection have their passband centered at the Raman shifted wavelengths of nitrogen (0.3777 μm), oxygen (0.3669 μm), and water vapor (0.3976 μm) for incident radiation at 0.3472 μm. The selected filter is placed in the collimated beam to allow monitoring the atmosphere at any of these wavelengths to measure the corresponding molecular profile. The photomultiplier outputs are displayed on separate dual-beam, dual-trace oscilloscopes along with their respective energy trace and are photographed.

The scanning system differs in that it utilizes a 1.52-meter-diameter searchlight mirror and a photomultiplier with color filter positioned behind a field stop located in the focal plane. The laser transmitter is housed in an environmental chamber and mounted on a rigid table, which is also micrometer adjustable in two degrees of freedom.

The high-power densities of the laser output pulse for these systems necessitate safety procedures for operation in the atmosphere. Therefore, a microwave radar system AN/APS-42A was incorporated into each laser-radar system. The microwave radar, using a horn transmitter receiver with a 12^{o} beam width, is alined parallel to the laser axis, thus it overlaps the 5-mrad laser beam width. Considering representative aircraft speeds, human reaction times, and laser power densities sufficient to cause eye damage, the APS-42A permits detection before the aircraft encounters the laser pulse. An A-scope presentation of the microwave return is viewed by the laser operator before each firing.

APPENDIX B

SYNOPTIC CONDITIONS

First Time Interval

2200 to 2400 August 26, 1970.- During the evening of August 26 a weak, onshore surface pressure gradient over western Oregon was associated with high pressure off the Oregon coast. The high-pressure cell weakened aloft, and at 850 and 700 millibars winds were light and variable with virtually no pressure gradient over western Oregon. At 500 millibars a trough located off the California coast induced moderate southwesterly winds over western Oregon.

Surface observations at the Salem airport indicated clear skies during the evening with visibility of 24 km. Surface winds were calm or less than 3 m/sec from the north and west.

0001 to 2400 August 27, 1970.- The onshore surface pressure gradient resulted in low stratus clouds along the Oregon coast during the early morning hours. The high pressure offshore lessened during the day as a weak low-pressure system approached the Washington coast. During the evening increasing cloudiness was observed from Salem northward. The weak pressure gradient and light and variable winds persisted throughout the day at 850 and 700 millibars, while winds at 500 millibars continued to be moderate from the southwest.

Salem airport observations indicated clear skies until approximately 1000, when a broken stratus layer, of between six- and nine-tenths sky cover, based between 460 and 610 meters was observed. This layer became scattered (one- to five-tenths sky cover) at 1200 and had dissipated by 1300. Clear skies prevailed until cirrus clouds were observed at approximately 2000. The cirrus layer increased in sky cover and was reported as a transparent broken layer at 2400. Visibility was greater than 10 km during the early morning and late evening. Smoke reduced visibility from 0700 to 1800 with the lowest visibility value being 3 km at 1600 and 1700. Surface winds were generally calm or less than 3 m/sec from the south until 1500, after which they were 2 to 5 m/sec from the west.

0001 to 2400 August 28, 1970.- The weak low-pressure system reached the Washington coast at approximately 1100 and then moved southward and decreased in intensity, becoming very weak along the Oregon coast. High surface pressure was off the Oregon coast at 2100, and an onshore pressure gradient was established. At 850 millibars a high-pressure cell with associated light winds moved in over western Oregon during the day. At 700 millibars a closed low-pressure system formed off the California

coast and caused light southerly winds over western Oregon. At 500 millibars moderate southwesterly winds over western Oregon were observed in the morning, becoming westerly during the afternoon and evening.

Salem reported decreasing cirrus cloud cover and lowering of cloud bases to approximately 3900 meters at 0400. Skies were clear from 0500 to 0700, and then the cloud cover increased with an altocumulus layer based at approximately 3650 meters. This layer resulted in overcast skies at 0900. Cloud cover again decreased after 0900, and clear skies were reported from 1200 to 2400. Visibility was 16 km or greater throughout the day. Surface winds were light and variable from 0001 to 0900 and northwesterly to northeasterly at 3 to 6 m/sec from 1100 to 2400.

Second Time Interval

0001 to 2400 August 31, 1970.- High surface pressure and an associated moderate onshore pressure gradient existed over western Oregon throughout the day. A low-pressure trough at 850 millibars moved eastward over Oregon during the day, and winds over western Oregon were light from the northwest. At 700 and 500 millibars the trough weakened, and the light winds shifted from southwesterly to westerly during the day.

Salem reported an overcast layer of stratocumulus based near 600 meters until 1000, at which time the base of the layer lifted to approximately 900 meters and dissipated. Skies were clear from 1300 to 1700, and scattered high clouds were reported from 1800 to 2100. A stratocumulus layer based near 750 meters was observed at 2200, and this layer had increased sky cover to broken conditions by 2400. Visibility was 13 km or greater throughout the day. Surface winds were southerly at 2 to 6 m/sec from 0001 to 0900, calm from 1000 to 1300, northerly at 2 to 6 m/sec from 1400 to 1800, and westerly to southwesterly at 3 to 6 m/sec from 1900 to 2400.

0001 to 2400 September 1, 1970.- High surface pressure and an associated strong onshore pressure gradient covered western Oregon throughout the day. At 850 millibars high pressure was off the Oregon coast, and a weak pressure gradient with resulting light westerly winds was observed over western Oregon. At 700 and 500 millibars a shallow trough centered over western Oregon resulted in light southwesterly to westerly winds over Oregon.

Throughout the day Salem reported an overcast layer of stratus clouds based between 600 and 900 meters. Drizzle was reported from approximately 0700 to 1000. Visibility was 11 km or greater during the day except for reported values of 5 and 8 km at 0900 and 1000, respectively. Surface winds were southerly at 3 m/sec or less until 1200 and northeasterly to northwesterly at 2 to 4 m/sec from 1300 to 2400.

0001 to 2400 September 2, 1970.- High surface pressure weakened during the day as a low-pressure system and an associated occluded front moved toward the Oregon coast, with the front reaching the coast at approximately 2400. At 850 millibars a moderate westerly air flow offshore diverged, resulting in light westerly winds over western Oregon. At 700 millibars the pressure gradient over western Oregon caused light westerly winds, and at 500 millibars a shallow trough with associated light northwesterly winds moved slowly in over Oregon.

Salem reported a scattered to broken cloud layer based between 900 and 1200 meters from 0001 to 1300. A smoke layer based at 1200 meters was observed from approximaterly 1400 to 1600. Cloud cover increased from 1700 to 2400, with a scattered cloud layer based at 4000 meters lowering during the evening and forming an overcast layer based near 1500 meters at 2400. Visibility was 11 km or greater throughout the day except at 1500, when smoke reduced the visibility to 8 km. Surface winds were variable at 4 m/sec or less throughout the day.

0001 to 0415 September 3, 1970.- At the surface the low-pressure system moved across western Oregon. Winds aloft were light westerly at 850 millibars increasing in speed up to 500 millibars.

Salem reported an overcast cloud layer based between 1100 and 1500 meters during the period. Visibility was 24 km or greater, and surface winds were southerly at 3 to 6 m/sec.

APPENDIX C

ANALYSIS OF DATA

All data in this paper are referenced to sea level. The absolute temperature at any given level, measured by rawinsonde or aircraft, differed by as much as 2° C because of aerodynamic heating of the aircraft-mounted sensor. However, the shapes of the temperature profiles are approximately the same and, therefore, so are the measured atmospheric stabilities. This finding is in general agreement with findings made by other investigators. (See ref. 8.)

Period 1 (2215 August 26 to 0415 August 27)

Data for period 1 (2215 August 26 to 0415 August 27) are shown in figure 14. The 2215 aircraft temperature sounding indicated a nocturnal inversion with the top at 210 meters. A second inversion was based at 1460 meters with the top at 1840 meters. The airborne particle counter measured high aerosol concentration near the surface and a rapid decrease from 150 to 200 meters indicating a trapping of aerosols in the lower inversion. It then showed an approximately constant particle concentration to about 1360 meters through the layer of thermal neutrality, where good mixing is expected. A rapid decrease in concentration is indicated between 1300 and 1510 meters. The concentration above 1510 meters was less than 500 cm^{-3} and nearly constant. Therefore, the actual mixing height, as defined in the section entitled "Data Presentation," would be approximately 1500 meters. Thus, a good correlation exists between the stability regime and the aerosol concentration regime, with the actual mixing height being within 100 meters of the base of the inversion aloft.

The 0415 rawinsonde also showed a nocturnal inversion near the surface that becomes nearly isothermal from 300 to 1920 meters. This would imply limited mixing to this altitude. The aircraft temperature data taken from 2215 to 2242 indicate very limited mixing to 200 meters and good mixing from 200 to 1460 meters. The laser-radar data were taken from 0210 to 0244, and the temperature profile during this time should be similar to and between the above two soundings. The laser-radar profile data agree very well with the particle-counter data, being nearly constant from 450 to 1250 meters and then decreasing to 1650 meters. The actual mixing height based on the laser-radar data was approximately 1450 meters, the average height between 1250 and 1650 meters.

Winds aloft at 0415 indicate a wind shear near 1100 meters. The 0415 water-vapor mixing-ratio values indicate a strong negative gradient between 1160 and 1510 meters, which closely correlates with the wind shear height and with the decrease in laser-radar and condensation nuclei data.

Period 2 (0800 to 1005 August 27)

Data for period 2 (0800 to 1005 August 27) are shown in figure 15. The aircraft temperature sounding at 0904 indicated a temperature inversion between 620 and 1060 meters, with a nearly isothermal layer extending from 1060 to 1770 meters. The simultaneous particle count decreased rapidly above 150 meters and again above 900 meters. The count indicated a secondary maximum particle count at 900 meters, or 160 meters below the top of the temperature inversion, associated with a layer of easterly air flow aloft. The actual mixing height was estimated to be 1280 meters. Particle counts remained nearly constant from 1370 to 2350 meters. The actual mixing height determined by laser radar was 1420 meters, which was not well defined. The laser-radar data also showed considerable variation between 630 and 1550 meters. The concentration in the mixing layer, which exceeded that of period 1, possibly resulted from the breaking up of the nocturnal inversion near the ground and the arrival of smoke from field burnings.

Wind shear occurred within the mixing layer with a strong shear at approximately 1100 meters, near the top of the temperature inversion. The 1005 mixing-ratio values indicated a strong negative water-vapor gradient, the bottom of which was at 1000 meters with a second decrease at approximately 1280 meters. Again, this "drying out" agrees well with the lidar and condensation nuclei measurements.

Period 3 (0855 to 1400 August 27)

Data for period 3 (0855 to 1400 August 27) are shown in figure 16. The 1050 aircraft temperature profile indicated two inversions: one between 700 and 1100 meters and a second based near 1300 meters. The lapse rate above approximately 1500 meters was nearly adiabatic (period 2). The particle counts decreased near the base of the first inversion and increased to a secondary maximum near the top of the first inversion. The counts decreased rapidly above 1430 meters, the actual mixing height. The laser-radar data from period 2 are replotted in this period for comparison. As shown in period 2, the mixing height determined by laser radar an hour earlier is 1420 meters, which agrees well with the mixing height determined by particle counts.

The 1200 and 1400 wind profiles are shown, and combined with the 0815 and 1005 wind profiles of period 2, show that wind shears occurred in the mixing layer throughout the morning and early afternoon. As discussed for period 2, the 1005 mixing-ratio profile indicates a strong negative water-vapor gradient above 1000 meters.

Period 4 (1517 to 1800 August 27)

Data for period 4 (1517 to 1800 August 27) are shown in figure 17. The 1517 aircraft temperature sounding indicated nearly adiabatic conditions below 930 meters with

a strong inversion above 930 meters. The particle count at 1517 remained nearly constant up to 1020 meters, about 100 meters above the base of the temperature inversion, and then decreased rapidly. The actual mixing height was estimated to be 1100 meters. The actual mixing height determined by laser radar at approximately 1640 was 1050 meters, which is the average height between the decrease in scattering at 850 meters and the near-molecular scattering at 1250 meters. The laser-radar data indicated the highest concentration of aerosols in the mixing layer during this period of the day, which correlated with the lowest visibility (3.2 km) measured during the day. (See appendix B for the synoptic conditions during this time period.) This reduction in visibility was attributed to smoke from field burnings in the valley. Also, mixing from the surface to the bottom of the inversion was very good causing the aerosols to be well mixed below the inversion.

In figure 17 a gradual wind shear can be seen in the 1600 sounding. A slight wind speed shear near 1200 meters is shown in the 1800 sounding. The 1615 mixing-ratio values indicated a significant negative water-vapor gradient, or drying out, between 850 and 1500 meters.

Figure 18 shows an isopleth of lidar scattering ratio for periods 1 to 4. As discussed in the text, the numbers in the figure indicate the ratio of the observed scattering to molecular scattering. In this manner, a plot of normalized scattering or aerosol-scattering ratio as a function of time and altitude depicts the temporal mixing of aerosols in the atmosphere. As can be seen in this figure, a steady increase in aerosol concentration occurred during the day.

Period 5 (2000 August 27 to 0003 August 28)

Data for period 5 (2000 August 27 to 0003 August 28) are shown in figure 19. A nocturnal inversion extending to 200 meters and three stable layers at 200 to 600, 600 to 900, and 1250 to 1350 meters were observed during the 2250 aircraft flight. The particle count decreased rapidly from the surface up to 300 meters and then decreased slowly up to 1250 meters. The actual mixing height was estimated to be 1200 meters, where the particle counts were 500 cm^{-3}.

Winds aloft indicated wind shears from the surface to 1700 meters with no clear indication of a discontinuity between the surface winds and the upper winds. The 2215 mixing-ratio values varied slightly up to 1100 meters, decreased rapidly from 1100 to 1650 meters, and decreased slowly above 1650 meters.

The Raman laser-radar water-vapor mixing-ratio measurements shown in figures 20 and 21 were related to rawinsonde measurements by performing a weighted least-squares fit, with the inverse of the variance as the weighting factor. In general, the two measurements agree. The earlier measurement (2102 to 2142) indicates the actual mix-

ing height to be near 1350 meters. A comparison of the two measurements indicates a change in the profile, with the actual mixing height increasing to 1550 meters in a period of approximately 1 hour.

Period 6 (0400 to 0717 August 28)

Data for period 6 (0400 to 0717 August 28) are shown in figure 22. The 0415 rawinsonde temperature profile indicated a surface inversion up to 1230 meters. The actual mixing height determined by laser radar at approximately 0700 was 850 meters with very little fluctuation in the scattering.

Winds aloft gave an indication of a gradual wind shear over the first 1200 meters. The 0415 mixing-ratio values were nearly constant up to 3100 meters with no indication of any equilibrium with the aerosol.

Period 7 (0810 to 1028 August 28)

Data for period 7 (0810 to 1028 August 28) are shown in figure 23. The 0938 aircraft temperature sounding indicated a strong inversion between 400 and 600 meters. Two shallower inversions based at 1310 and 1740 meters were observed. Particle counts increased from the surface up to 400 meters, decreased rapidly up to 500 meters, increased to a secondary maximum at 550 meters, and decreased rapidly above 550 meters, with the actual height being approximately 600 meters. Several maximums occurred near the shallow temperature inversions; these indicate secondary haze layers. The actual mixing height determined by laser radar during this period was 600 meters; a secondary aerosol layer was indicated at 1350 meters. The profiles for periods 6 and 7 were very similar, with more fluctuation and a lower mixing height in period 7.

A significant wind shear occurred at 1250 meters, with an easterly flow of air associated with the lower inversion. The 1015 mixing-ratio values were nearly constant up to 1650 meters and then decreased slowly above 1650 meters. As in period 6, there seems to be no drying out near the top of the mixing layer.

Period 8 (1200 to 1800 August 28)

Data for period 8 (1200 to 1800 August 28) are shown in figure 24. The 1634 aircraft temperature sounding indicated a strong temperature inversion between 1500 and 1580 meters. The particle count was nearly constant up to 1450 meters and then decreased rapidly. The actual mixing height determined from the particle counts was 1650 meters. The nearly constant particle counts up to 1450 meters were associated with strong vertical mixing, as indicated by the nearly-dry-adiabatic lapse rate from 300 to 1500 meters. The sudden decrease in particles indicated trapping of particles by the shallow but intense inversion. The actual mixing height determined by laser radar during this period was 1630 meters.

The actual mixing height determined by laser radar and particle count was observed to remain near a temperature inversion throughout the afternoon. The height changed with the inversion and was approximately 750 meters between 1300 and 1400 and 1400 meters between 1538 and 1552. The temporal change of the actual mixing height was thus documented; an isopleth including this period is shown subsequently. It is also interesting to note that the lidar scattering ratio was very low during this period correlating with high measured visibility. (See appendix B for the synoptic weather conditions.)

Wind shears occurred within the mixing layer with shearlines marking the transition to geostrophic flow gradually moving higher during the afternoon and in general associated with the inversion aloft. At 1800 pronounced shearing occurred near 1500 meters. The 1615 mixing-ratio values decreased very slowly up to 2200 meters; a steep negative gradient, which seems to have no relationship to the measured mixing height, was observed between 2200 and 2450 meters.

Period 9 (2140 to 2251 August 28)

Data for period 9 (2140 to 2251 August 28) are shown in figure 25. The 2209 rawinsonde temperature profile indicated an inversion between 1120 and 1540 meters. The actual mixing height determined by laser radar at approximately 2145 was 1500 meters.

The laser-radar data showed the aerosols to increase to a peak at 1300 meters in a well-defined layering and then decrease to nearly molecular scattering at 1650 meters. The air over Salem was relatively clean during the day until approximately 1700, when smoke and haze started to move in over the area. The haze layer seemed to be trapped in the inversion and was fairly stable in space and time. This is shown in figures 26 and 27, where isopleths for August 28 are presented. Figure 26 was constructed with data from the zenith system, and figure 27 was constructed with data from the scanning system. The layer, approximately 500 meters thick, developed and dissipated over a period of about 4 hours, that is, it moved overhead during this period. However, since the only continuous data were taken from 2145 to 2251, the time cross section in figure 26 might be misleading, since linear interpolations were made in its construction from 1712 to 2148. The rawinsonde-derived wind speed was approximately 5 m/sec from the north at this altitude, and assuming it constant during the 4 hours would give this haze layer a horizontal (north-south) dimension of about 72 000 meters.

In order to investigate the spatial cross section of this haze layer, the scanning laser radar made a series of elevation angle measurements pointing to the west of the field site. The results of these scans are shown in figure 28. These data show that the center or region of maximum scattering intensity was not overhead but approximately 1400 meters to the west. The east-west extent of the layer was approximately 3000 meters; this observation suggests that this layer was indeed smoke from a field

burn drifting south through the valley. A secondary maximum is indicated about 400 meters over Salem. The utility of a scanning laser radar is shown by these measurements.

A wind shear was observed within the inversion at approximately 1500 meters. The 2209 mixing-ratio values indicated a strong negative gradient between 1130 and 1540 meters. The Raman water-vapor data shown in figures 29 and 30 indicate that the atmosphere below 1800 meters was stable over the period 2210 to 2240, whereas at 2000 meters there appeared to be a statistically significant increase of water vapor during this time. This increase may be indicative of a moist air mass moving into the region at this altitude.

Period 10 (1030 to 1452 August 31)

Data for period 10 (1030 to 1452 August 31) are shown in figure 31. The laser-radar profile taken at approximately 1140 indicated a cloud layer based near 900 meters, which was in agreement with surface observations taken at the National Weather Service station at the Salem airport. At 1300 the clouds had dissipated, as indicated in the laser-radar profile taken at approximately 1300. The actual mixing height determined by laser radar at approximately 1300 was 1000 meters.

Period 11 (1509 to 1645 August 31)

Data for period 11 (1509 to 1645 August 31) are shown in figure 32. No temperature inversion was observed in the 1615 rawinsonde temperature profile. Superadiabatic conditions existed from the surface up to 820 meters, and an average lapse rate occurred from 820 meters to 3110 meters. The particle count at 1535 was high from the surface up to 1150 meters and then decreased rapidly up to 1250 meters. The count averaged near 600 cm^{-3} between 1450 and 3040 meters. The high particle counts up to 3040 meters agreed with the fact that the temperature lapse rates up to that height indicated moderate vertical mixing of the air. The actual mixing height probably occurred above 3040 meters. The laser-radar profile average during 1600 to 1613 indicated moderately well mixed air up to at least 2000 meters with very little fluctuation in the data and a low scattering ratio. This agreed with the high visibility during this period.

In a general sense, there is agreement between the lidar and particle-counter data. Point-to-point differences can be explained since the lidar data is an average of many instantaneous zenith profiles, whereas the condensation nuclei data is a composite of single-point measurements at different times and locations in space. Also, as mentioned previously, the instrument size sensitivities are different. The lidar data definitely indicate a well-mixed boundary layer with low aerosol concentration and, therefore, good visibility.

No definite wind shear existed below 3000 meters. The mixing-ratio values decreased slowly with height and showed no strong gradients.

Period 12 (2043 to 2400 August 31)

Data for period 12 (2043 to 2400 August 31) are shown in figure 33. The 2043 aircraft temperature sounding indicated inversion conditions below 320 meters, between 620 and 1060 meters, and a shallow inversion based at 2000 meters. The 2210 rawinsonde showed an inversion based at 2850 meters, which was above the maximum flight altitude. The particle count indicated a rapid decrease of particles with height through the onsetting nocturnal inversion up to 450 meters and another rapid decrease between 1060 and 1220 meters. The actual mixing height was estimated to be 1170 meters although the counts remained constant, about 400 cm^{-3} up to above 2000 meters. The laser-radar profile averaged over 2203 to 2237 indicated moderately well mixed air up to at least 3000 meters with little fluctuation in the data and relatively high concentrations. There appeared to be small enhancements from 850 to 1150 meters and 2150 to 2550 meters. Evidently, the aerosols which were mixed vigorously in the afternoon were continuing to be well mixed and reside at these altitudes. It also appeared that more aerosols were being distributed in the mixing layer under the 3000-meter inversion. The condensation nuclei counter did not appear to show this buildup. It is unfortunate that data were not obtained above 3000 meters.

The isopleth constructed with data from the zenith system, shown in figure 34, shows this uniform mixing throughout the day. The data from the scanning system confirmed that the aerosols were well mixed throughout the valley with only a few plumes indicated. These data are plotted in figures 35, 36, and 37 for three azimuths, west and $\pm 28^{o}$ from west.

The 2210 mixing-ratio values indicated a moderate negative gradient between 880 and 1800 meters. The laser-radar water-vapor data agreed well with the 2210 rawinsonde mixing-ratio profile and indicated little change over the period 2130 to 2312, as shown in figures 38 and 39. Slight wind speed shears were associated with the inversion between 620 and 1060 meters.

Period 13 (0955 to 1645 September 1)

Data for period 13 (0955 to 1645 September 1) are shown in figure 40. The 1615 rawinsonde sounding indicated a nearly adiabatic lapse rate up to 1850 meters and a strong inversion between 1850 and 2500 meters. The winds aloft indicated a wind shear near 1800 meters. The 1615 mixing-ratio values indicated a strong negative gradient from 1510 to 1850 meters and a peak near 2000 meters associated with the inversion aloft. Since cloud cover and rain continued during this period, no laser-radar data were obtained.

Period 14 (0914 to 1020 September 2)

Data for period 14 (0914 to 1020 September 2) are shown in figure 41. The 1006 aircraft temperature sounding indicated a nearly adiabatic lapse rate from the surface with a strong inversion between 1150 and 1370 meters and a nearly isothermal layer between 1370 and at least 2140 meters. Particle counts decreased to 100 cm^{-3} above 750 meters, with the actual mixing height estimated to be 680 meters. The actual mixing height determined by laser radar averaged between 0914 and 1010 was 1400 meters with little data fluctuation. The condensation nuclei and lidar data do not seem to agree in this case. It is interesting to point out that the lidar data indicate a capping of aerosols under the temperature inversion, whereas the smaller particles measured by the aircraft particle counter are concentrated below approximately 700 meters.

A wind shear occurred near 1000 meters and was associated with the inversion aloft. The 1012 mixing-ratio values indicated a significant negative gradient between the surface and 200 meters and between 1180 and 1380 meters. This gradient correlates with the temperature inversion and the mixing height measured with laser radar.

Period 15 (1147 to 1417 September 2)

Data for period 15 (1147 to 1417 September 2) are shown in figure 42. The 1214 aircraft temperature sounding indicated a nearly adiabatic lapse ratio from the surface capped by a strong inversion between 1150 and 1370 meters, with isothermal conditions from 1370 to at least 1660 meters. The particle count decreased rapidly between 1130 and 1250 meters; the actual mixing height determined by this technique was estimated to be 1230 meters. The actual mixing height determined by laser radar averaged at 1147, 1235, and 1400 was approximately 1200 meters, which is in good agreement with the condensation nuclei counter. The laser-radar data also show the buildup of a smoke layer at 1200 meters starting at approximately 1230. This correlates with the synoptic weather discussion in appendix B.

A wind shear occurred near 1600 meters, with an easterly wind associated with the inversion aloft. The 1012 mixing-ratio values indicated a negative gradient between the ground and 200 meters and between 1180 and 1380 meters.

Period 16 (1604 to 1814 September 2)

Data for period 16 (1604 to 1814 September 2) are shown in figure 43. The 1604 aircraft temperature sounding indicated a nearly-dry-adiabatic lapse rate below 1070 meters, shallow inversions between 1070 and 1460 meters, and an isothermal lapse rate from 1460 to at least 1980 meters. The particle count was nearly constant up to 1060 meters, with a moderate decrease in count between 1060 and 1440 meters and a rapid decrease in count between 1440 and 1550 meters. The actual mixing height was estimated, therefore,

to be 1420 meters. The actual mixing height determined by laser radar at approximately 1728 was estimated to be 1100 meters although not definitive because of lack of data.

A definite wind shear at 1605 occurred near 1000 meters. The 1615 mixing-ratio values decreased slowly with height, similar to the profile for period 15.

Period 17 (2007 to 2353 September 2)

Data for period 17 (2007 to 2353 September 2) are shown in figure 44. The 2007 aircraft temperature sounding indicated an average lapse rate up to 2120 meters with a slight ground-based inversion. Particle counts decreased rapidly between 300 and 450 meters and decreased gradually from 620 to 1670 meters. The actual mixing height measured was approximately 1370 meters. The laser-radar profile averaged from 2040 to 2049 indicated moderately well mixed air up to at least 1950 meters. The data showed low concentrations near the surface, building up to a nearly constant value above 750 meters. The height of the mixing layer measured with lidar is approximately 2000 meters, which is much higher than that indicated by the particle counter. A time cross section for periods 14, 15, 16, and 17 is shown in figure 45, and a cross section based on the scanning-system data from 2109 September 2 to 0257 September 3 is shown in figure 46. As mentioned in the discussion of period 15, a heavy buildup of aerosols began near noon with the field burning. Later the aerosols seem to become relatively well mixed throughout the mixing layer.

A significant wind direction shear occurred near 1500 meters. The 2208 mixing-ratio values indicated a significant positive gradient between 1460 and 1730 meters. The Raman water-vapor measurements for this period are shown in figures 47 and 48. The later lidar profile (fig. 48) indicated that possibly the moist layer near 1800 meters was dissipating.

Period 18 (0117 to 0415 September 3)

Data for period 18 (0117 to 0415 September 3) are shown in figure 49. The 0415 rawinsonde sounding indicated a temperature inversion between 220 and 330 meters and an average lapse rate above 330 meters. An isopleth for the period 0114 to 0147 is presented in figure 46 and indicates the possible existence of a layer near 600 meters.

A gradual wind direction shear was observed below 500 meters at 0415. The mixing-ratio values for this sounding increased rapidly between 200 and 580 meters and decreased slowly above 580 meters.

REFERENCES

1. Holzworth, George C.: Meteorological Potential for Urban Air Pollution in the Contiguous United States. Proceedings of the Second International Clean Air Congress, H. M. Englund and W. T. Beery, eds., Academic Press, Inc., 1971, pp. 1076-1080.

2. Olsson, Lars E.; and Tuft, Wesley L.: A Study of the Natural Ventilation of the Columbia-Willamette Valleys. Tech. Rep. No. 70-6, Dep. Atmos. Sci., Oregon State Univ., June 1970.

3. Olsson, Lars E.; and Peterson, Ernest W.: A Study of the Natural Ventilation in Western Oregon. Proceedings of the Second International Clean Air Congress, H. M. Englund and W. T. Beery, eds., Academic Press, Inc., 1971, pp. 979-982.

4. Olsson, Lars E.; Tuft, Wesley L.; Elliott, William P.; and Egami, Richard: The Study of the Natural Ventilation of the Columbia-Willamette Valleys: II. Tech. Rep. No. 71-2, Dep. Atmos. Sci., Oregon State Univ., Apr. 1971.

5. McCormick, M. P.: Simultaneous Multiple Wavelength Laser Radar Measurements of the Lower Atmosphere. Electro-Optics '71 International Conference, Ind. & Sci. Conf. Management, Inc., c.1971, pp. 495-512.

6. Anon.: Federal Meteorological Handbook No. 3 – Radiosonde Observations. U.S. Dep. Com., Jan. 1, 1969. (Supersedes Seventh ed. of WBAN Circ. P.)

7. Anon.: Manual of Winds-Aloft Observations (WBAN). Circ. O, Fifth ed., U.S. Govt. Printing Office, Sept. 1959.

8. McCaldin, R. O.; and Sholtes, R. S.: Mixing Height Determinations by Means of an Instrumented Aircraft. PB193419 (Contract No. PHS CPA 22-69-76), Eng. Ind. Exp. Sta., Univ. of Florida, June 1970.

TABLE 1.- SUMMARY OF OBSERVATIONS MADE OVER SALEM, OREGON, DURING THE PERIOD AUGUST 26 TO SEPTEMBER 3, 1970

Period	Day/Time	Time of observation by –			
		Rawinsonde [a]	Aircraft [b]	Laser radar [b]	Winds aloft [a]
1	26/2215 to 27/0415	0415	2215 to 2242	0210 to 0244	0415
2	27/0800 to 27/1005	1005	0904 to 0938	0855 to 0938	0815, 1005
3	27/0855 to 27/1400	1005	1050 to 1119	0855 to 0938	1200, 1400
4	27/1517 to 27/1800	1615	1517 to 1537	1612 to 1710	1600, 1800
5	27/2000 to 28/0003	2215	2250 to 2313	2100 to 0003	2215
6	28/0400 to 28/0717	0415	----------	0417 to 0717	0415
7	28/0810 to 28/1028	1015	0938 to 1027	0935 to 1028	0810, 1010
8	28/1200 to 28/1800	1615	1343 to 1720	1300 to 1713	1200, 1400 1600, 1800
9	28/2140 to 28/2251	2209	----------	2140 to 2251	2209
10	31/1030 to 31/1452	----	----------	1030 to 1452	---------
11	31/1509 to 31/1645	1615	1535 to 1645	1509 to 1613	1615
12	31/2043 to 31/2400	2210	2043 to 2058	2131 to 2400	2210
13	01/0955 to 01/1645	1615	----------	----------	1410, 1615
14	02/0914 to 02/1020	1012	1006 to 1020	0914 to 1010	1012
15	02/1147 to 02/1417	1012	1214 to 1235	1147 to 1417	1200, 1400
16	02/1604 to 02/1814	1615	1604 to 1625	1728 to 2049	1605, 1814
17	02/2007 to 02/2353	2208	2007 to 2025	2109 to 2352	2208
18	03/0117 to 03/0415	0415	----------	0117 to 0147	0415

[a] Time of balloon launch.

[b] Period during which measurements were made.

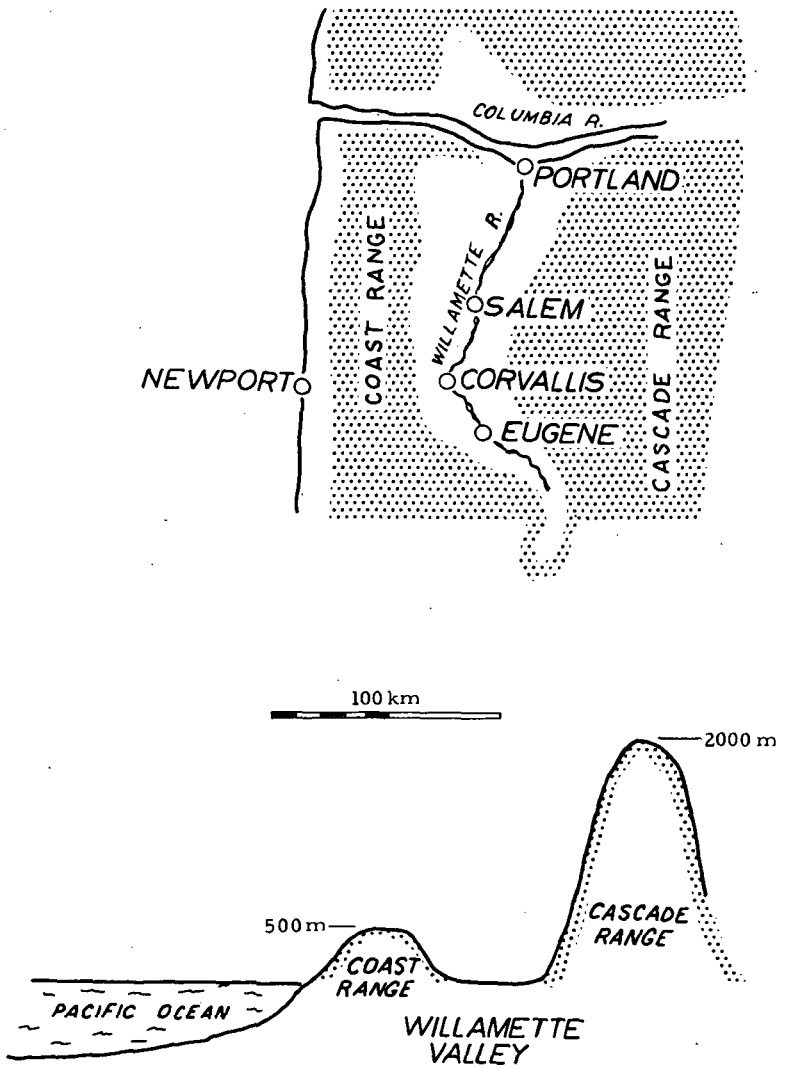

Figure 1.- Map and cross section of Willamette Valley.

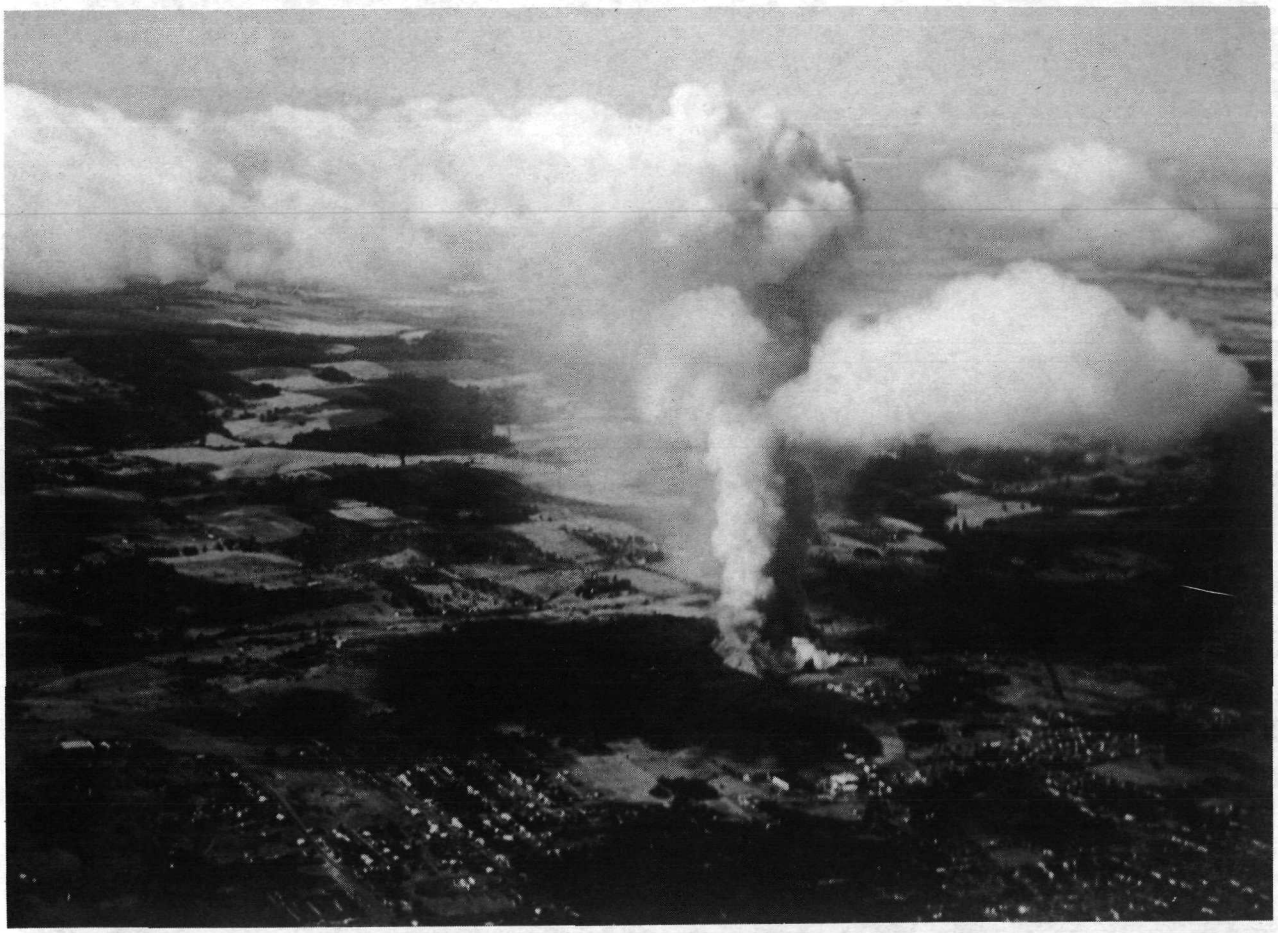

L-71-902

Figure 2.- Willamette Valley field burning.

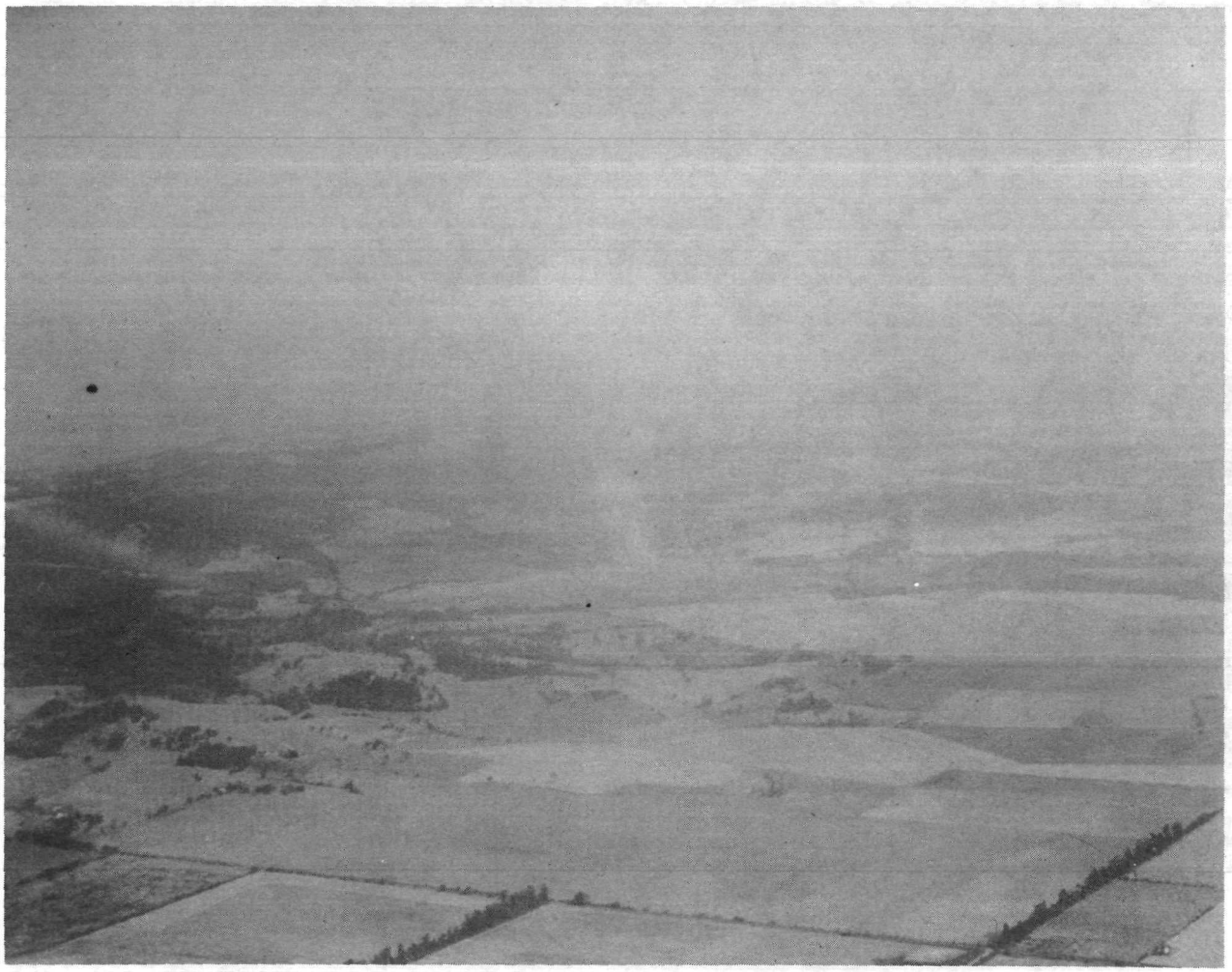

L-72-6582

Figure 3.- Willamette Valley field burning.

L-69-393

Figure 4.- Laser radar (van) system.

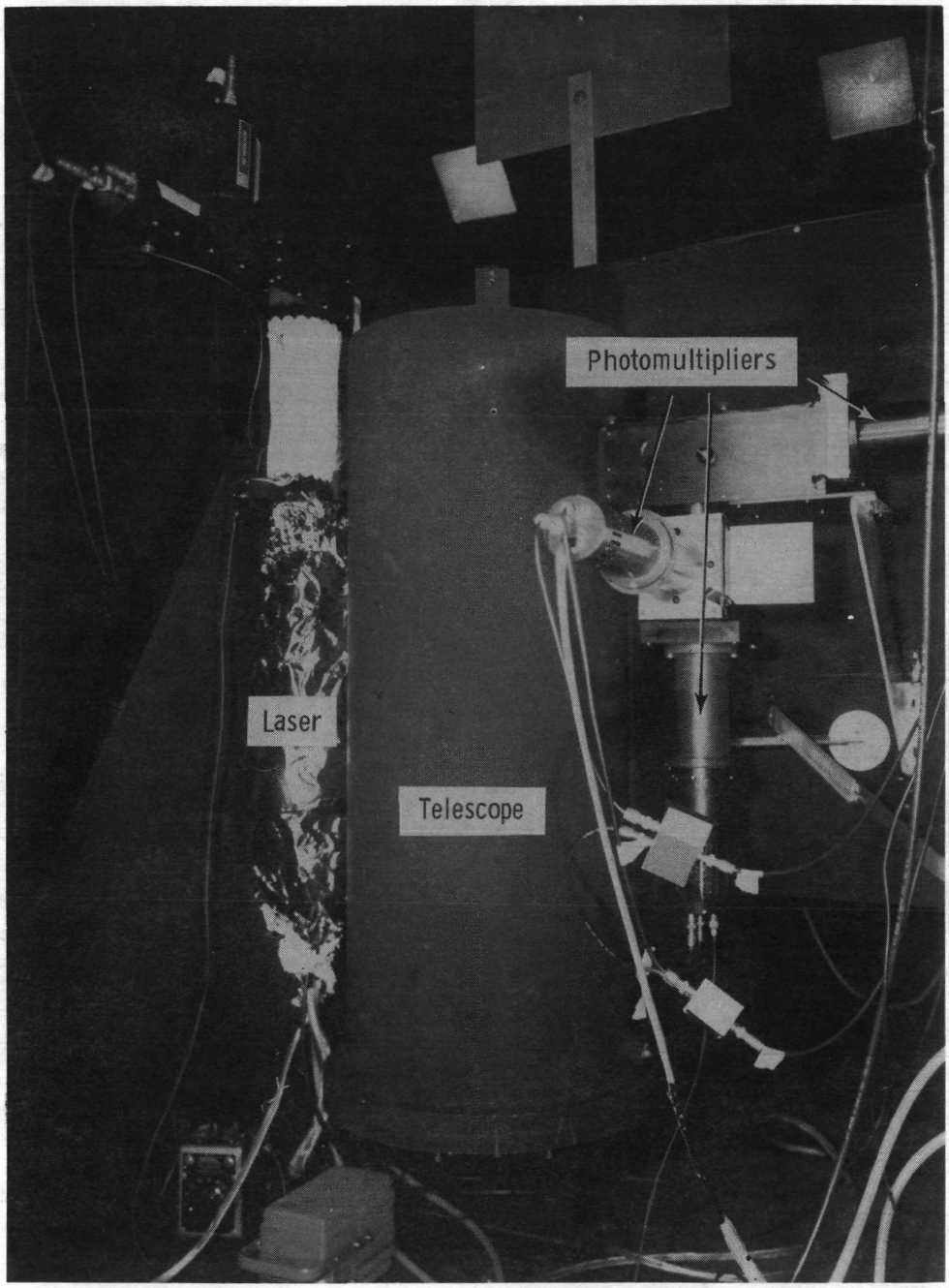

L-69-390.1

Figure 5.- Laser radar (van) interior.

L-69-385

Figure 6.- Laser-radar scanning system.

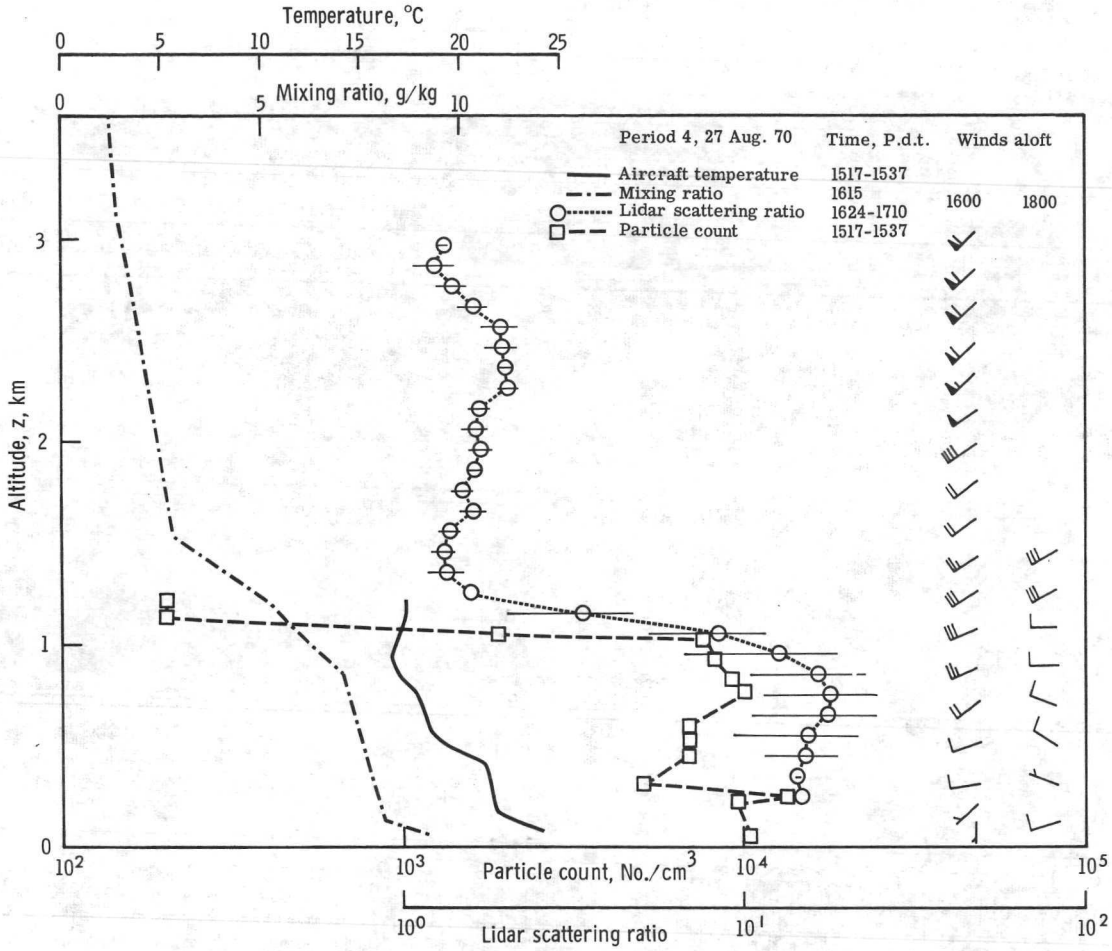

Figure 7.- Vertical profiles of temperature, water vapor, winds aloft, and aerosol concentrations measured over Salem, Oregon, during period 4, August 27, 1970.

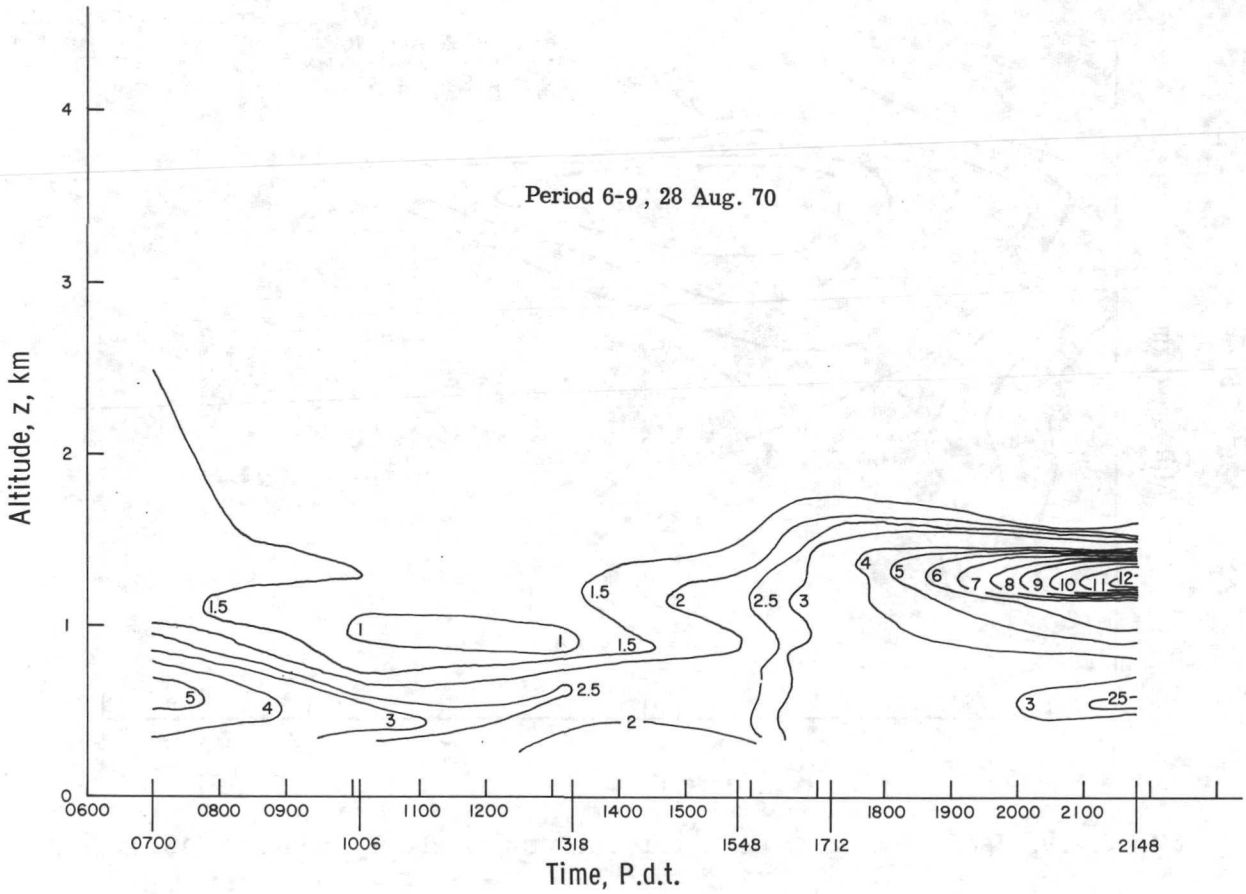

Figure 8.- Isopleth of lidar scattering ratio for periods 6 to 9, August 28, 1970.

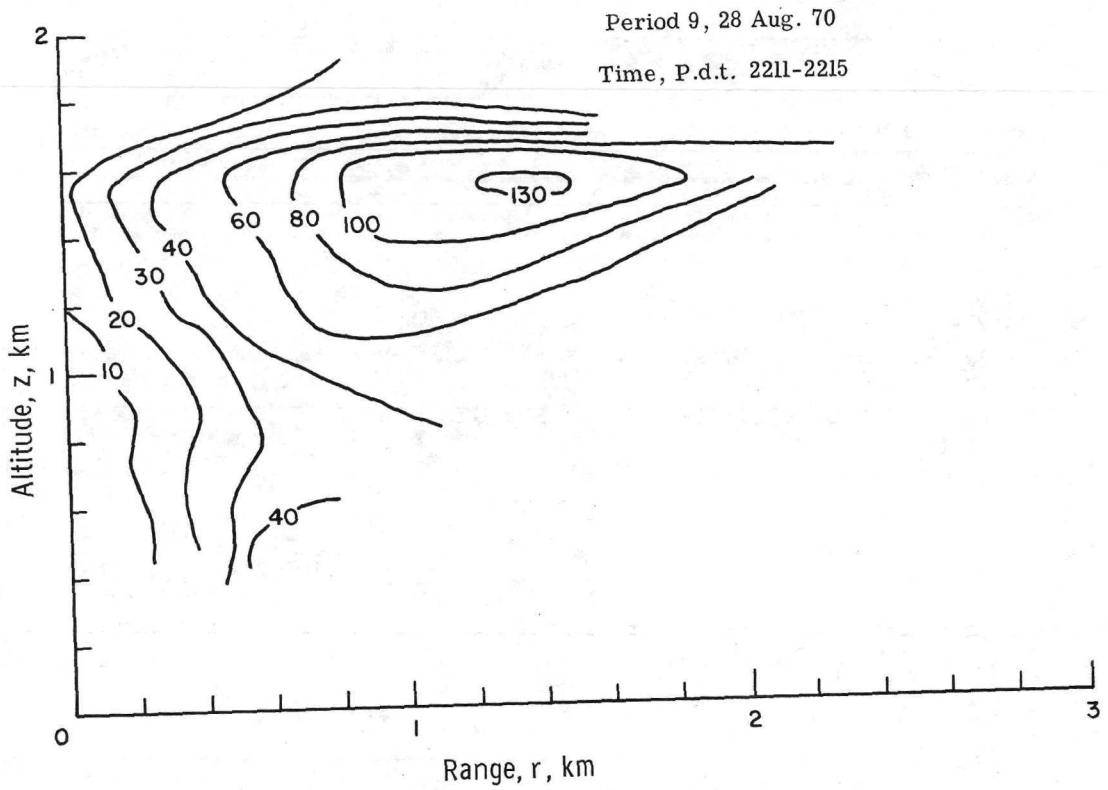

Figure 9.- Isopleth of lidar scattering ratio for period 9, August 28, 1970.

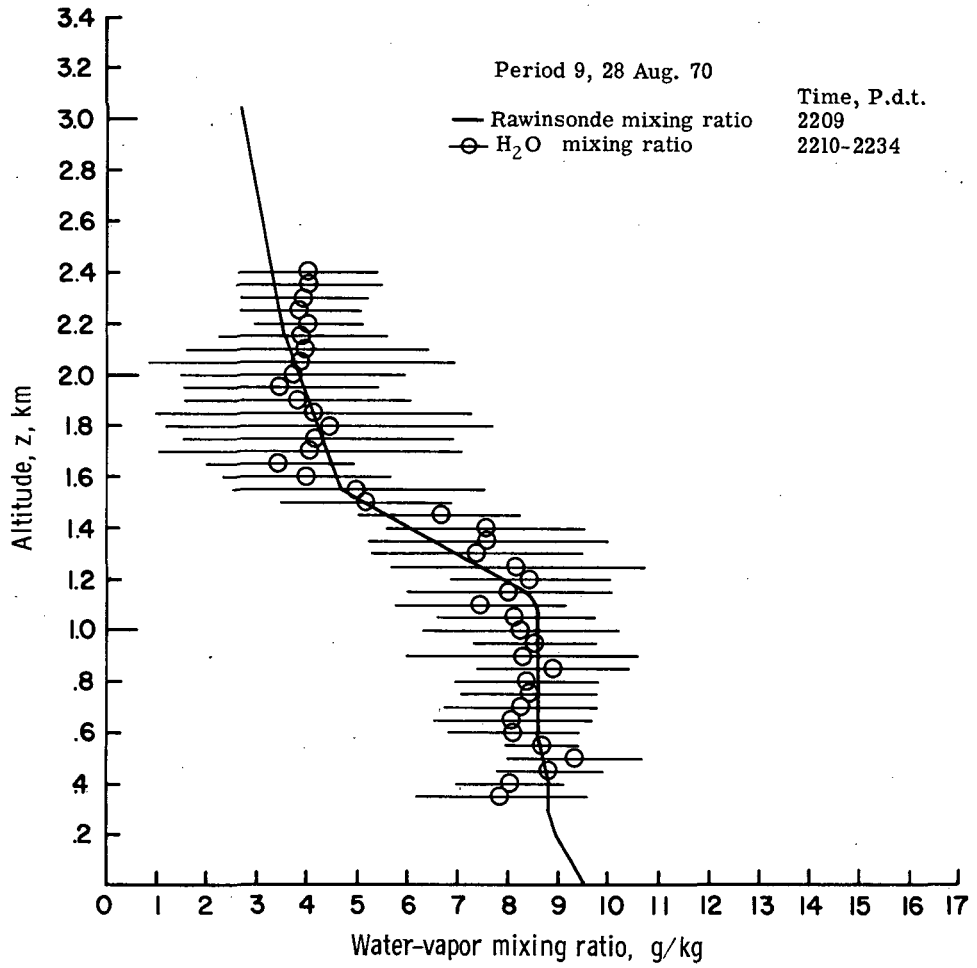

Figure 10.- Comparison of vertical profiles of lidar and rawinsonde water-vapor mixing ratios for period 9, August 28, 1970.

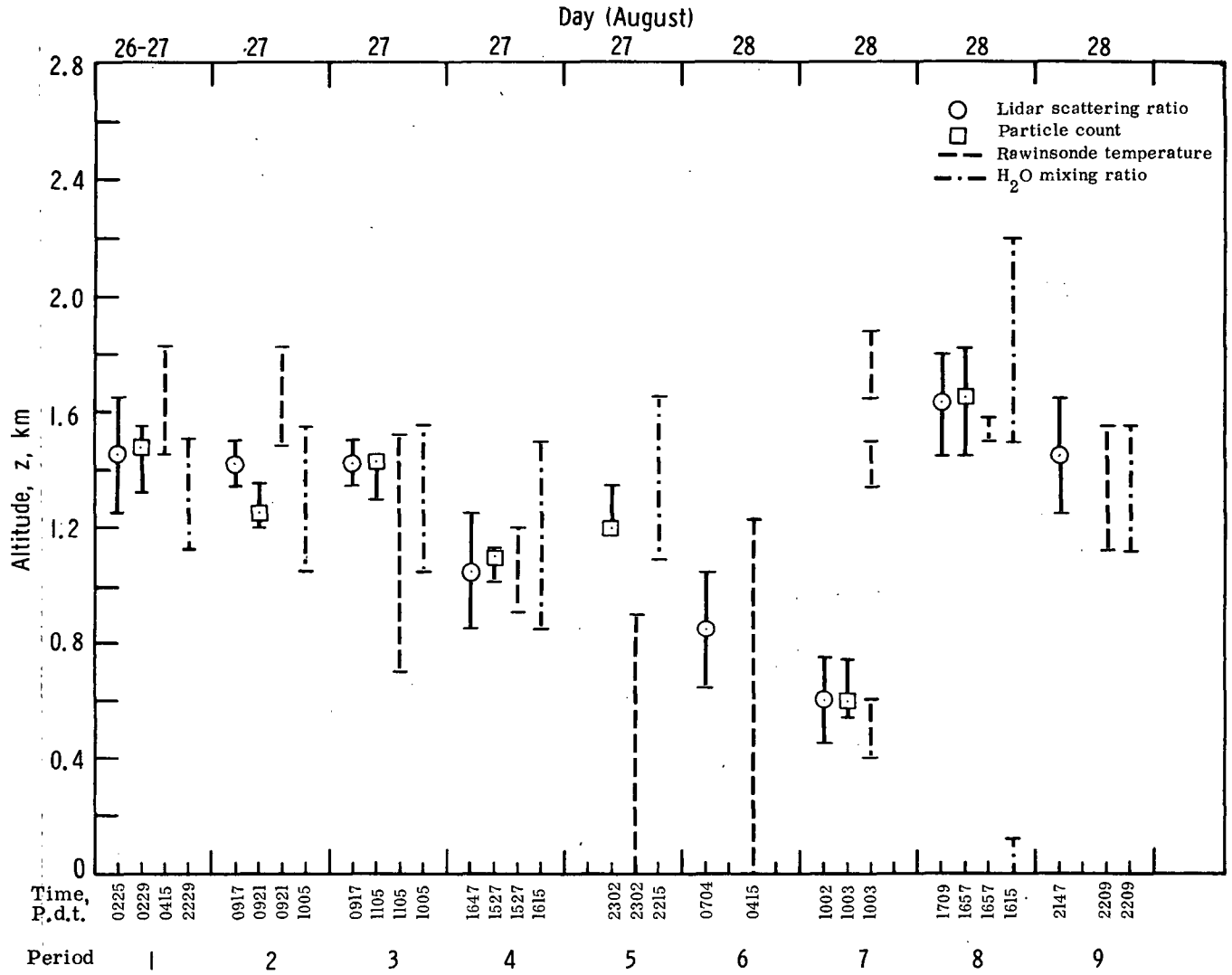

Figure 11.- Summary of data taken during periods 1 to 9. The top of the mixing layer as determined by lidar and particle counter, the altitude region of temperature inversion, and the region of decreasing water vapor are shown. Also shown are the altitude regions of significant decrease in lidar scattering ratio and particle count.

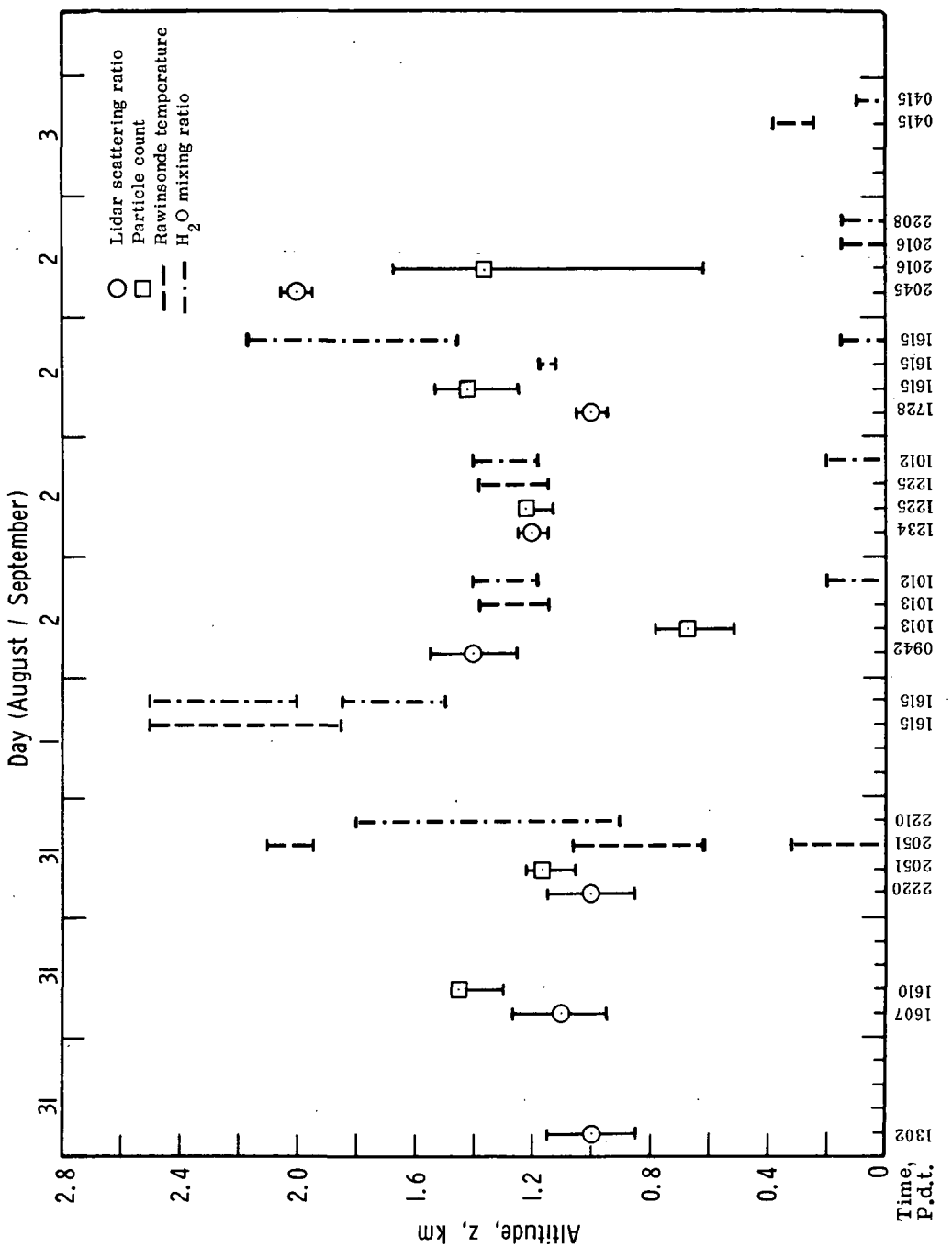

Figure 12.- Summary of data taken during periods 10 to 18. The top of the mixing layer as determined by lidar and particle counter, the altitude region of temperature inversion, and the region of decreasing water vapor are shown. Also shown are the altitude regions of significant decrease in lidar scattering ratio and particle count.

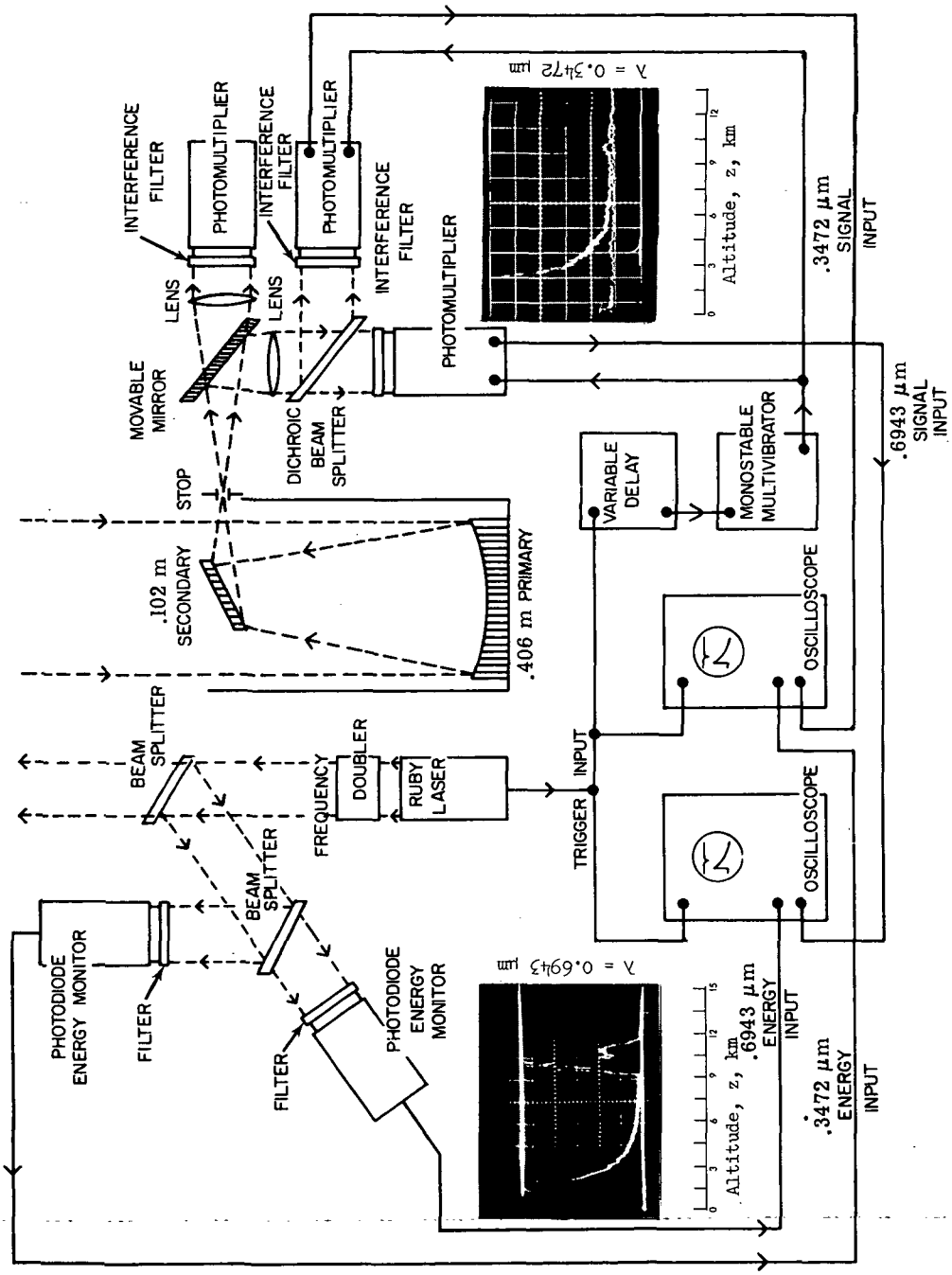

Figure 13.- Diagram of experimental arrangement.

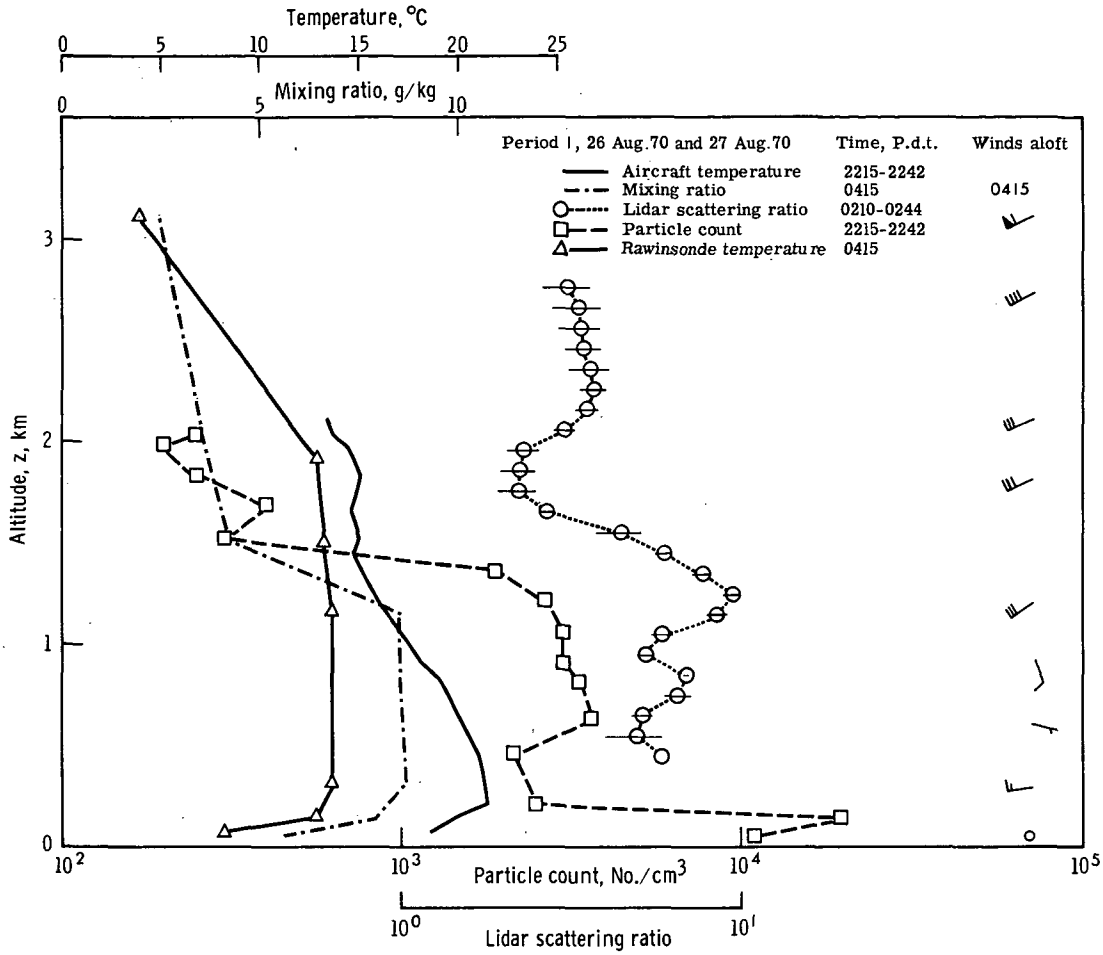

Figure 14.- Vertical profiles of temperature, water vapor, winds aloft, and aerosol concentrations measured over Salem, Oregon, during period 1, August 26 and 27, 1970.

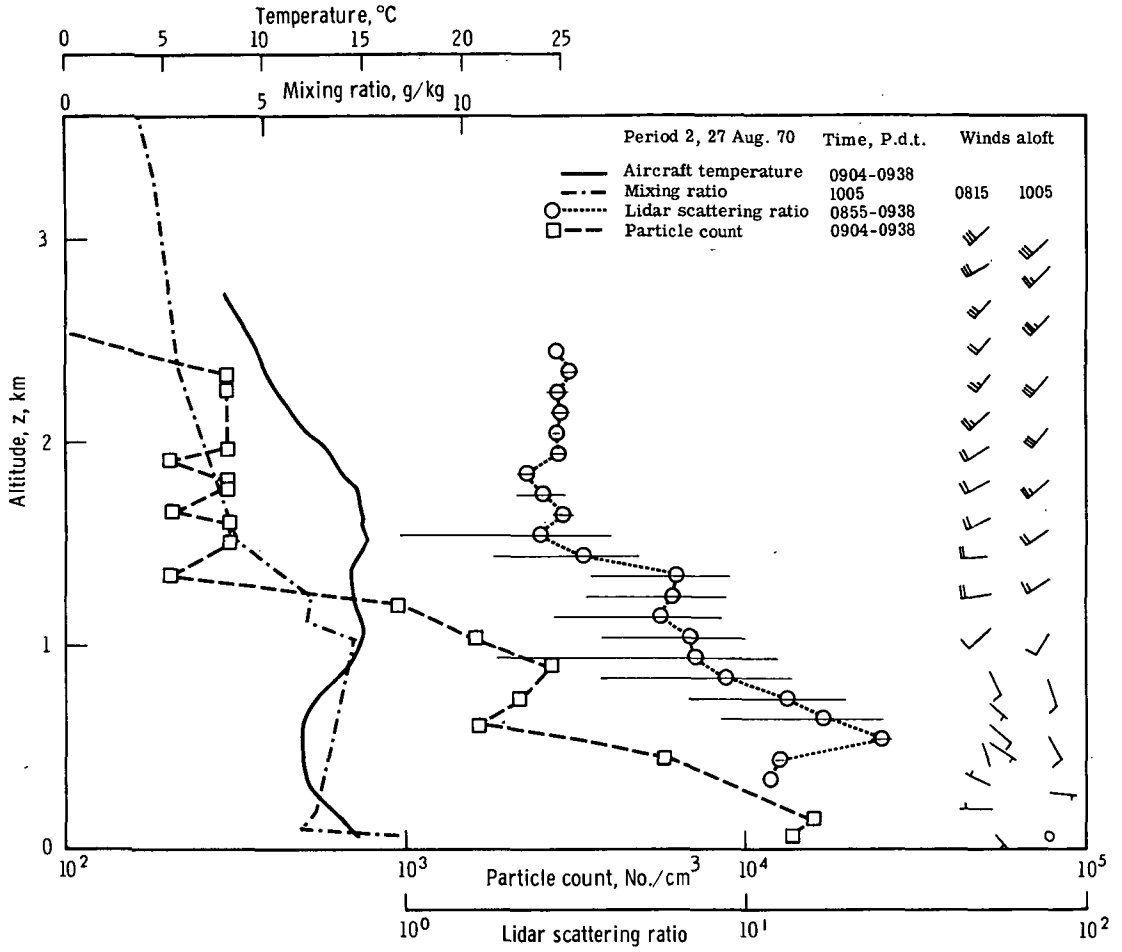

Figure 15.- Vertical profiles of temperature, water vapor, winds aloft, and aerosol concentrations measured over Salem, Oregon, during period 2, August 27, 1970.

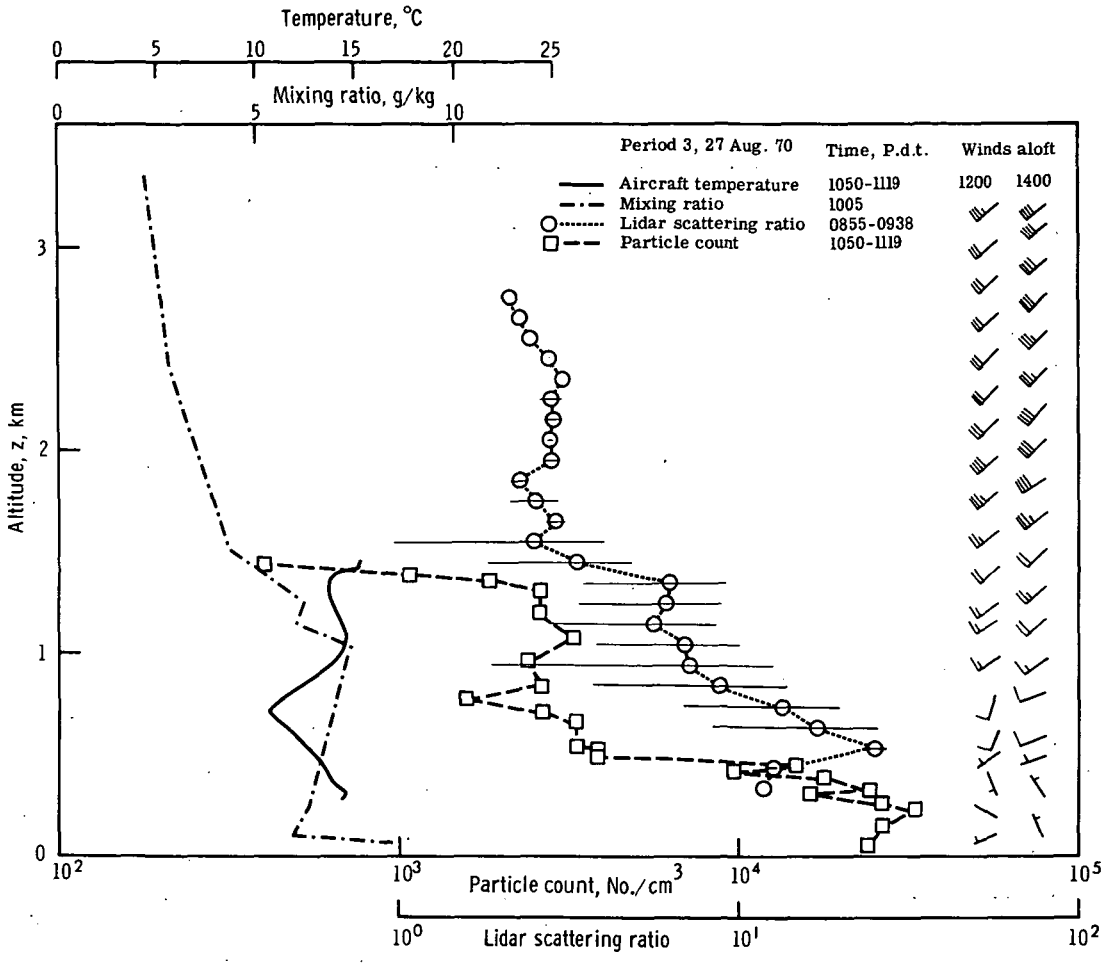

Figure 16.- Vertical profiles of temperature, water vapor, winds aloft, and aerosol concentrations measured over Salem, Oregon, during period 3, August 27, 1970.

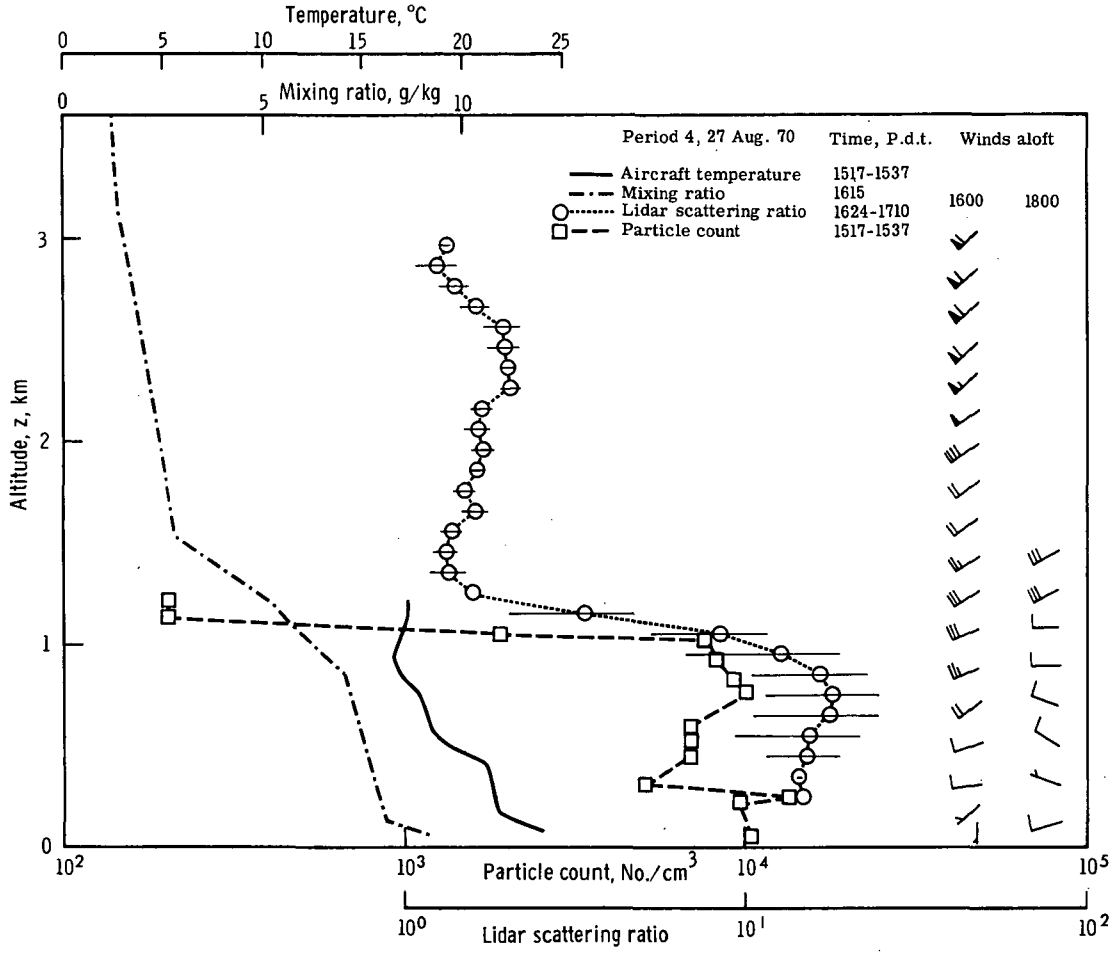

Figure 17.- Vertical profiles of temperature, water vapor, winds aloft, and aerosol concentrations measured over Salem, Oregon, during period 4, August 27, 1970.

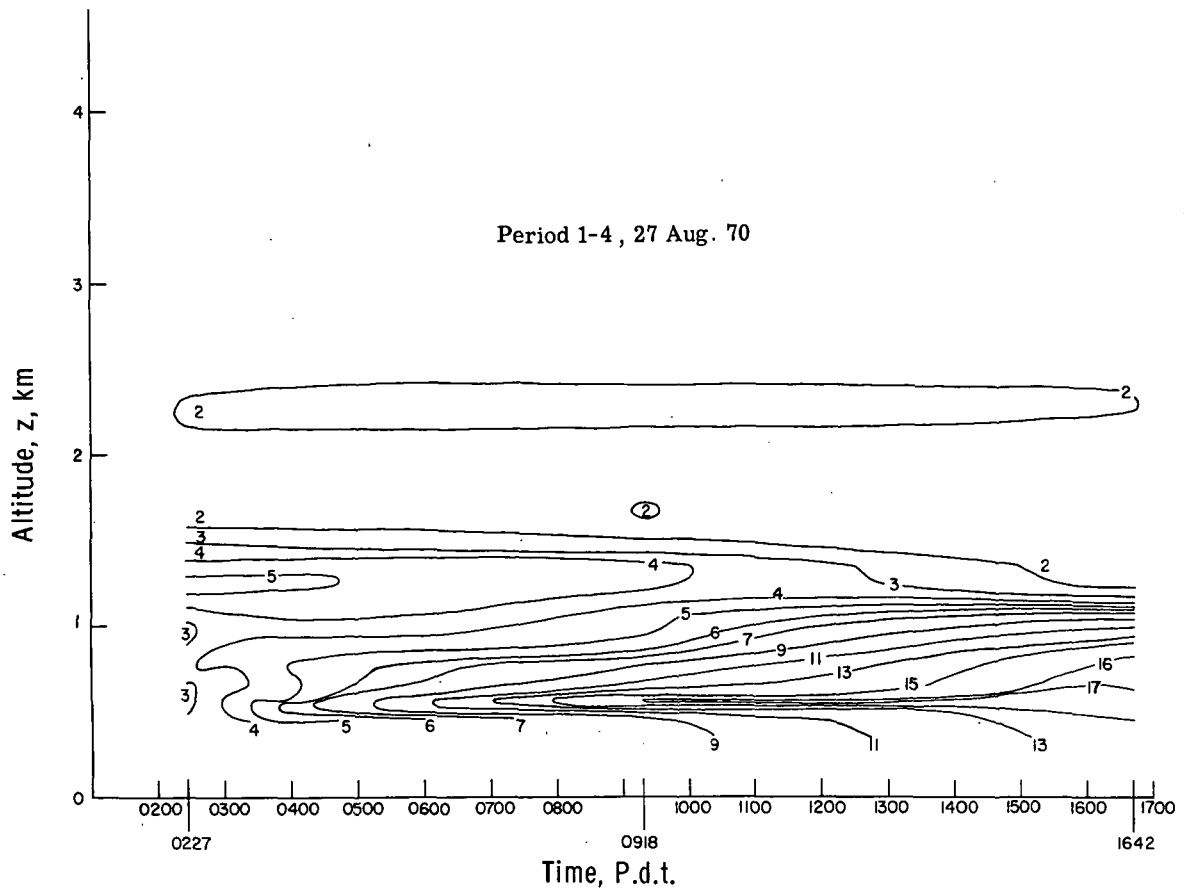

Figure 18.- Isopleth of lidar aerosol scattering ratio for periods 1 to 4, August 27, 1970.

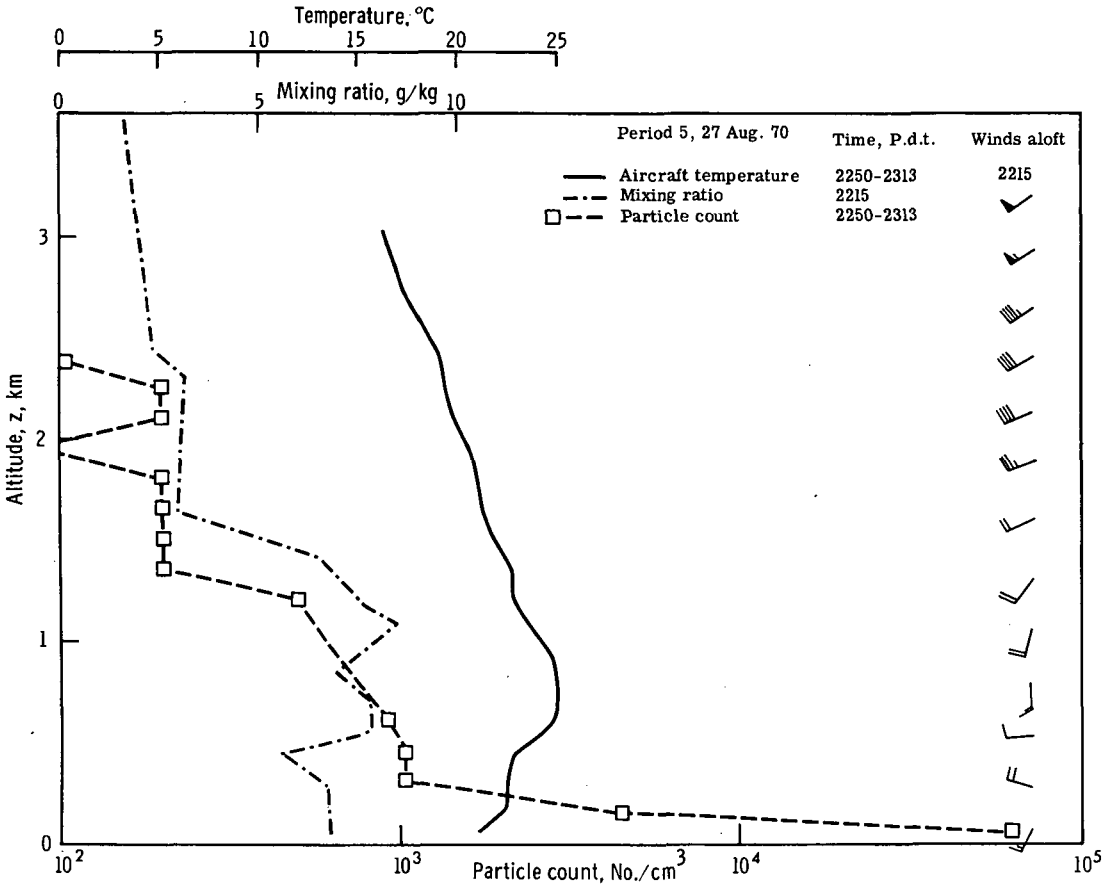

Figure 19.- Vertical profiles of temperature, water vapor, winds aloft, and aerosol concentrations measured over Salem, Oregon, for period 5, August 27, 1970.

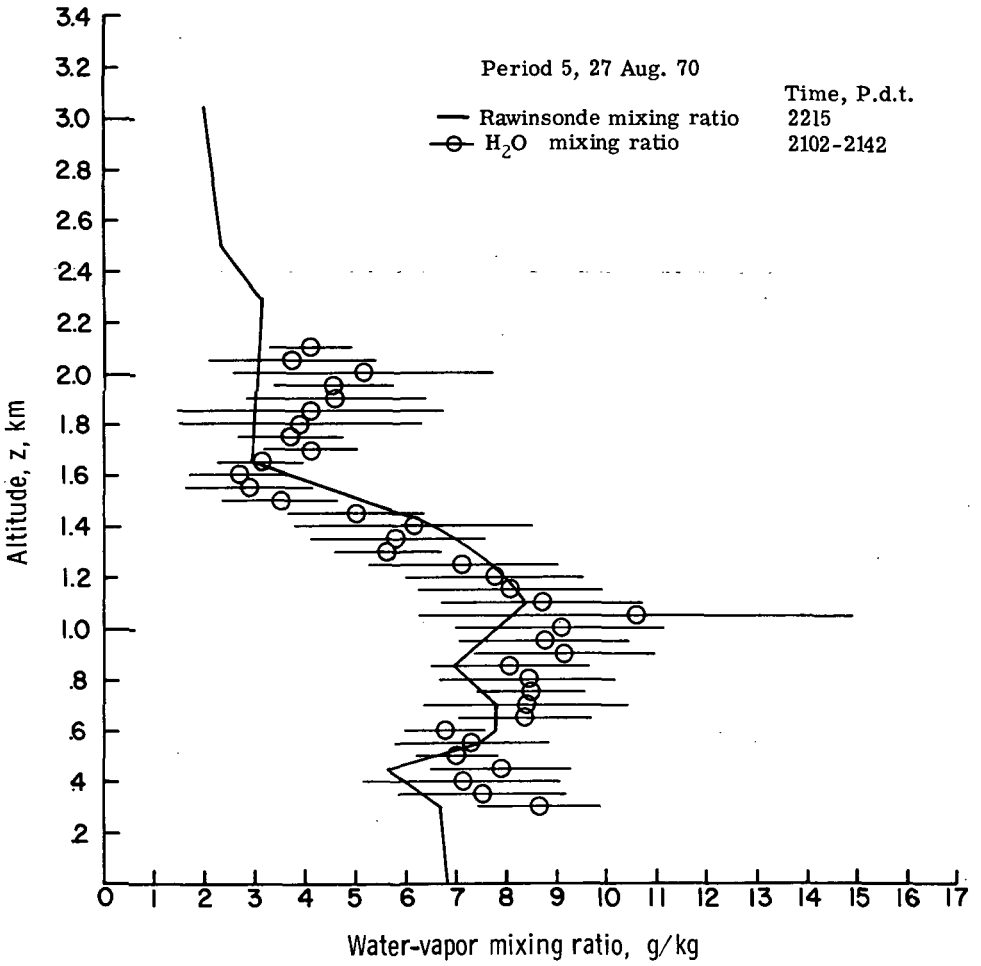

Figure 20.- Comparison of vertical profiles of lidar and rawinsonde water-vapor mixing ratios for period 5, August 27, 1970.

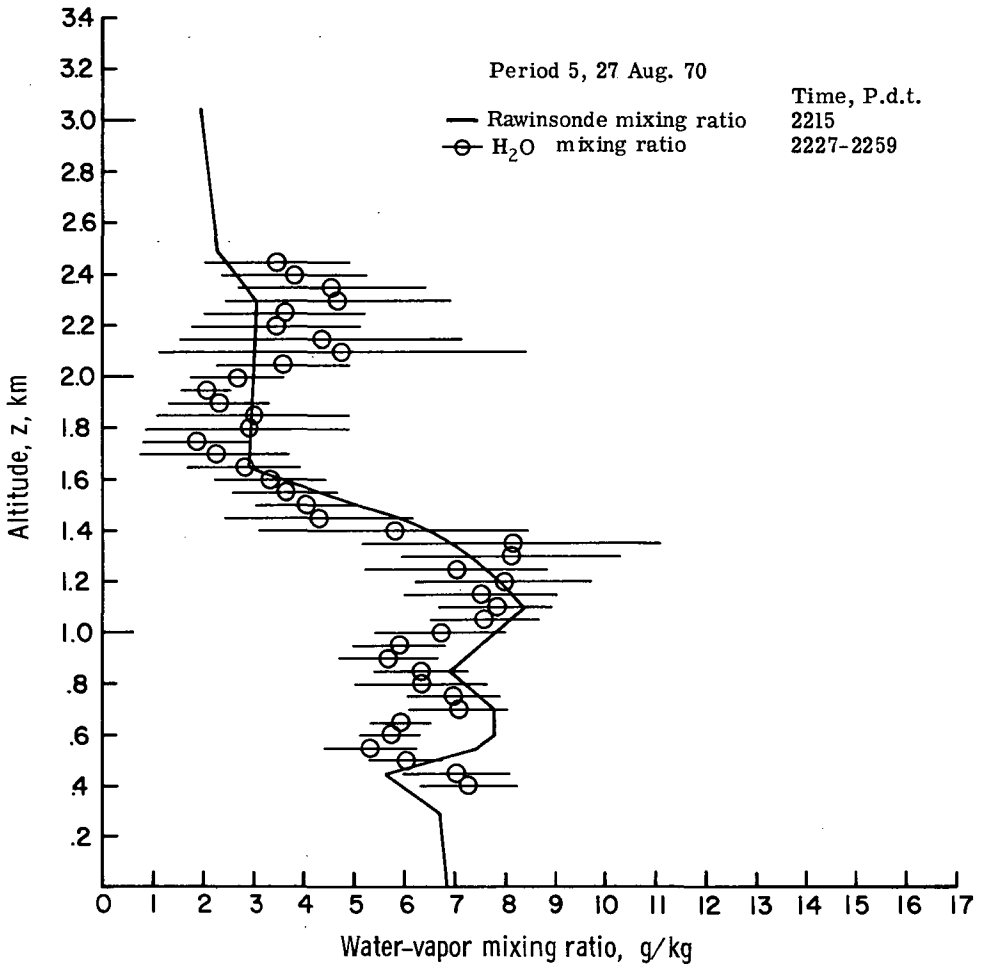

Figure 21.- Comparison of vertical profiles of lidar and rawinsonde water-vapor mixing ratios for period 5, August 27, 1970.

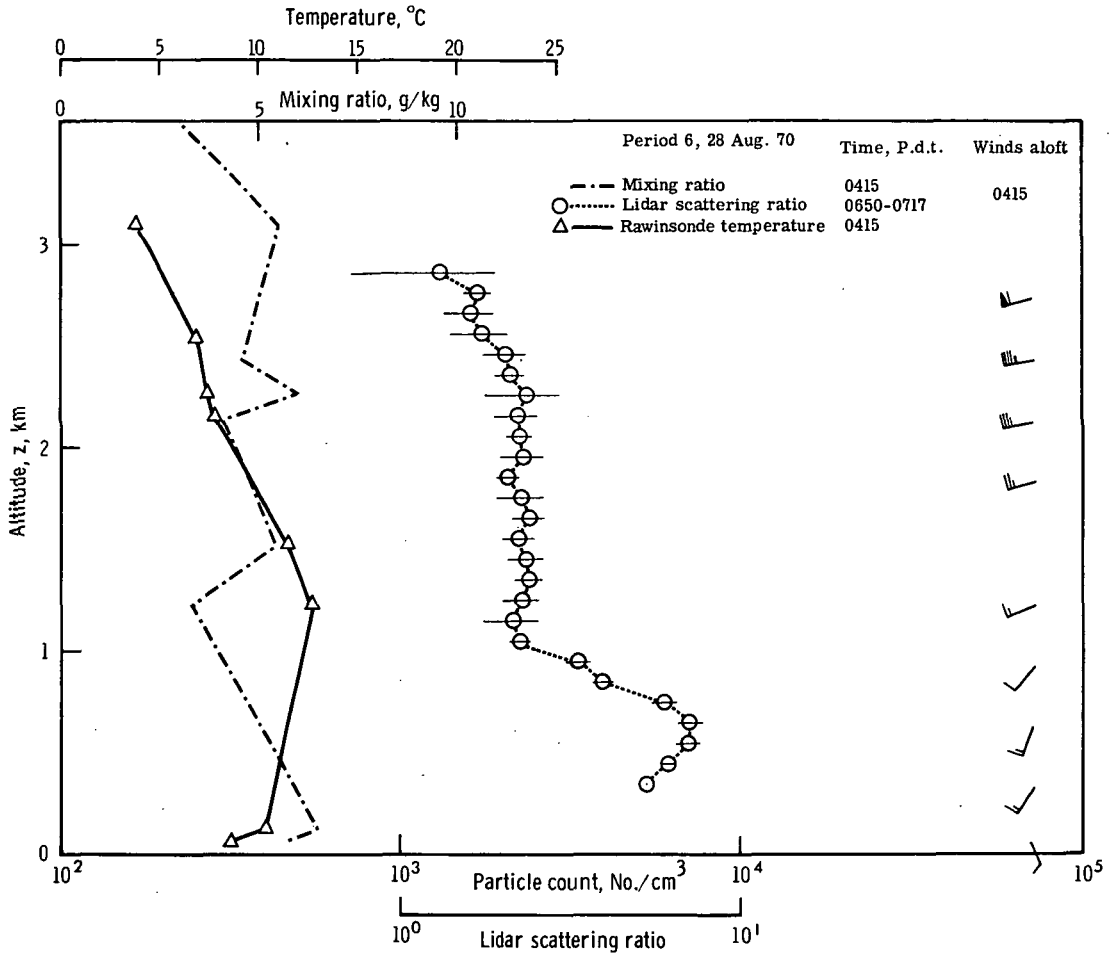

Figure 22.- Vertical profiles of temperature, water vapor, winds aloft, and aerosol concentrations measured over Salem, Oregon, during period 6, August 28, 1970.

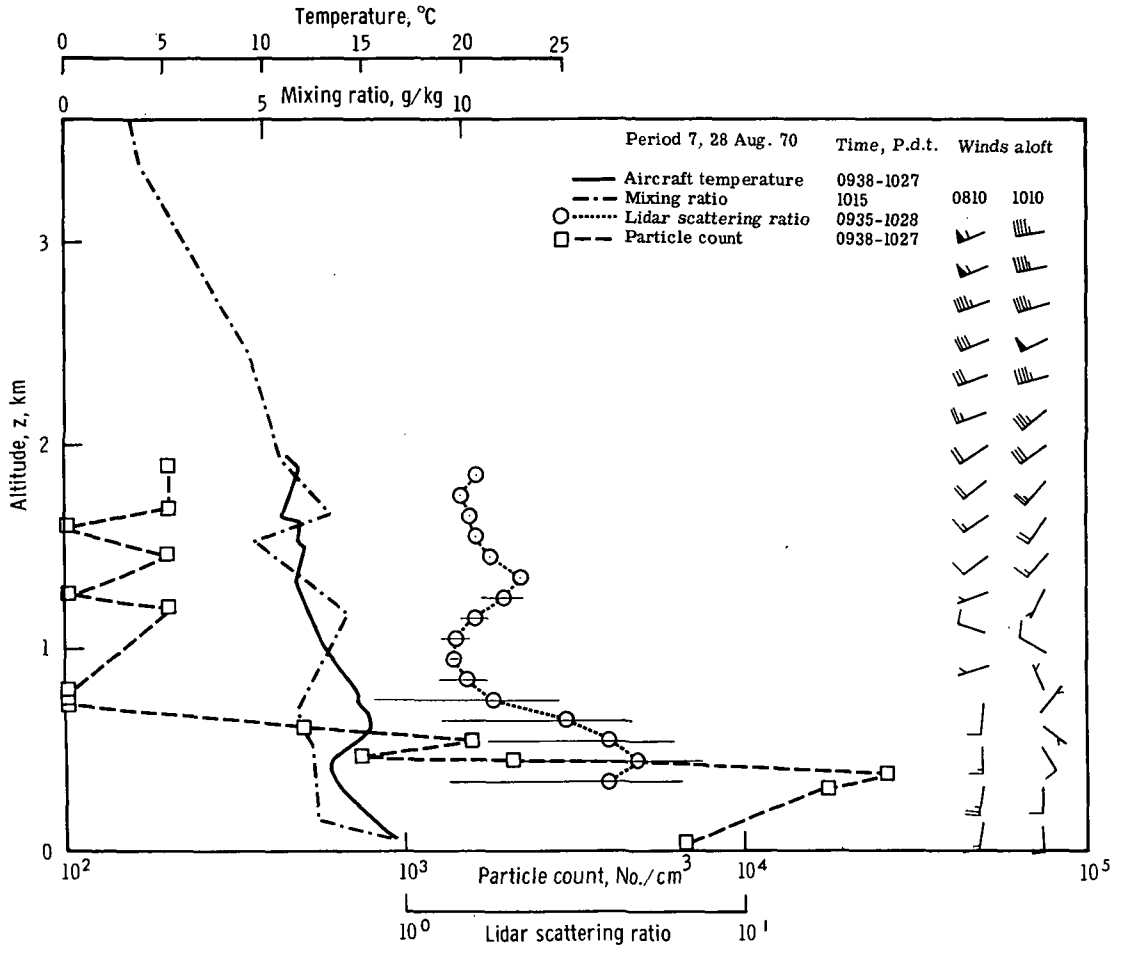

Figure 23.- Vertical profiles of temperature, water vapor, winds aloft, and aerosol concentrations measured over Salem, Oregon, during period 7, August 28, 1970.

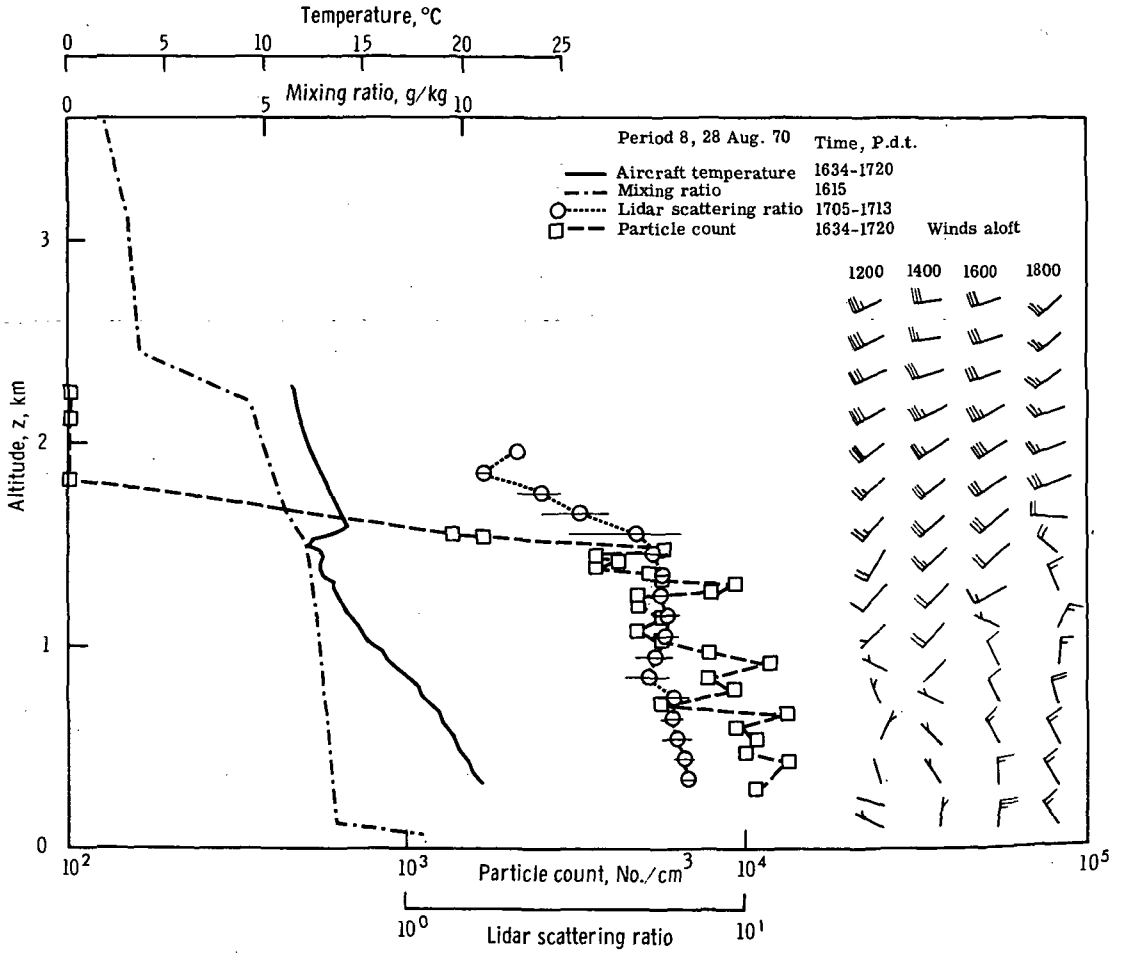

Figure 24.- Vertical profiles of temperature, water vapor, winds aloft, and aerosol concentrations measured over Salem, Oregon, during period 8, August 28, 1970.

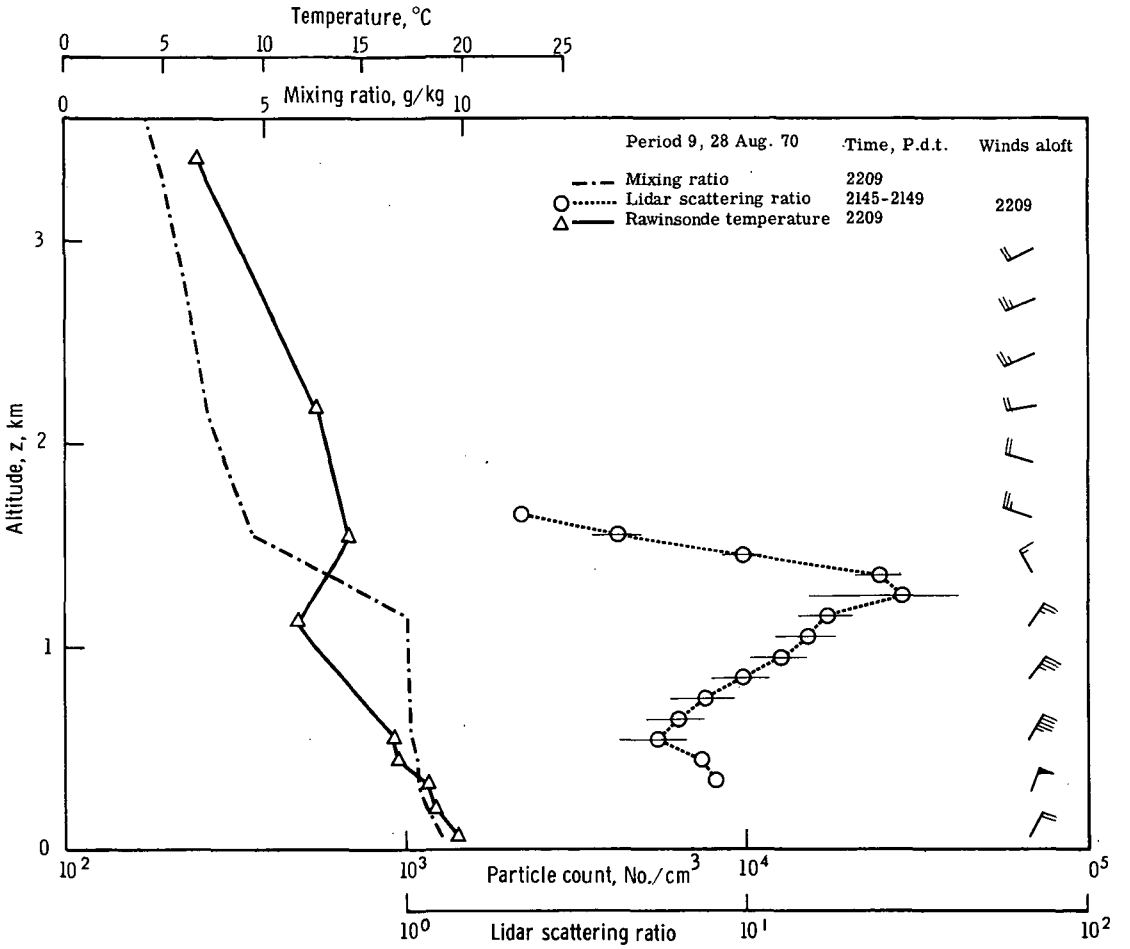

Figure 25.- Vertical profiles of temperature, water vapor, winds aloft, and aerosol concentrations measured over Salem, Oregon, during period 9, August 28, 1970.

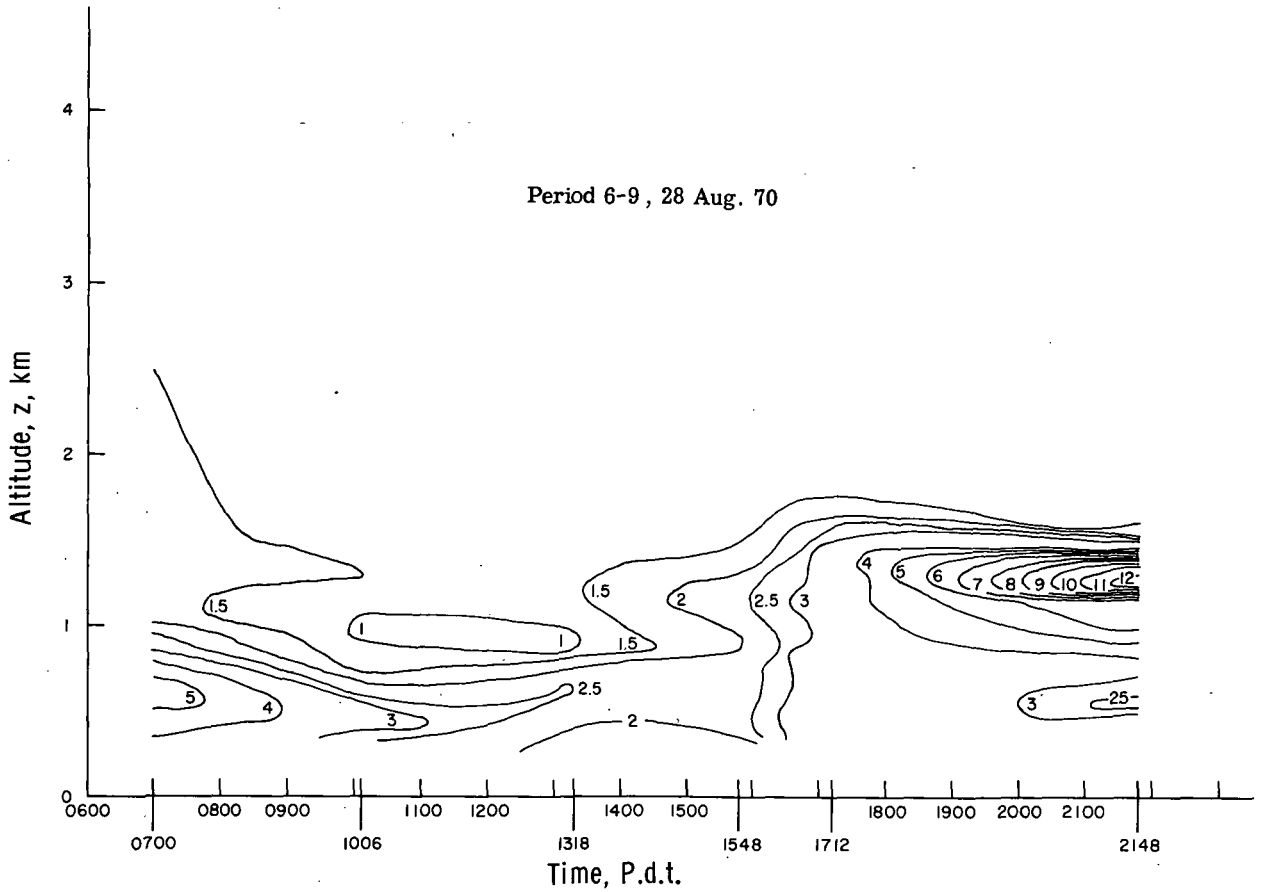

Figure 26.- Isopleth of lidar scattering ratio for periods 6 to 9, August 28, 1970.

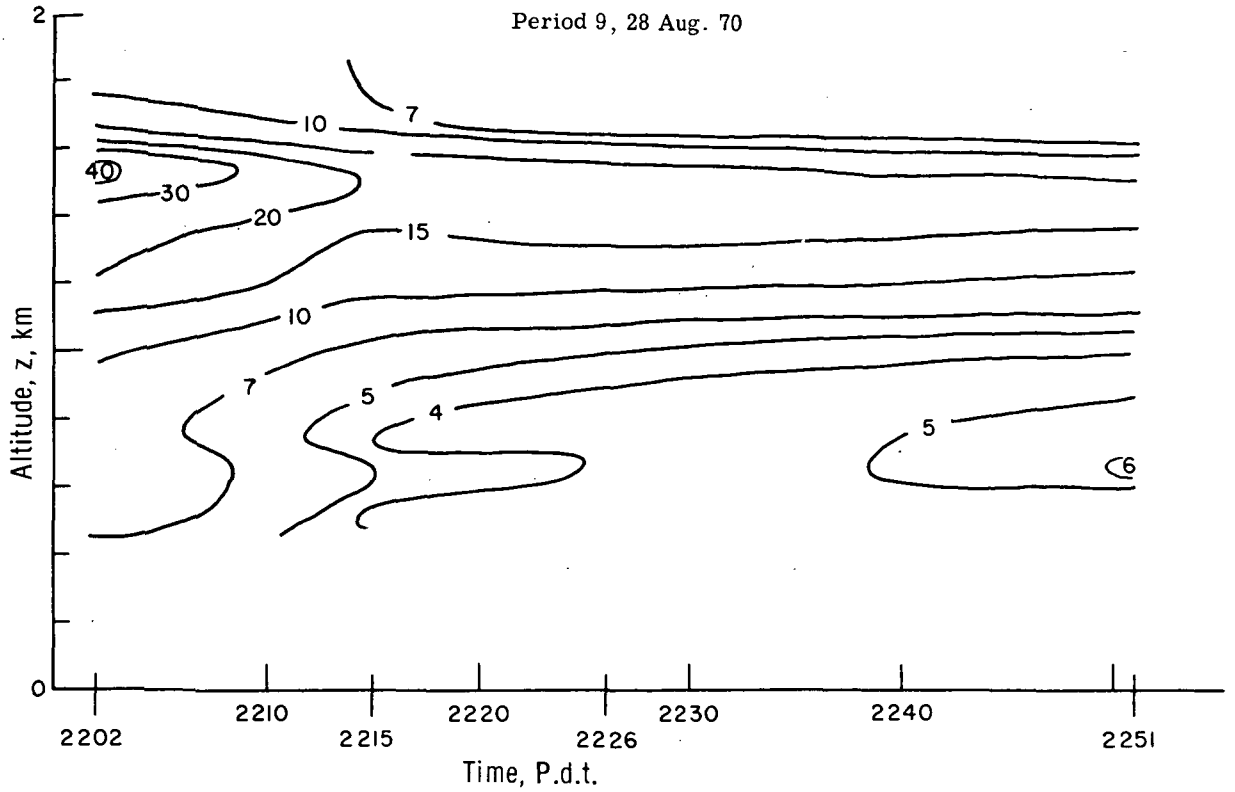

Figure 27.- Isopleth of lidar scattering ratio for period 9, August 28, 1970.

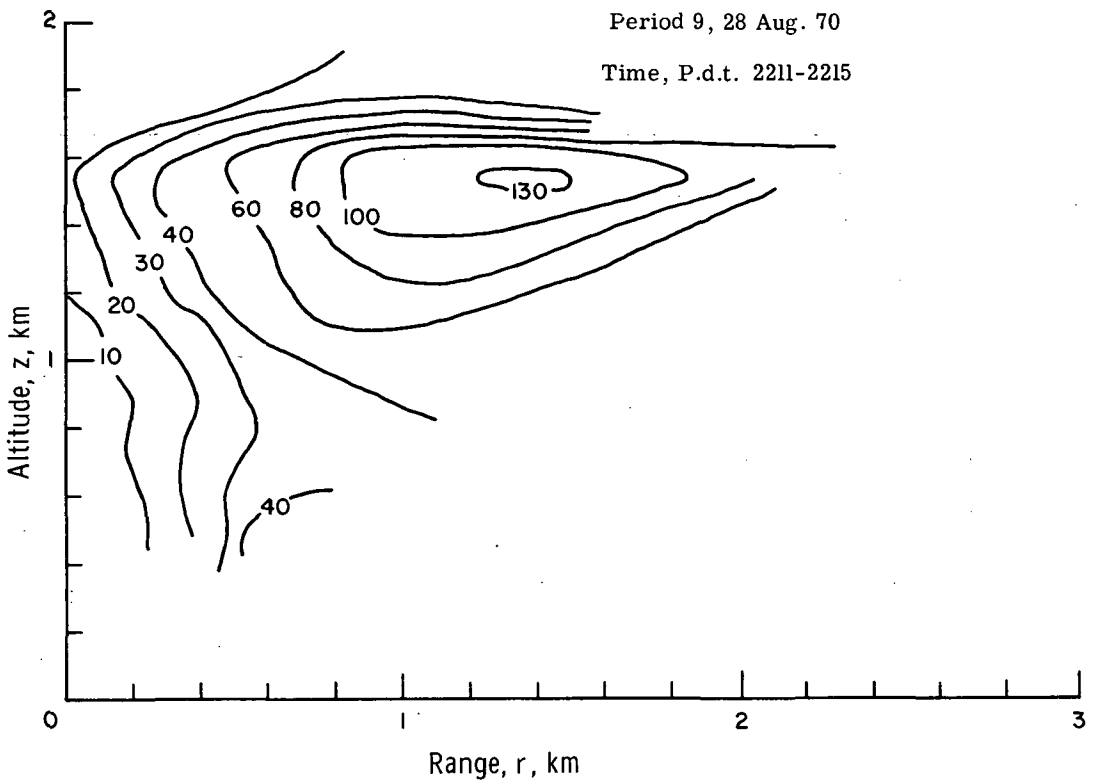

Figure 28.- Isopleth of lidar scattering ratio for period 9, August 28, 1970.

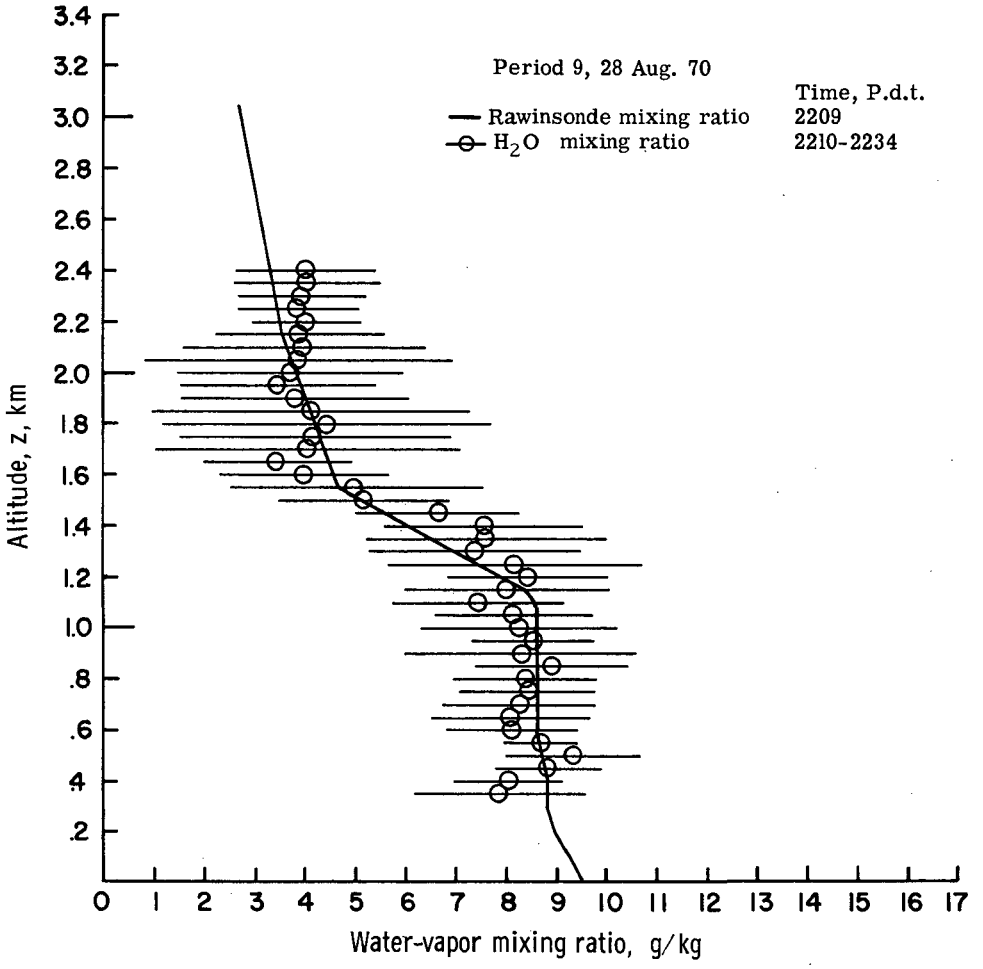

Figure 29.- Comparison of vertical profiles of lidar and rawinsonde water-vapor mixing ratios for period 9, August 28, 1970.

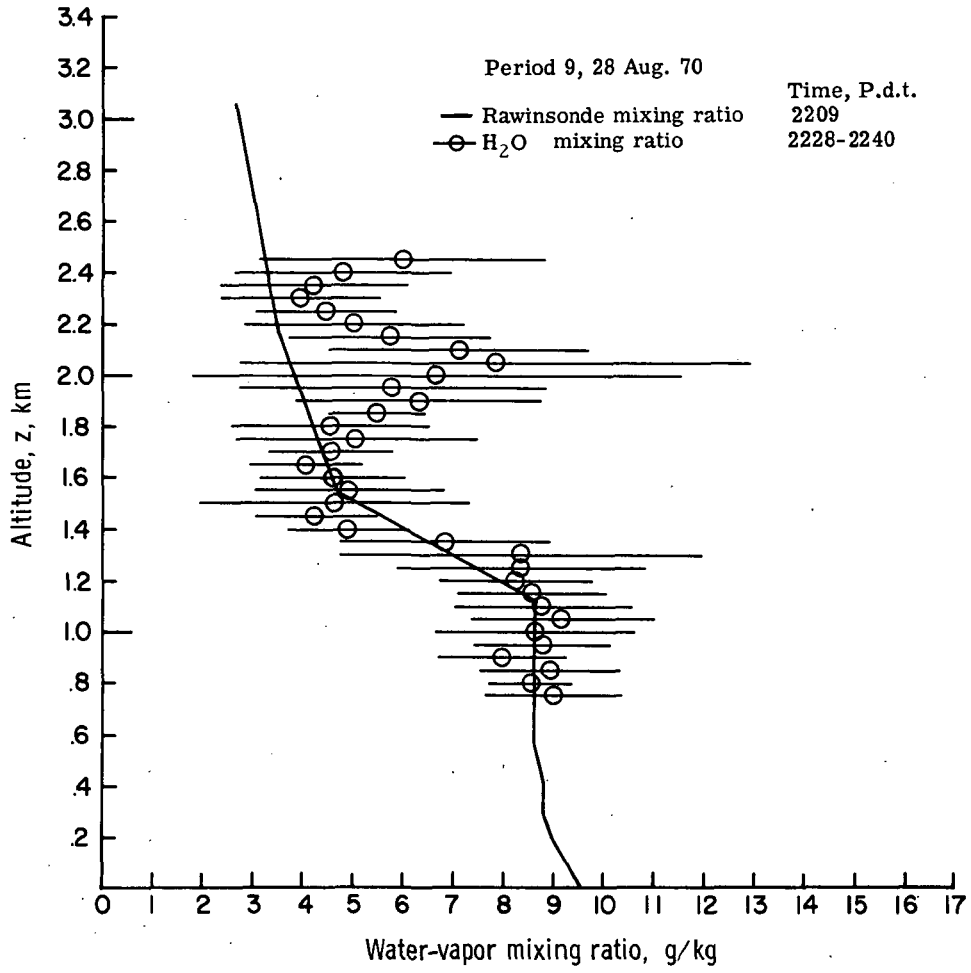

Figure 30.- Comparison of vertical profiles of lidar and rawinsonde water-vapor mixing ratios for period 9, August 28, 1970.

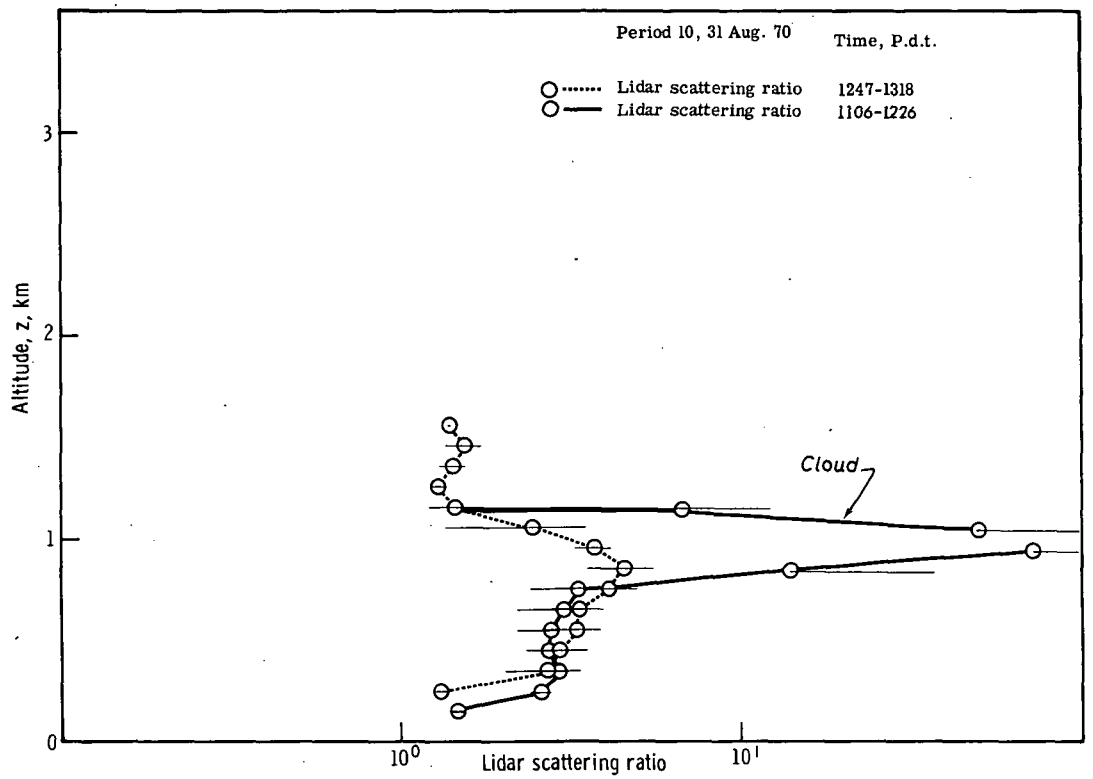

Figure 31.- Vertical profiles of aerosol concentrations measured over Salem, Oregon, during period 10, August 31, 1970.

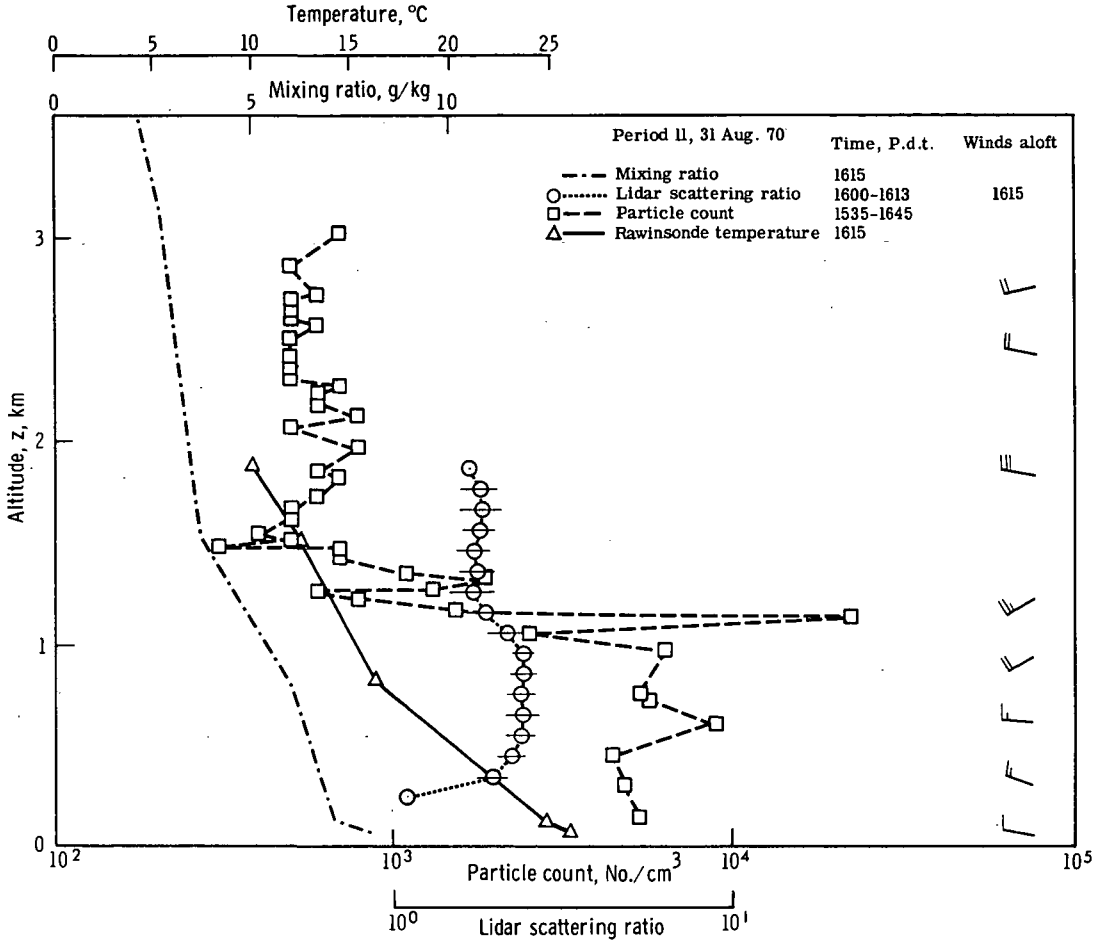

Figure 32.- Vertical profiles of temperature, water vapor, wind aloft, and aerosol concentrations measured over Salem, Oregon, during period 11, August 31, 1970.

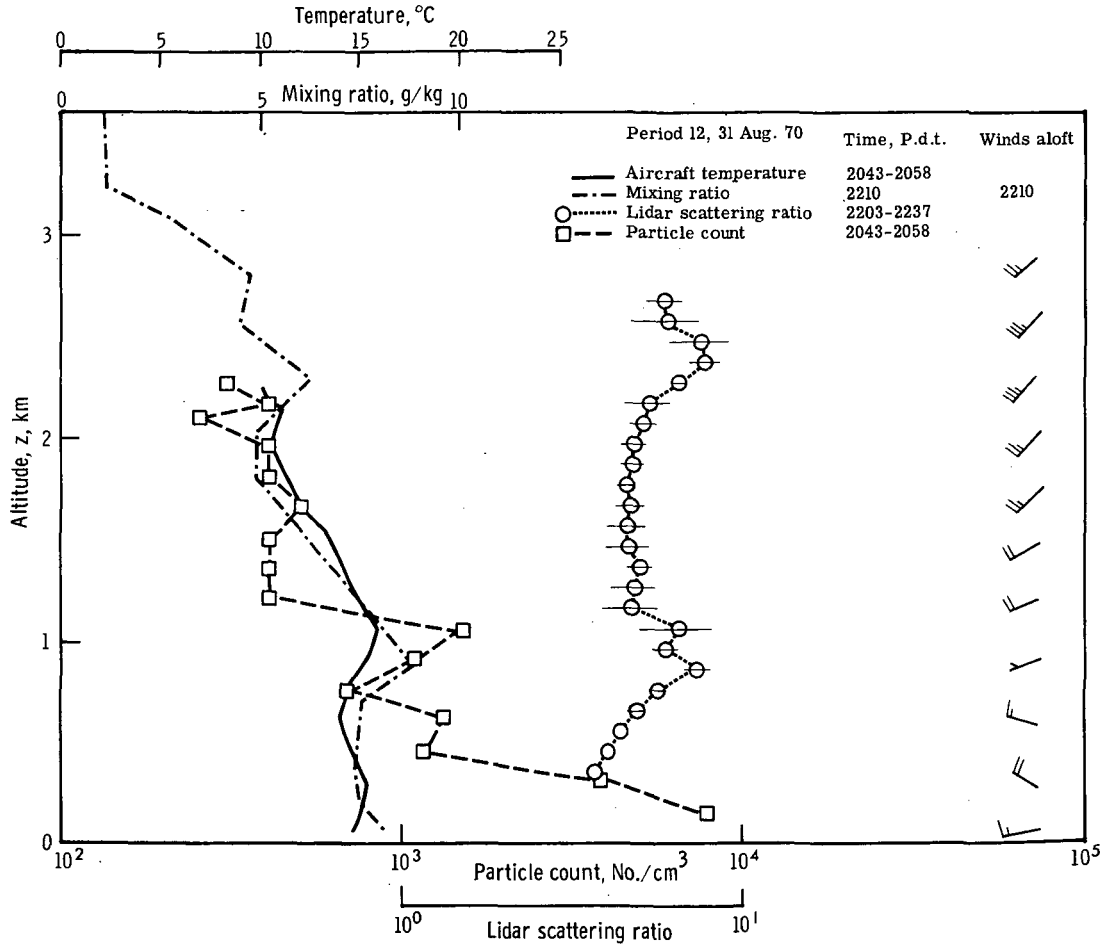

Figure 33.- Vertical profiles of temperature, water vapor, winds aloft, and aerosol concentrations measured over Salem, Oregon, during period 12, August 31, 1970.

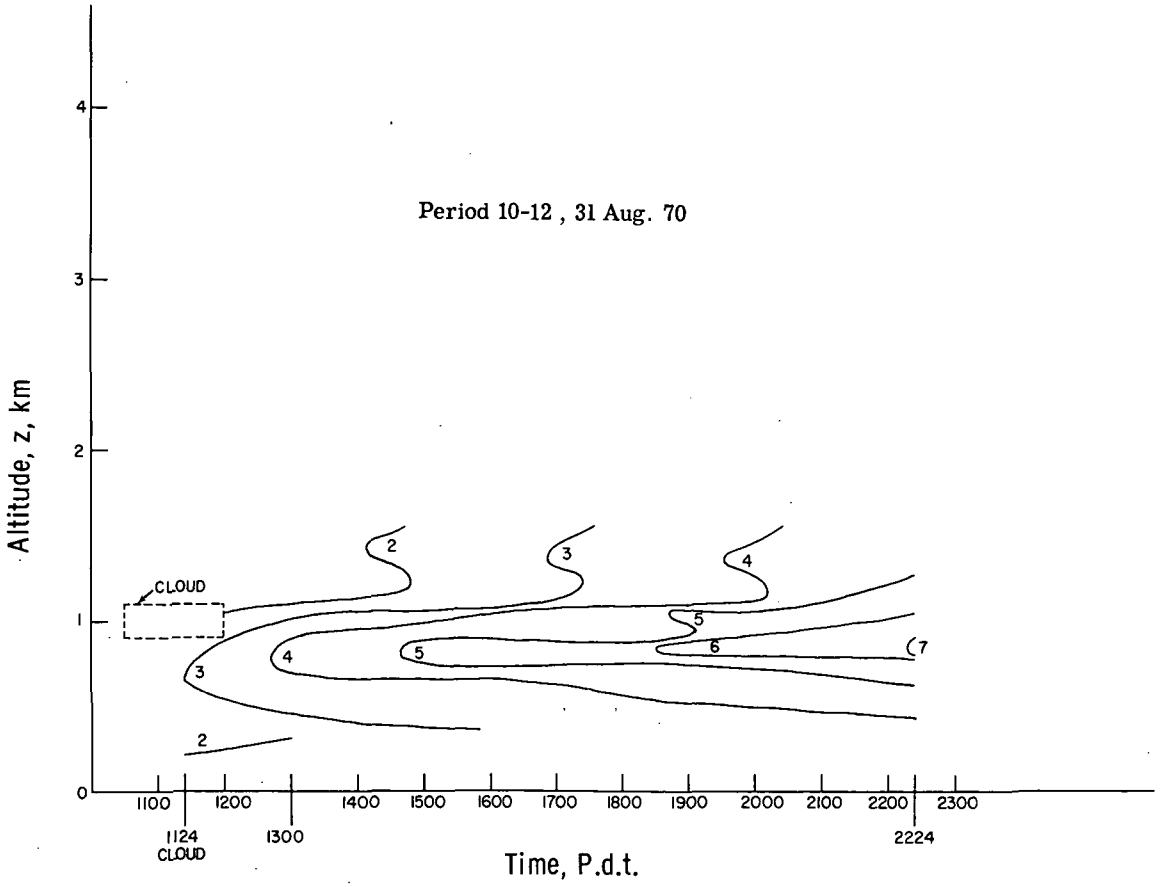

Figure 34.- Isopleth of lidar scattering ratio for periods 10 to 12, August 31, 1970.

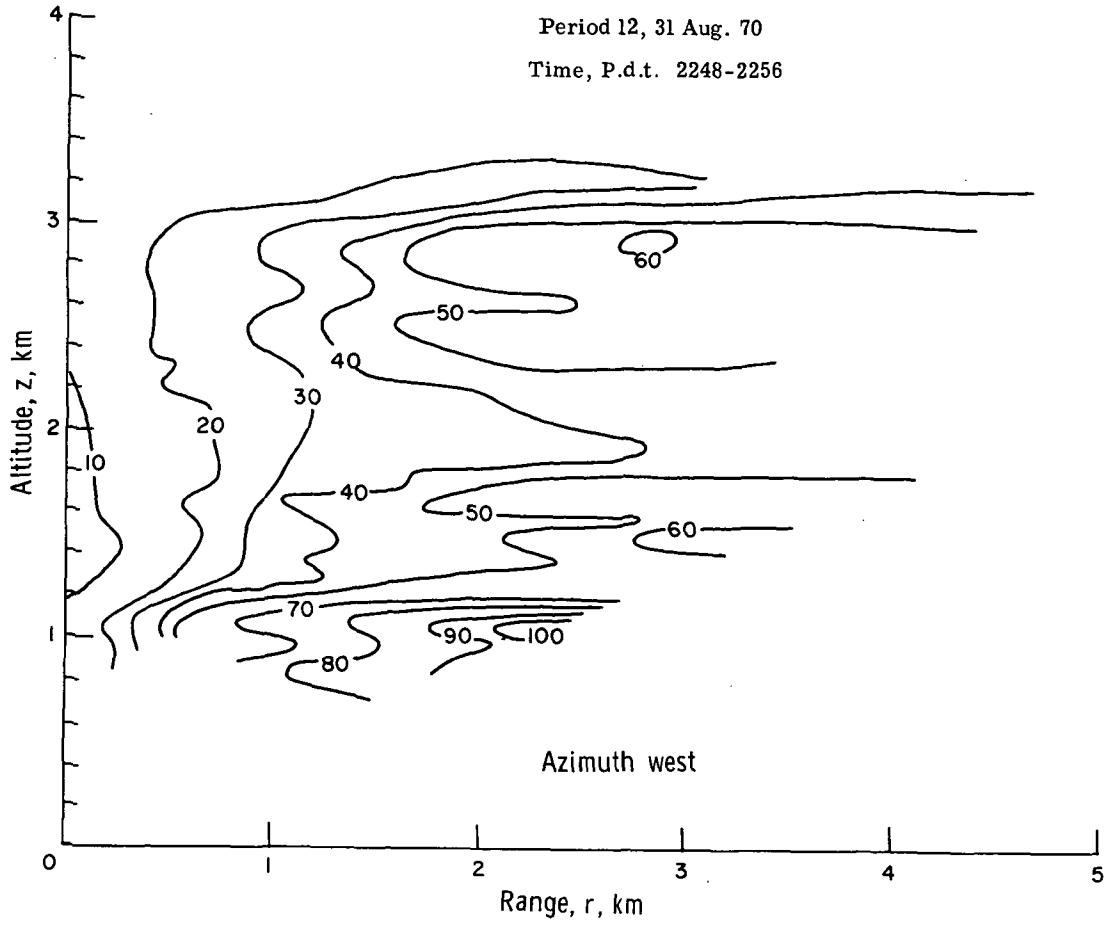

Figure 35.- Isopleth of lidar scattering ratio, azimuth west, during period 12, August 31, 1970.

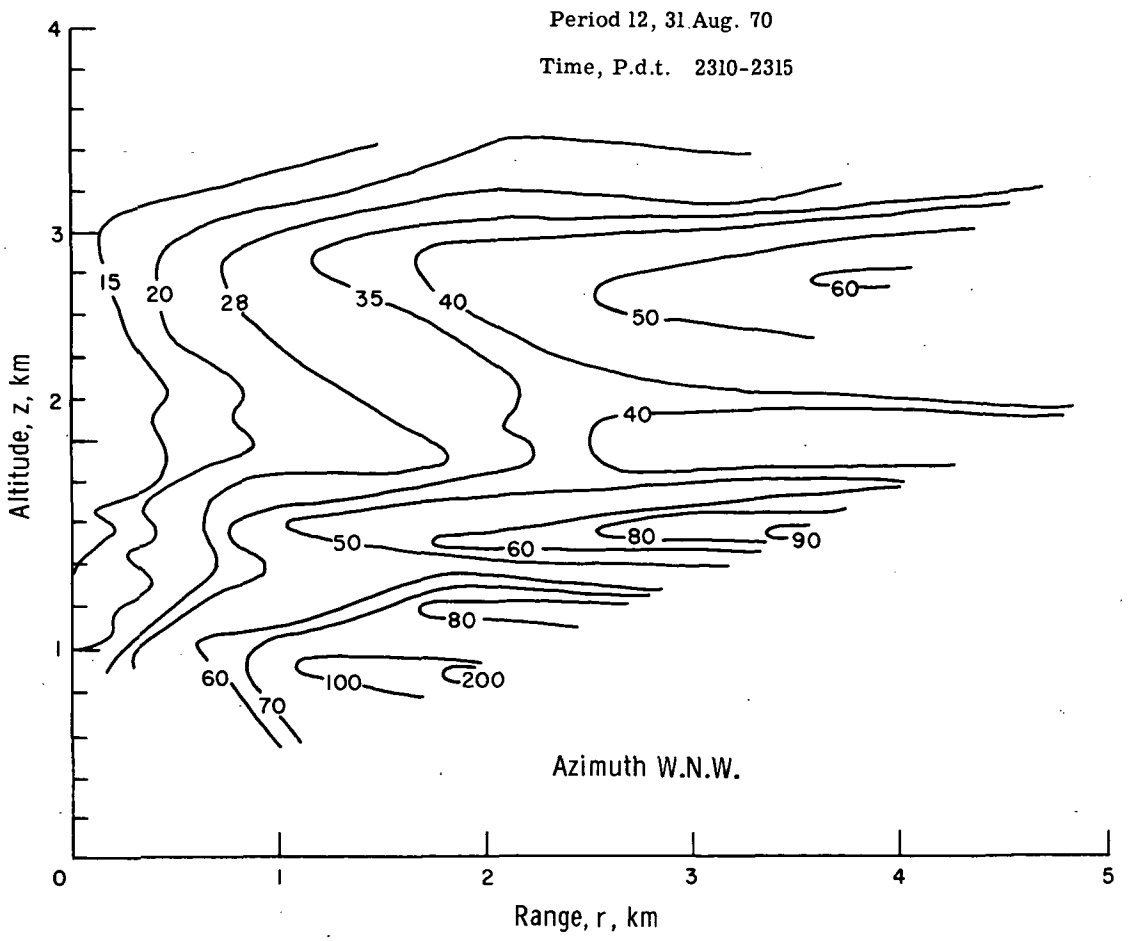

Figure 36.- Isopleth of lidar scattering ratio, azimuth W.N.W., during period 12, August 31, 1970.

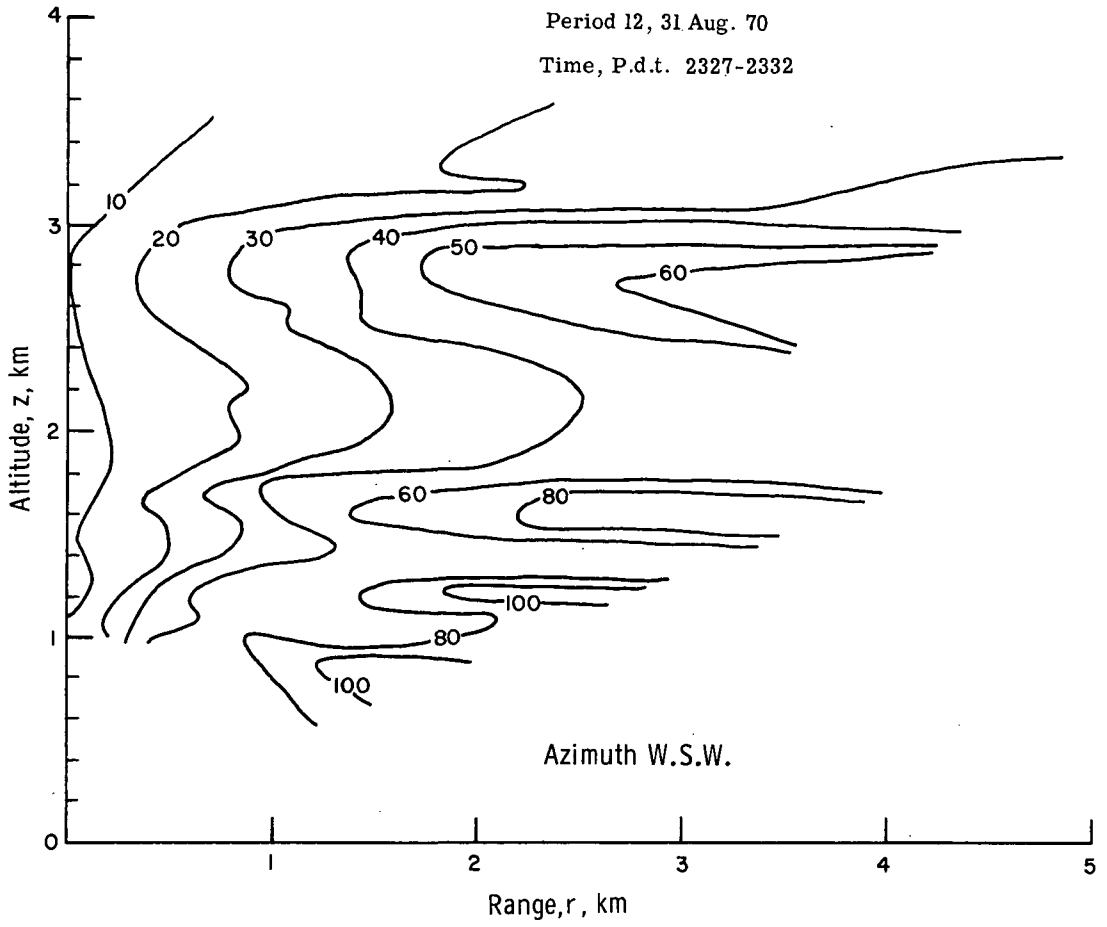

Figure 37.- Isopleth of lidar scattering ratio, azimuth W.S.W., during period 12, August 31, 1970.

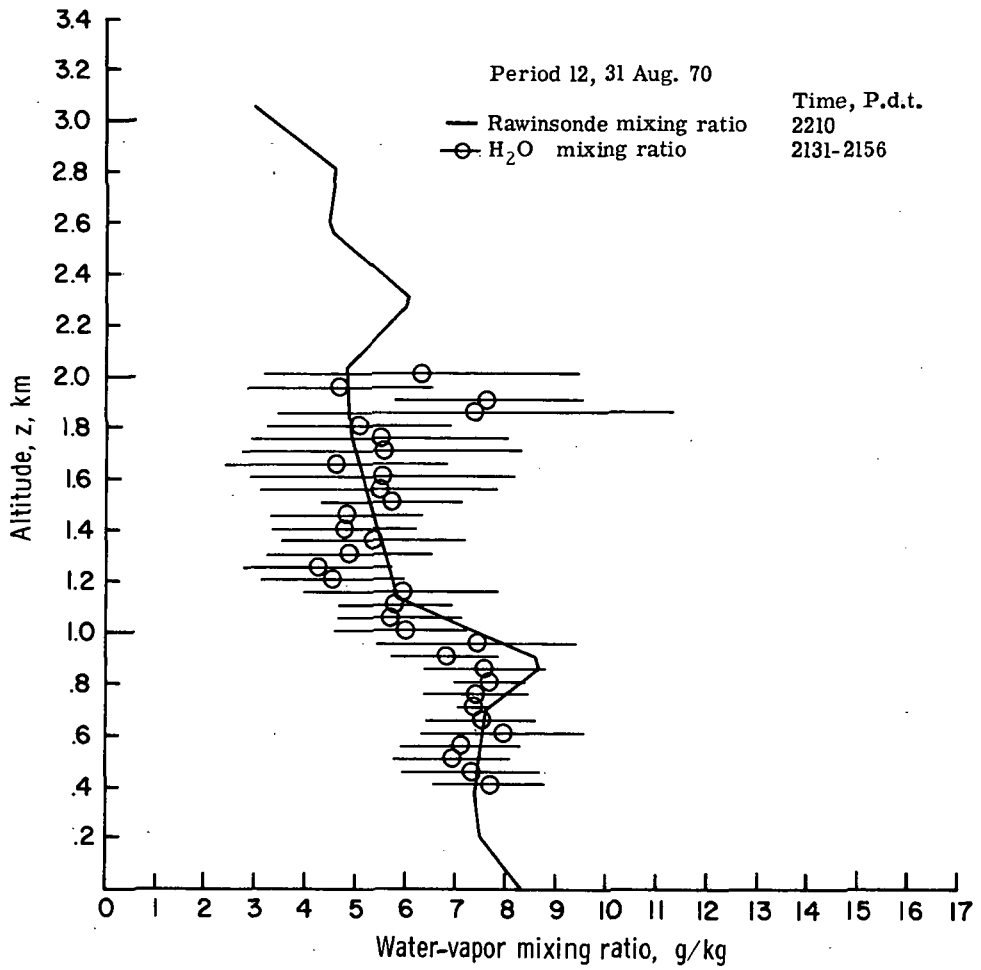

Figure 38.- Comparison of vertical profiles of lidar and rawinsonde water-vapor mixing ratios for period 12, August 31, 1970.

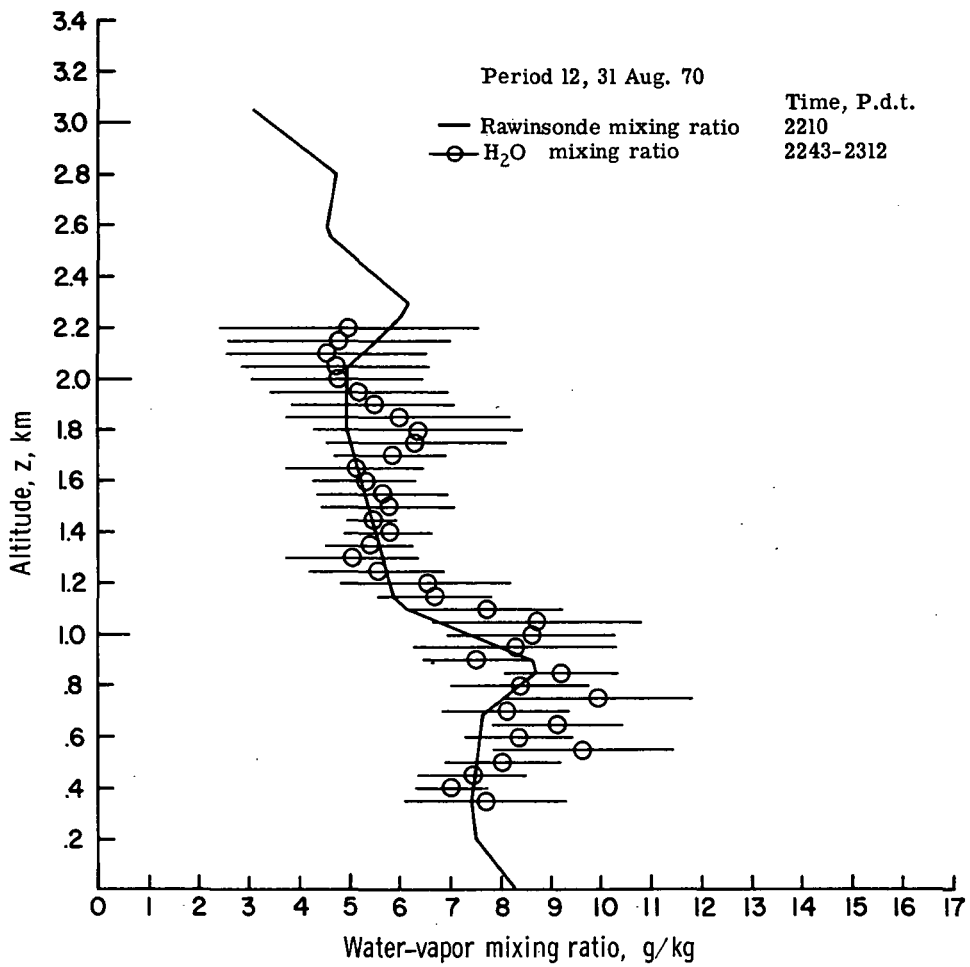

Figure 39.- Comparison of vertical profiles of lidar and rawinsonde water-vapor mixing ratios for period 12, August 31, 1970.

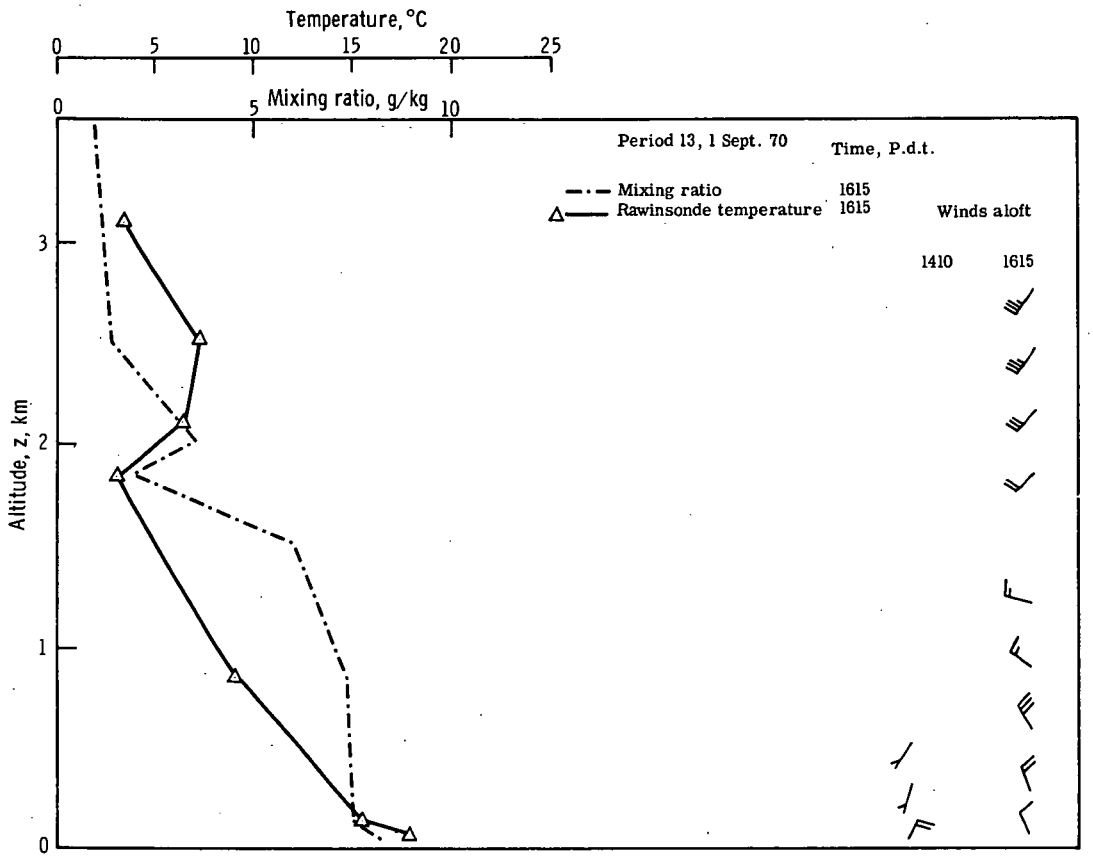

Figure 40.- Vertical profiles of temperature, water vapor, and winds aloft measured over Salem, Oregon, during period 13, September 1, 1970.

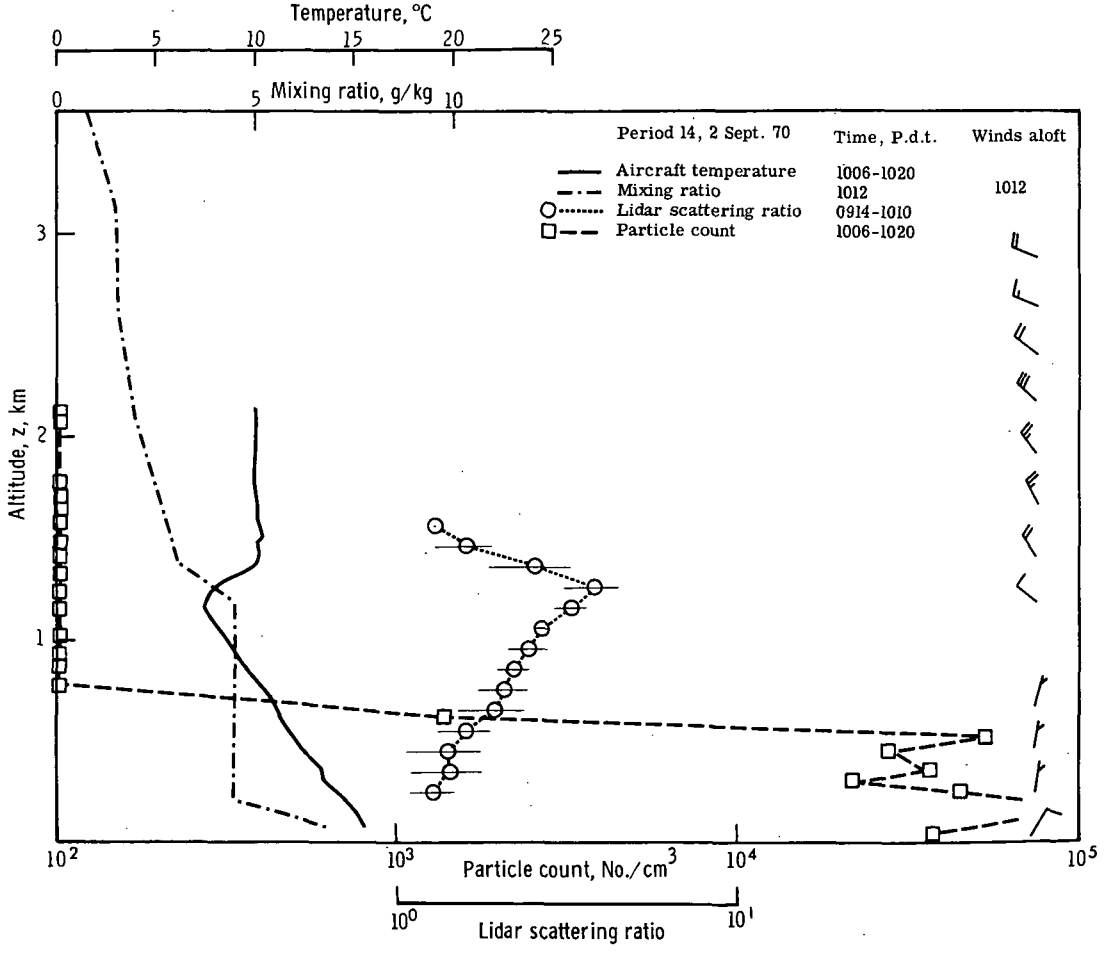

Figure 41.- Vertical profiles of temperature, water vapor, winds aloft, and aerosol concentrations measured over Salem, Oregon, during period 14, September 2, 1970.

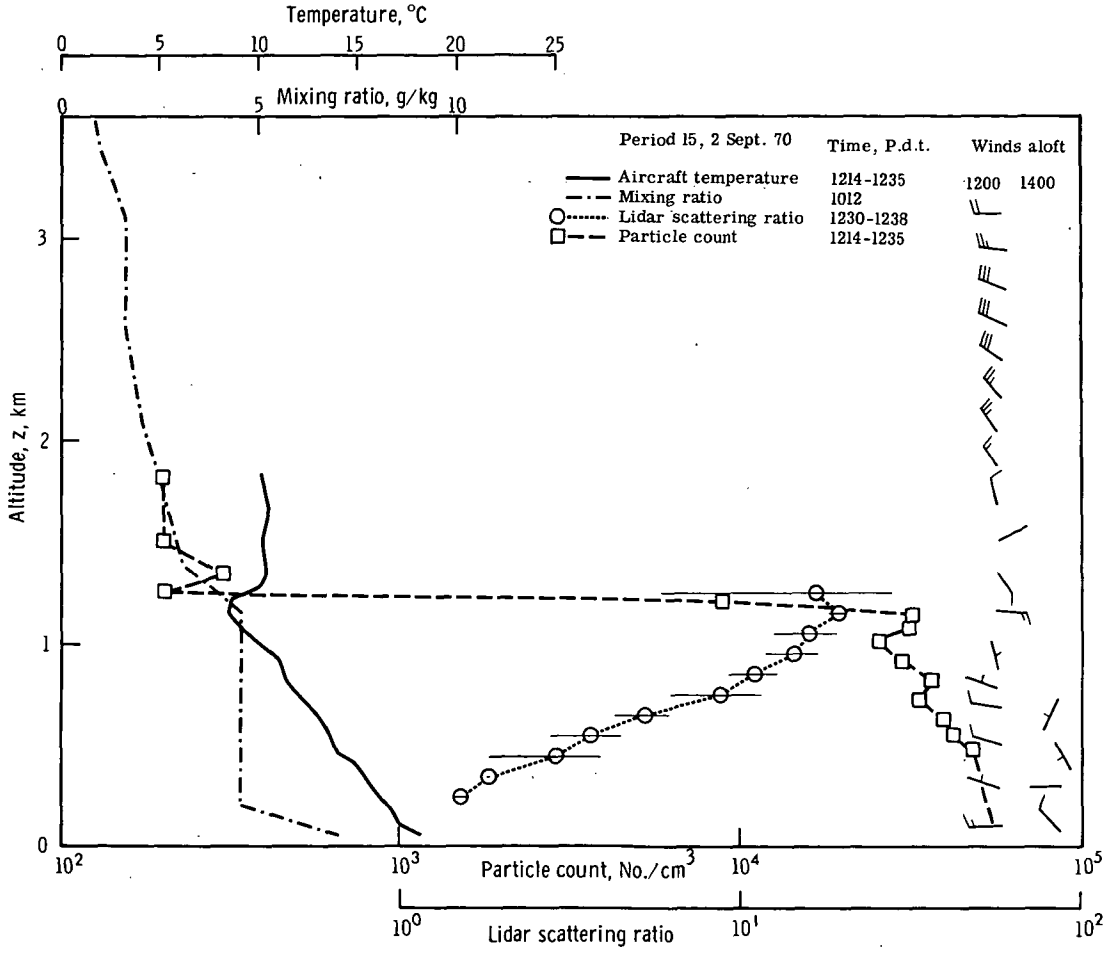

Figure 42.- Vertical profiles of temperature, water vapor, winds aloft, and aerosol concentrations measured over Salem, Oregon, during period 15, September 2, 1970.

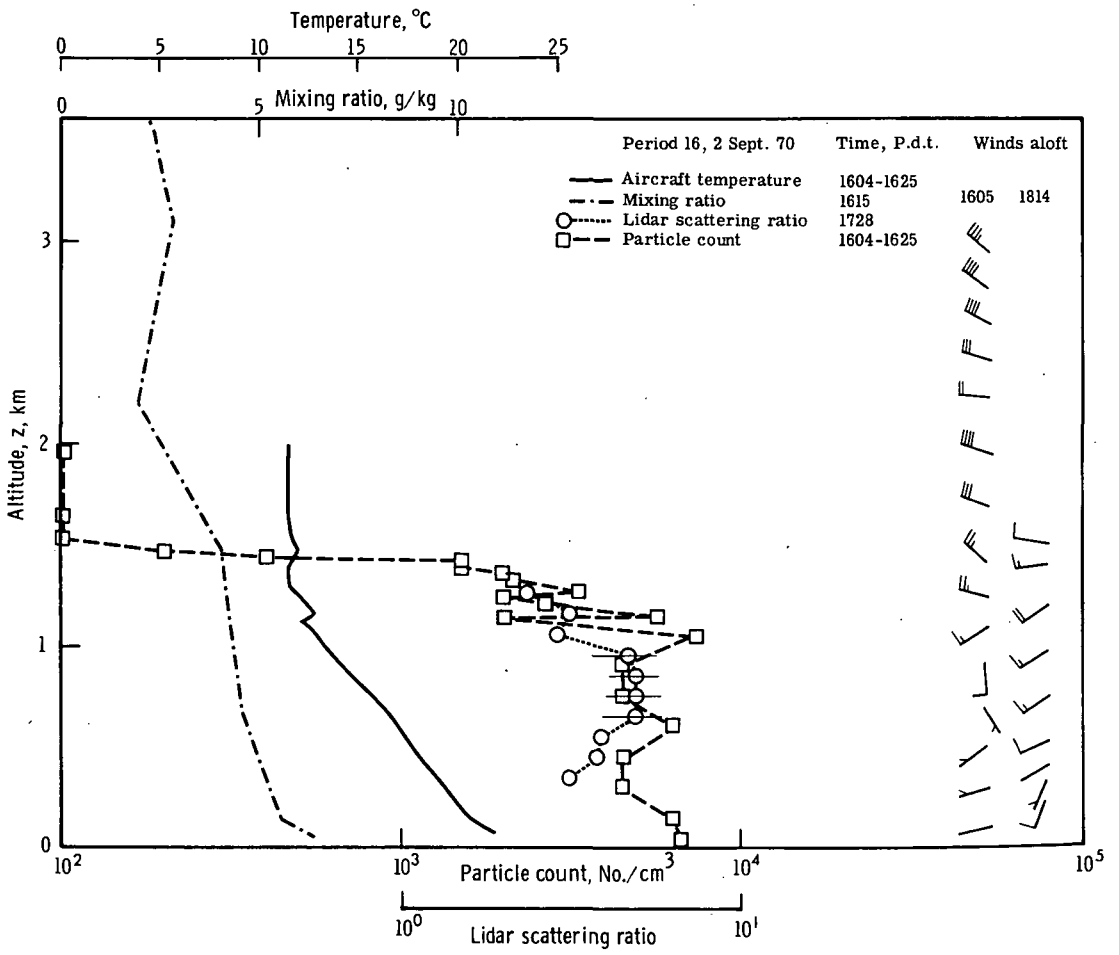

Figure 43.- Vertical profiles of temperature, water vapor, winds aloft, and aerosol concentrations measured over Salem, Oregon, during period 16, September 2, 1970.

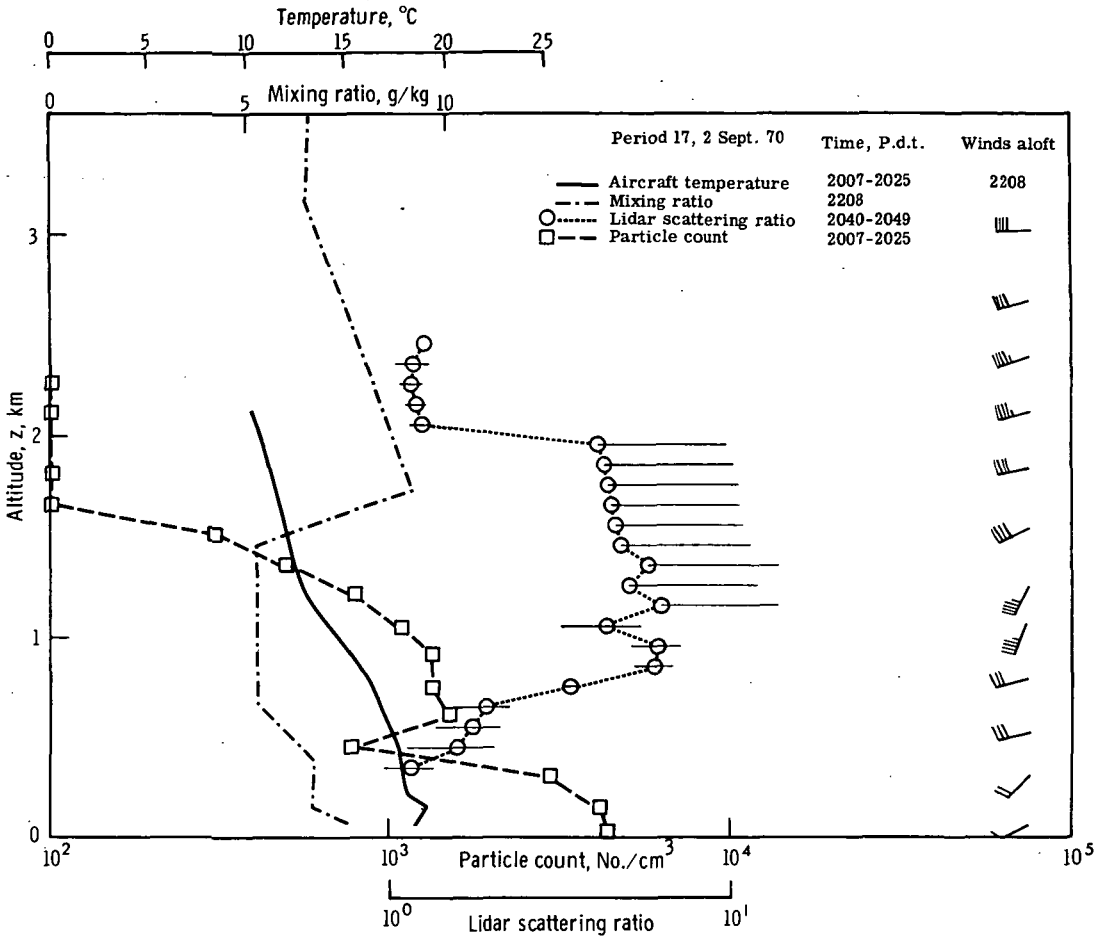

Figure 44.- Vertical profiles of temperature, water vapor, winds aloft, and aerosol concentrations measured over Salem, Oregon, during period 17, September 2, 1970.

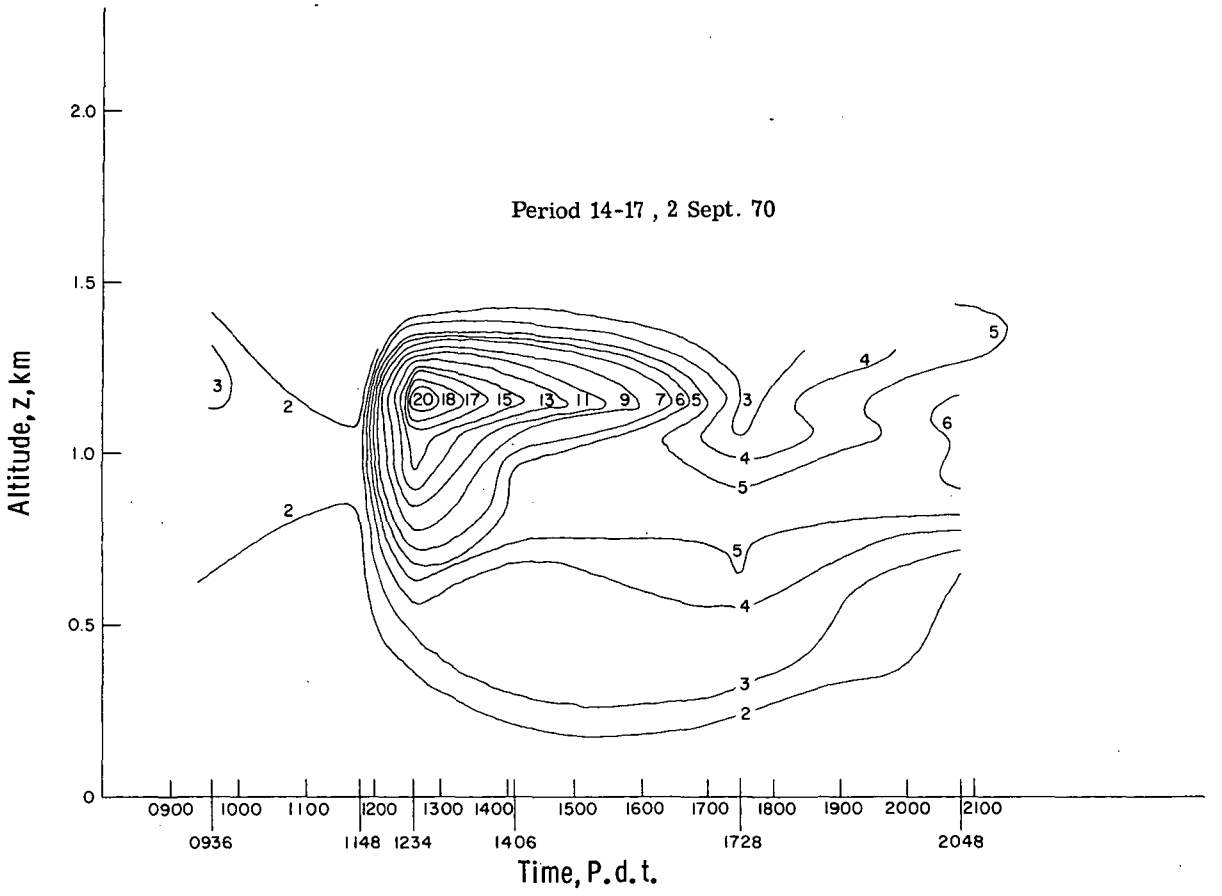

Figure 45.- Isopleth of lidar scattering ratio for periods 14 to 17, September 2, 1970.

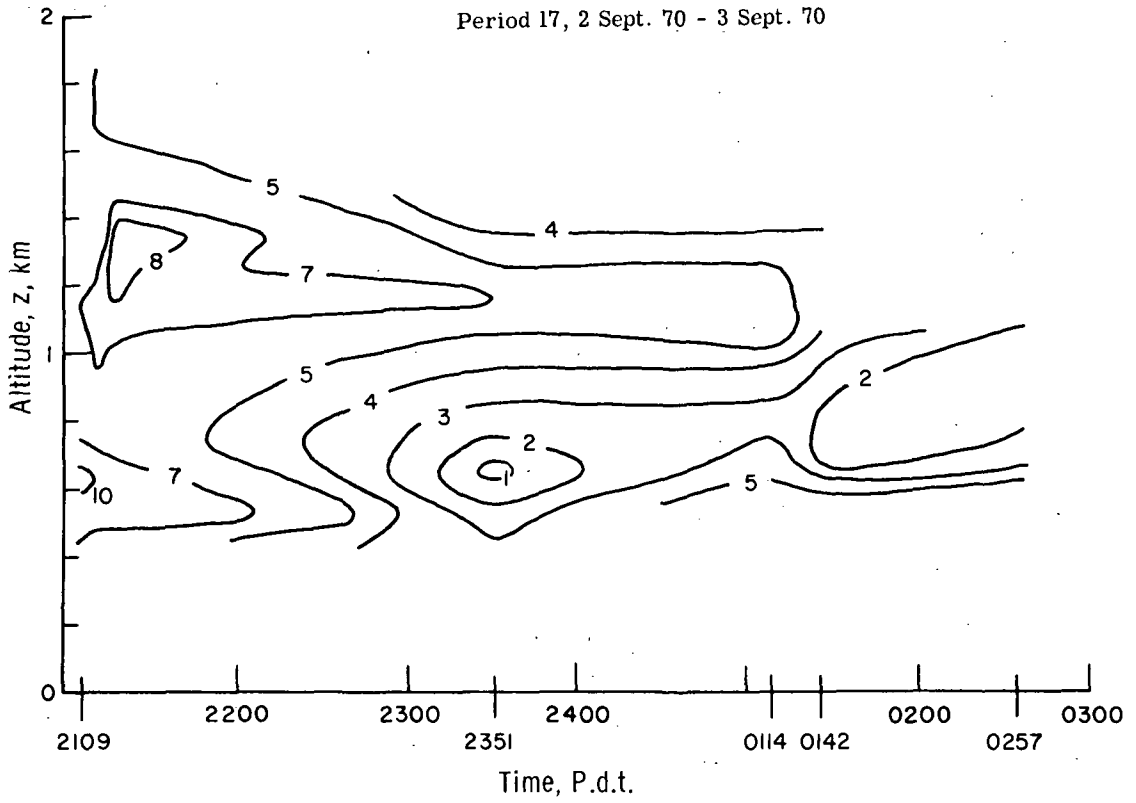

Figure 46.- Isopleth of lidar scattering ratio for period 17, September 2, 1970.

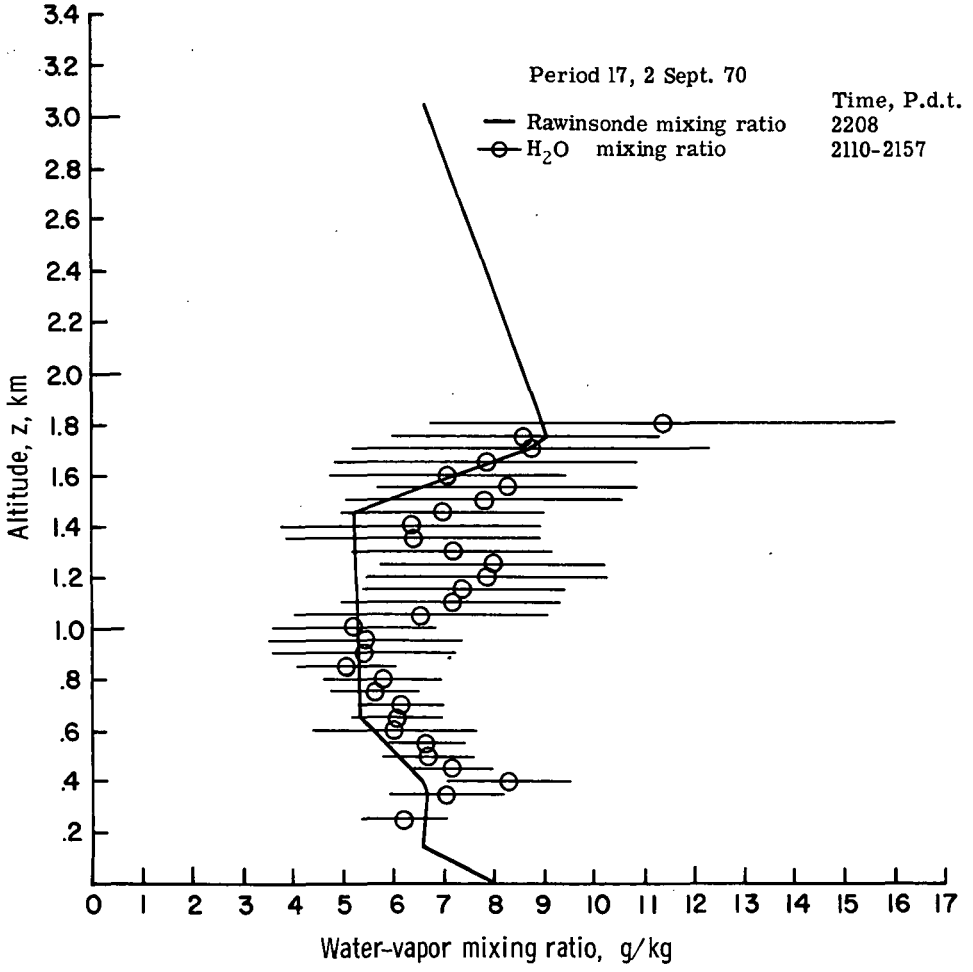

Figure 47.- Comparison of vertical profiles of lidar and rawinsonde water-vapor mixing ratios for period 17, September 2, 1970.

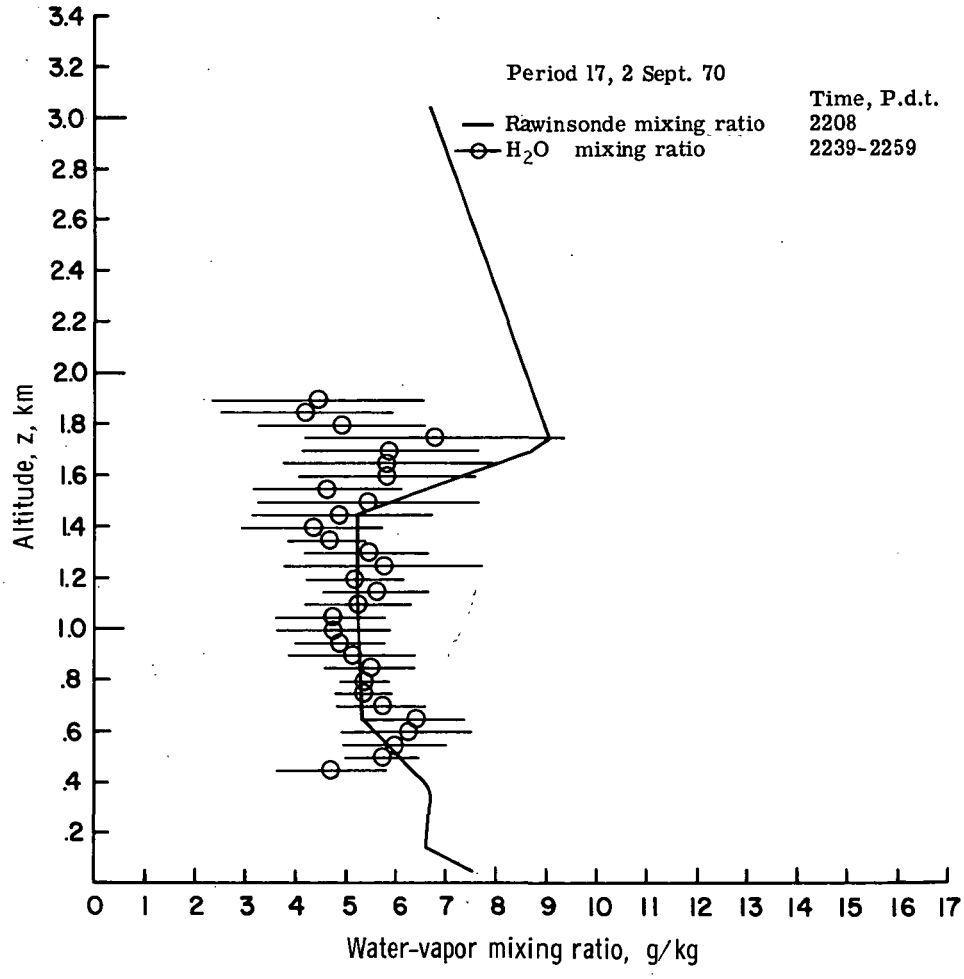

Figure 48.- Comparison of vertical profiles of lidar and rawinsonde water-vapor mixing ratios for period 17, September 2, 1970.

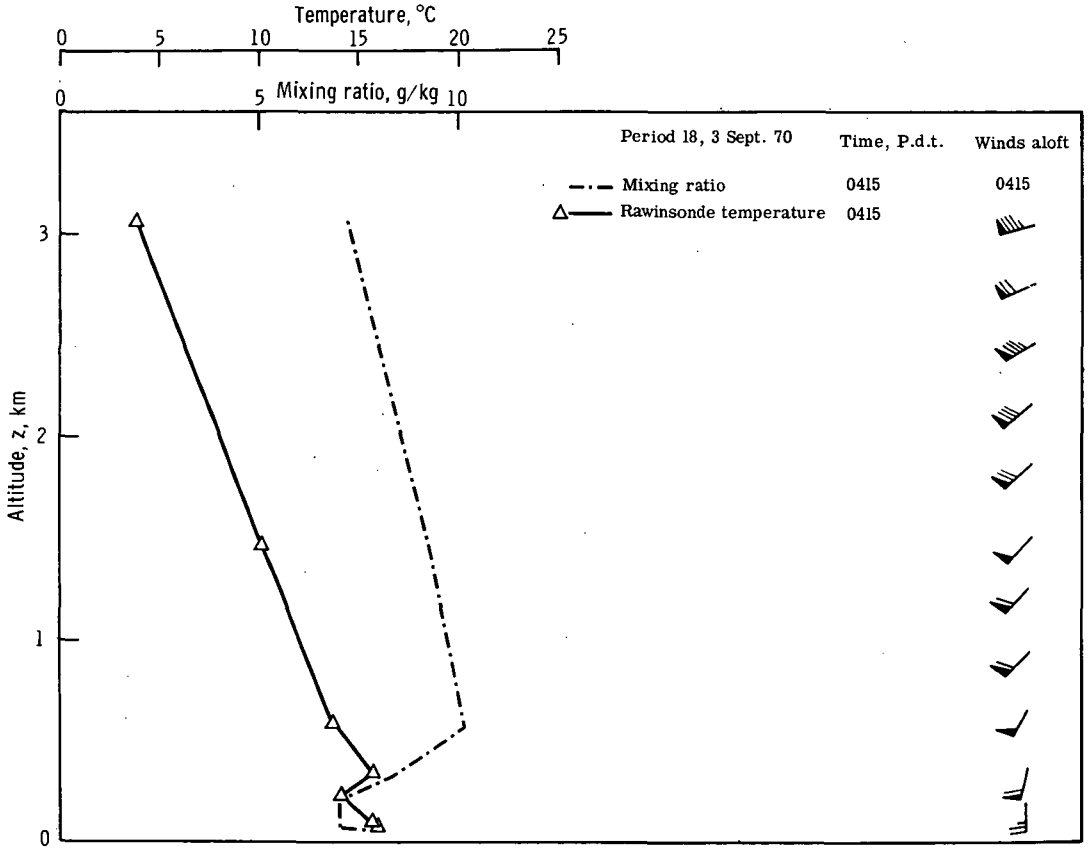

Figure 49.- Vertical profiles of temperature, water vapor, and winds aloft measured over Salem, Oregon, during period 18, September 3, 1970.

NASA-Langley, 1972 — 20 L-8279

"The aeronautical and space activities of the United States shall be conducted so as to contribute . . . to the expansion of human knowledge of phenomena in the atmosphere and space. The Administration shall provide for the widest practicable and appropriate dissemination of information concerning its activities and the results thereof."

— NATIONAL AERONAUTICS AND SPACE ACT OF 1958

NASA SCIENTIFIC AND TECHNICAL PUBLICATIONS

TECHNICAL REPORTS: Scientific and technical information considered important, complete, and a lasting contribution to existing knowledge.

TECHNICAL NOTES: Information less broad in scope but nevertheless of importance as a contribution to existing knowledge.

TECHNICAL MEMORANDUMS: Information receiving limited distribution because of preliminary data, security classification, or other reasons.

CONTRACTOR REPORTS: Scientific and technical information generated under a NASA contract or grant and considered an important contribution to existing knowledge.

TECHNICAL TRANSLATIONS: Information published in a foreign language considered to merit NASA distribution in English.

SPECIAL PUBLICATIONS: Information derived from or of value to NASA activities. Publications include conference proceedings, monographs, data compilations, handbooks, sourcebooks, and special bibliographies.

TECHNOLOGY UTILIZATION PUBLICATIONS: Information on technology used by NASA that may be of particular interest in commercial and other non-aerospace applications. Publications include Tech Briefs, Technology Utilization Reports and Technology Surveys.

Details on the availability of these publications may be obtained from:

SCIENTIFIC AND TECHNICAL INFORMATION OFFICE

NATIONAL AERONAUTICS AND SPACE ADMINISTRATION

Washington, D.C. 20546